IDŐJÁRÁS

QUARTERLY JOURNAL
OF THE HUNGARIAN METEOROLOGICAL SERVICE

CONTENTS

****

http://www.met.hu/Journal-Idojaras.php

VOL. 117* NO. 3 * JULY – SEPTEMBER 2013

IDŐJÁRÁS

Quarterly Journal of the Hungarian Meteorological Service

Editorial Office: Kitaibel P.u. 1, H-1024 Budapest, Hungary
P.O. Box 38, H-1525 Budapest, Hungary
E-mail: journal.idojaras@met.hu
Fax: (36-1) 346-4669

Indexed and abstracted in Science Citation Index Expanded™ and Journal Citation Reports/Science Edition
Covered in the abstract and citation database SCOPUS®

Subscription by mail:
IDŐJÁRÁS, P.O. Box 38, H-1525 Budapest, Hungary
E-mail: journal.idojaras@met.hu

IDŐJÁRÁS

Quarterly Journal of the Hungarian Meteorological Service
Vol. 117, No. 3, July – September, 2013, pp. 239–275

Evaluation and validation of a CFD solver adapted to atmospheric flows: Simulation of topography-induced waves

Norbert Rácz[1*], **Gergely Kristóf**[1], and **Tamás Weidinger**[2]

[1]*Department of Fluid Mechanics, Budapest University of Technology and Economics (BME), Bertalan L. u. 4-6, H-1111 Budapest, Hungary*
E-mails: racz@ara.bme.hu; kristof@ara.bme.hu

[2]*Department of Meteorology, Eötvös Loránd University, P.O. Box 32, H-1518 Budapest, Hungary*
weidi@caesar.elte.hu

**Corresponding author*

(Manuscript received in final form December 15, 2012)

Abstract–Mountain wave phenomena have been simulated by using a well-known general purpose computational fluid dynamic (CFD) simulation system adapted to atmospheric flow modeling. Mesoscale effects have been taken into account with a novel approach based on a system of transformations and customized volume sources acting in the conservation and governing equations. Simulations of linear hydrostatic wave fields generated by a two-dimensional obstacle were carried out, and the resulting vertical velocity fields were compared against the corresponding analytic solution. Validation with laboratory experiments and full-scale atmospheric flows is a very important step toward the practical application of the method. Performance measures showed good correspondence with measured data concerning flow structures and wave pattern characteristics of non-hydrostatic and nonlinear mountain waves in low Reynolds number flows. For highly nonlinear atmospheric scale conditions, we reproduced the well-documented downslope windstorm at Boulder in January 1972, during which extreme weather conditions, with a wind speed of approximately 60 m s^{-1}, were measured close to the ground. The existence of the hydraulic jump, the strong descent of the stratospheric air, wave breaking regions, and the highly accelerated downslope wind were well reproduced by the model. Evaluation based on normalized mean square error (NMSE), fractional bias (FB), and predictions within a factor of two of observations (FAC2) show good model performance, however, due to the horizontal shift in the flow pattern, a less satisfactory hit rate and correlation value can be observed.

Key-words: complex terrain, gravity waves, CFD simulation, model validation, numerical weather prediction

1. Introduction

An extension of the physical model used in general purpose computational fluid dynamic (CFD) solvers has been developed recently in order to simulate mesoscale atmospheric flow phenomena in the same model with finely structured microscale flow around complex geometries (*Castro et al.*, 2008). We suggested a novel approach by utilizing a system of transformations and additional volume sources in the governing equations. Atmospheric stratification, adiabatic temperature change caused by vertical motion, baroclinicity, and Coriolis force are taken into account through this method (*Kristóf et al.,* 2009). The model uses only one single unstructured grid, and a uniform physical description for close- and far-field flow avoiding interpolation errors and model uncertainties due to model nesting. The authors intended purpose, furthermore, is to create a more general method, which is easy to implement in any CFD solver allowing programmable user defined volume sources in the governing equations. This new approach can be applied in several areas of practice, but before the application of the method, it is an important step to validate the model and to understand the capabilities of the technique.

In the early model validation steps (the implementation of the energy source term and the Coriolis force was investigated), large-eddy simulations (LES) of small scale thermal convection problems were carried out in order to simulate urban heat island circulation problem (*Noto,* 1996; *Lu et al.,* 1997; *Cenedese* and *Monti,* 2003). Good qualitative and quantitative agreement was found regarding the velocity and temperature profiles and the general flow pattern as well. Behavior of a spreading density current has also been simulated by solving the unsteady Reynolds averaged Navier-Stokes (URANS) equations, to study the behavior of the dynamical model core and compare the differences between the incompressible and compressible versions of the model (*Kristóf et al.,* 2009). The correct implementation of the Coriolis force was also tested in this work.

These validation cases have the advantage of that they have more control over the measured parameters due to the nature of the measuring device. However, they have low Reynolds number range, the cases are mainly hydrostatic, the vertical extent is limited to a certain height, and the density current study used a fixed turbulence viscosity model.

The purpose of the present paper is to further extend the validation cases characterized by non-hydrostatic and strong nonlinear situations. Further differences compared to previous validations (*Kristóf et al.,* 2009) are the complex topography, the extended simulation domain height incorporating the tropopause, and that all the source terms are activated (see Eqs.(30)–(35)). Results of gravity wave simulations compared against the corresponding analytic solution, small scale water-tank experiments (*Gyüre* and *Jánosi,* 2003), and full scale observations (*Lilly* and *Zipser,* 1972) will be presented. The

simulation of such cases has been found to be ideal for testing and evaluating mesoscale numerical models due to the presence of complex flow patterns and wave breaking phenomena.

Atmospheric waves form when stable air flow passes over an obstacle. Fluid parcels tend to return into their original height due to the restoring forces caused by stratification. Various types of oscillatory flow responses occur depending on the state of stratification and geometric parameters (*Holton,* 2004) One can see two divisions of mountain waves, vertically propagating and trapped lee waves. Mountain waves vertically propagating over a barrier may have horizontal wavelengths of many tens of kilometers, even reaching the lower stratosphere (*Lin,* 2007). The vertical propagation of trapped lee waves is limited to a certain height due to the presence of a highly stable layer when waves can be reflected in such situations. In general, gravity waves can modify the local weather situation near mountains: they can create rotor motions, hydraulic jumps, and they have the capability of concentrating momentum on the lee slopes, or occasionally leading to violent downslope windstorms. (*Klemp* and *Lilly,* 1975; *Simon et al.,* 2006) Lee waves can be a potential hazard for wave gliders, by producing rotors or clear air turbulence. Flow beneath the wave crests can be extremely turbulent, thus causing a potential hazard for low-level aviation as well (National Research Council, 1983). The simulations of atmospheric scale flows around mountains can also have economical importance when the future location of a wind farm is to be estimated (*Montavon,* 1998; *Lopes da Costa et al.,* 2006; *Palma et al.,* 2008).

One can observe mountain waves (*Smith et al.,* 2002) with the help of various types of clouds, altocumulus or wave clouds at wave crests. Rotor clouds may dye some parts of the wave field if the appropriate amount of moisture is present. In some cases they are marked by regularly spaced clouds, and may be of great help to the flight of gliders (*Lesieur,* 2008).

Several researchers examined mountain waves and established theories to describe the basic phenomena (*Scorer,* 1949; *Long,* 1953; *Doyle and Durran,* 2002; *Smith,* 2002). One can also find experimental works dealing with the examination of flows around small scale, simplified, two-dimensional isolated obstacles (*Gyüre* and *Jánosi,* 2003). Gravity waves can be a good basis for the validation of atmospheric simulation models, as their structure strongly depends on the state of stratification. Indeed, one can see numerous works dealing with the validation of mesoscale models against mountain waves (*Durran* and *Klemp,* 1983; *Yang,* 1993; *Thunis* and *Clappier,* 2000; *Xue et al.,* 2000), such as the ones caused by a severe downslope windstorm event of Boulder. Similar events can occur in mountainous regions all over the world (*Colle and Mass,* 2000; *Belušič* and *Klai,* 2004). Postevent analysis of severe windstorms are often performed to study the future predictability of such events and also to test model performance and validity. A recent study dealt with the November 19, 2004 windstorm in the High Tatras in Slovakia (*Simon et al.,* 2006). The authors

concluded that an increased 2.5 km resolution mesoscale model can forecast downslope windstorms.

In the following section the main aspects of numerical models used in meteorological codes and in engineering CFD will be compared together with a brief description of the model transformations (for the full description see *Kristóf et al.,* 2009). Simulation results will be shown in the third section in comparison with analytical solutions, water-tank experiments, and full scale downlsope windstorm observations. Conclusions and further investigations are outlined in Section 4.

2. Model overview

In this section a brief overview will be given on the governing equations, numerical methods, and parameterizations applied in numerical weather prediction (NWP) and CFD models in order to show the similarities and differences between the meteorological and engineering assumptions.

2.1. Meteorological outlook

The Navier-Stokes (N-S) equitation describes all types of fluid motion of our interest. It can be seen that today's NWP and CFD models are based on these equations of different forms.

2.1.1. Equations, numerical solution

Modern numerical forecast models are based on a formulation of the dynamical equations, which is essentially the formulation proposed by Richardson (*Lynch,* 2006):

$$\frac{d\mathbf{v}}{dt} = -2\boldsymbol{\Omega}\times\mathbf{v} - \frac{1}{\rho}\nabla p + \mathbf{g} + \mathbf{F_r} \ , \tag{1}$$

where $\mathbf{v}, \boldsymbol{\Omega}, \rho, p, \mathbf{g}$ *and* $\mathbf{F_r}$ are the velocity vector, angular velocity of the Earth, air density, pressure, gravity term, and the frictional force, respectively. The centrifugal force is combined with gravitation in the gravity term $\mathbf{g}$. This form of the N-S equation is basic to most work in dynamic meteorology and solved together with the continuity and thermodynamic equations and the equation of state in NWP-s. After expanding the components of Eq. (1), one arrives to the eastward, northward, and vertical components in spherical coordinate system, respectively (*Holton,* 2004):

$$\frac{du}{dt} - \frac{u\,v\tan\varphi}{a} + \frac{u\,w}{a} = -\frac{1}{\rho}\frac{\partial p}{\partial x} + 2\Omega v\sin\varphi - 2\Omega w\cos\varphi + F_{rx}, \tag{2}$$

$$\frac{dv}{dt} - \frac{u^2\tan\varphi}{a} + \frac{v\,w}{a} = -\frac{1}{\rho}\frac{\partial p}{\partial y} - 2\Omega u\sin\varphi + F_{ry}, \tag{3}$$

$$\frac{dw}{dt} - \frac{u^2 + v^2}{a} = -\frac{1}{\rho}\frac{\partial p}{\partial z} - g + 2\Omega u\cos\varphi + F_{rz}, \tag{4}$$

where u, v, w are the velocity components, a is the curvature of the Earth, φ is the latitude, and F_{ri} are the components of the frictional force. The terms standing with $1/a$ in Eqs. (2) – (4) are so-called curvature terms, and they arise due to the curvature of the Earth and often neglected in midlatitude synoptic scale motions.

The precise form of equations depends on the vertical coordinate system chosen as well, such as pressure coordinates, log pressure coordinates, sigma coordinates, hybrid coordinates, etc. (*Kasahara,* 1974; *Klemp et al.,* 2007; *Saito et al.,* 2007). Furthermore, the variables may be decomposed into mean and perturbation components. Equation systems using perturbation variables reduce the truncation errors in the horizontal pressure gradient calculations, in addition to reducing machine rounding errors in the vertical pressure gradient and buoyancy calculations. For this purpose, new variables are defined as perturbations from a hydrostatically-balanced reference state, and reference state variables are defined to satisfy the governing equations for an atmosphere at rest. (*Skamarock et al.,* 2005) As an example, in the hydrostatic model version of the Fifth-Generation Penn State/NCAR Mesoscale Model (MM5), the state variables are explicitly forecasted while in the non-hydrostatic model version (*Dudhia,* 1993) or in the more advanced Weather Research and Forecasting modeling system (WRF), pressure, temperature, and density are defined in terms of a reference state and perturbation components. When Reynolds averaging is applied, various covariance terms will appear in the system, representing turbulent fluxes. For many boundary layers, the magnitudes of the turbulent flux terms are of the same order as the other terms in Eqs. (2) – (4). In these cases one cannot neglect these fluxes even if it is not of direct interest.

There are tendencies towards higher spatial resolution models, but the resolution of most NWP models is yet too coarse to resolve boundary layer eddies, and parameterizations of them are usually necessary as the complete energy cascade cannot be resolved. (The High Resolution Limited Area models (HIRLAM), or ALADIN operate on horizontal grids in the range of 1–10 km.) Thus a number of turbulent mixing and filtering formulations were developed in the past. Some of these filters are for numerical reasons. For example,

divergence damping filters acoustic modes from the solution. Other filters represent sub-grid processes that cannot be resolved on the given spatial resolution.

2.1.2. Filtering of acoustic modes

The complete equations of motion (Eqs. (2) – (4)) describes all types and scales of atmospheric motion. The elimination of terms on scaling considerations has an important advantage of simplified mathematics and filtering of a range of unwanted type of motions.

These high-frequency acoustic modes would limit the time step during the calculation. To circumvent, different time discretization techniques are developed, see, e.g., the Runge-Kutta time-split scheme in *Wicker* and *Skamarock* (2002) or *Almut* and *Herzog* (2007). The efficiency of the time-split scheme arises from that the large time step Δt is much larger than the acoustic time step $\Delta\tau$, so the most costly calculations are only done in the less-frequent large steps. There are less efficient methods than the leapfrog-based models (e.g. in MM5 or WRF) resulting typically a factor of two greater time step. In the non-hydrostatic model of MM5, a semi-implicit scheme based on *Wilhelmson* and *Klemp* (1978) is used to filter the acoustic waves, while in the hydrostatic model, a split-explicit scheme based on *Madala* (1981) is used to filter gravity waves from the solution. The time differencing in MM5 is extensively discussed in *Grell et al.* (1995). In highly complicated systems, also involving pollution transport and chemical reactions, efficient operator splitting methods are developed recently to reduce computational time. The method is well spread in related fields of applied mathematics (*Geiser,* 2008) and in circulation and pollution models (*Havasi et al.,* 2001; *Faragó,* 2006; *Kocsis et. al,* 2009)

2.1.3. Planetary boundary layer (PBL) and surface-layer schemes, turbulence, closure problem

NWP and air pollution models must contain proper treatment for the PBL since it couples energy, momentum, and mass transfer between the land and atmosphere. The importance of its modeling is increasing nowadays due to environmental requirements, including human health, urban air quality, local and global warming trends, or homeland security problems. The PBL parameterization is especially important for predicting pollutant transport and dispersion (*Lundquist* and *Chan,* 2006).

In order to solve the equations of motion (Eqs. (2)–(4)), closure assumptions must be made to approximate the unknown fluxes as a function of known quantities and parameters (*Holton,* 2004). Turbulent fluxes provide a lower boundary condition for the vertical transport done in the PBL schemes. The PBL schemes determine the flux profiles within the well-mixed boundary layer and the surface layer providing tendencies of temperature, moisture, and

horizontal momentum in the entire column. Thus, when a PBL scheme is activated, explicit vertical diffusion is de-activated assuming that the PBL scheme will handle the process. Most PBL schemes apply dry mixing, but can also include moisture effects in the vertical stability that determines the mixing. The schemes are one-dimensional, since the horizontal large gradients cannot be resolved, and assume a clear scale separation between sub-grid eddies and resolved eddies. This assumption is less clear below a certain grid size, where boundary layer eddies may start to be resolved. In these situations the scheme is replaced by a fully three-dimensional local sub-grid turbulence scheme such as the turbulent kinetic energy (TKE) diffusion scheme (see in the WRF model: *Knievel et al.,* 2007; *Nagy,* 2010). Numerical simulations of PBL have been performed by many authors in the past resulting in different model complexity ranging from very simple zero dimensional parameterization to 3-D high resolution models. In the following sections a brief description will be given on the commonly used closure models.

2.1.3.1. First order closure

Operational NWP, emergency response, and air-quality models usually are of a RANS type (solving Reynolds averaged Navier-Stokes equations), and they employ first- or 1.5-order turbulence closures. The simplest turbulent transport parameterization is the first-order closure based on the K-theory (*Corrsin,* 1975; *Wyngaard* and *Brost,* 1984; *Holtslag* and *Moeng,* 1991; *Stull,* 1993). It is robust and requires low computational resources but gives poor approximation in the boundary layer, where the scale of typical turbulent eddies is strongly dependent on the distance to the surface and static stability. In many cases the most intense eddies have scales comparable to the boundary layer depth, and there the momentum and heat fluxes are not proportional to the local gradient of the mean. In much of the mixed layer, heat fluxes are positive even with neutral conditions.

To improve the model behavior, alternative approaches have been developed. An example is the modified first-order closure (*Townsend,* 1980; *Troen* and *Mahrt,* 1986; *Hong* and *Pan,* 1996). This scheme employs a counter-gradient flux for heat and moisture in unstable situations. It uses enhanced vertical flux coefficients in the PBL, and the PBL height is determined from a critical bulk Richardson number (Ri). It handles vertical diffusion with an implicit local scheme, and it is based on local Ri in the free atmosphere (Ri_{free}).

In spite of its drawbacks, the first-order closure based models remain the most popular parameterization for stable conditions, although alternative approaches have been used for the daytime convective period, e.g., the Blackadar (BK) non-local mixing scheme (*Blackadar,* 1976; *Zhang* and *Anthes,* 1982) and non-local K-theory (*Hong* and *Pan,* 1996). The BK scheme is a first-order hybrid local and nonlocal scheme in which eddy diffusivity, a function of

the local Ri number, is applied to the stable and forced convective regimes, while nonlocal mixing is used for free convective cases. The BK scheme's closure is based on an expression for the mass that is exchanged between individual layers in the boundary layer.

Recent improvements of first order schemes include the Yonsei University model (YSU, *Hong et al.,* 2006) or the asymmetrical convective models ACM1 (*Pleim* and *Chang,* 1992) and ACM2 (*Pleim,* 2007). YSU is based on the K profile for the convective cases as a function of local wind shear and local Ri_{free}. It also considers non-local mixing by adding a non-local gradient adjustment term to the vertical diffusion equation. Moreover, it contains additional terms to describe entrainment at the top of PBL proportional to the surface flux. For stable cases, the original mixing coefficient (*Hong et al.,* 2006) is replaced by an enhanced diffusion based on the bulk Ri number between the surface and top layers (*Hong,* 2010). The ACM1 and ACM2 models are modifications of the BK scheme. In ACM1 the symmetrical downward transport of BK scheme is replaced by an asymmetrical layer-by-layer model. In order to produce more realistic vertical profiles, the ACM2 model, a combination of local and non-local closures, was introduced (*Pleim,* 2007), that adds an eddy diffusion component to the non-local transport. With this addition the ACM2 scheme can better represent the shape of the vertical profiles in the near surface region. Both ACM1 and ACM2 models are available in the MM5 and WRF solvers.

2.1.3.2. Higher order closures

Given the known drawbacks of these simpler models, new approaches are developed with increasing complexity of turbulence description. The Gayno–Seaman (GS) scheme is a 1.5-order local closure scheme that computes eddy diffusivities based on local vertical wind shear, stability, turbulent kinetic energy (TKE) predicted by a prognostic equation (*Shafran et al.,* 2000), and length scale. The Eta PBL scheme, also known as the Mellor-Yamada-Janjic (MYJ) scheme (*Janjic,* 1990; *Mellor* and *Yamada,* 1982, *Janjic,* 1996, 2002), is a level-1.5 local closure scheme that computes vertical eddy diffusivities based on TKE predicted by a prognostic equation as a function of local vertical wind shear, stability, and turbulence length scale. The effects of the viscous sub-layer are taken into account through variable roughness length for temperature and humidity (*Zilitinkevich,* 1995). Other more sophisticated schemes are based on ensemble-averaged turbulence models (*Xue et al.,* 1996) with varying orders of closure (e.g., *Mellor* and *Yamada,* 1974; *Wyngaard et al.,* 1974; *Andre et al.,* 1978). These schemes often perform remarkably well under horizontally homogeneous conditions in modeling the horizontally (ensemble) averaged profiles of quasi-conservative quantities. However, the 3-D structures of the boundary layer is not predicted well. They are more complicated, and require solving equations of higher order moments, limiting their practical application

(*Lee et al.,* 2006). Several researcher proposed modifications to the original MY model improving the master length scale equation (*Sušelj and Sood,* 2010) or the pressure-strain, pressure –temperature covariance closures (*Nakanishi* and *Niino,* 2009)

Other researchers, however, showed that there is little gain in accuracy with increasing scheme complexity using different turbulence parameterizations. Increasing the complexity of the turbulence parameterization not just increased the computational resources but did not show obvious improvement, sometimes producing equally poor, if not worse, predictions (*Zhong et al.,* 2007) of the simulated mean and turbulent properties in the boundary layer, even around complex regions (*Berg et al.,* 2005).

Traditional PBL schemes were adequate for flat, horizontally homogeneous surfaces under steady-state conditions with different stratification. They cannot cope, however, with increased-resolution models that require more detailed and accurate representations of physical processes (*Baklanov et al.,* 2011). Therefore, different approaches are developed where the calculation of eddies was done explicitly in the PBL using 3-D high resolution models. Since only a small portion of the turbulence is handled by the subgrid scale (SGS) scheme, the results are less sensitive to turbulence closure assumptions. The first LES models and work in this area was pioneered by *Deardorff* (1974a,b). For PBL applications, LES models typically require horizontal resolutions on the order of 100 m (see, e.g., ARPS, MESO-NH codes), and they are typically used for research applications (e.g., *Weigel et al.,* 2007). *Deardorff* (1980) designed a simplified 1.5-order closure scheme that requires the solution of only one additional prognostic equation for the SGS turbulent kinetic energy, where the eddy coefficient was assumed to be proportional to the square root of TKE. This scheme has been widely used by researchers (*Klemp* and *Wilhelmson,* 1978) to handle SGS turbulence in cloud-scale models. Such models have a horizontal resolution in the order of 1 km, and they are expected to resolve cloud structures and limited turbulent eddies.

2.2. Engineering outlook

CFD tools have been in use for decades with success for solving engineering related problems involving broad range of physics. Spatial scales are extended to urban scales to handle flows involving pollution dispersion and can be even extended to mesoscale problems by the presented transformation method. Therefore, it is interesting to show the main aspects and some of the current problems of CFD solvers in this field.

2.2.1. Governing equations, simulation of turbulent flows

In engineering CFD, continuity, momentum, and energy equations are usually solved based on the finite volume method in an unsteady conservative form.

Because of numerous advantages of the finite volume method, it is widely spread among commercial and open source fluid mechanical solvers. Although the instantaneous Navier–Stokes equations exactly define all fluid flow, it is essentially impossible to solve these equations for turbulent flows over domains of significant spatial scale. Therefore, the exact equations are often Reynolds averaged to create a set of equations that can be solved for the spatial scales of engineering interest. The current adaptation method was developed for the commercial fluid mechanical solver ANSYS-FLUENT, but it can be implemented in other solvers as well, having user defined function (UDF) capabilities such as the commercial codes ANSYS-CFX and StarCD or the open source solver Openfoam. Through UDF-s, the user can modify the governing equations of the CFD code by adding appropriate source/sink terms to the equations.

The governing equations (Eqs. (5)–(7)) are solved by using the Boussinesq approximation (Eq. (10)) for the density.

$$\nabla \cdot \tilde{\mathbf{v}} = 0\,, \tag{5}$$

$$\frac{\partial}{\partial t}\left(\rho_0 \tilde{\mathbf{v}}\right) + \nabla \cdot \left(\rho_0\, \tilde{\mathbf{v}} \otimes \tilde{\mathbf{v}}\right) = -\nabla \tilde{p} + \nabla \cdot \boldsymbol{\tau} + \left(\tilde{\rho} - \rho_0\right)\mathbf{g} + \mathbf{F} \tag{6}$$

$$\frac{\partial}{\partial t}\left(\rho_0 c_p \tilde{T}\right) + \nabla \cdot \left(\tilde{\mathbf{v}}\ \rho_0\ c_p \tilde{T}\right) = \nabla \cdot \left(K_t \nabla \tilde{T}\right) + S_T\,, \tag{7}$$

$$\frac{\partial}{\partial t}\left(\rho_0\ k\right) + \nabla \cdot \left(\rho_0\ \tilde{\mathbf{v}}\ k\right) = \nabla \cdot \left(\frac{\mu_t}{\sigma_k} \nabla k\right) + G_k + G_b - \rho_0\ \varepsilon + S_k\,, \tag{8}$$

$$\frac{\partial}{\partial t}\left(\rho_0\ \varepsilon\right) + \nabla \cdot \left(\rho_0\ \tilde{\mathbf{v}}\ \varepsilon\right) =$$

$$= \nabla \cdot \left(\frac{\mu_t}{\sigma_\varepsilon} \nabla \varepsilon\right) + \rho_0\ C_1\ S\ \varepsilon - \rho_0\ C_{2\varepsilon} \frac{\varepsilon^2}{k + \sqrt{\nu\ \varepsilon}} + C_{1\varepsilon} \frac{\varepsilon}{k} C_{3\varepsilon} G_b + S_\varepsilon\,, \tag{9}$$

$$\tilde{\rho} = \rho_0 - \rho_0\ \beta\left(\tilde{T} - T_0\right). \tag{10}$$

In the equation system $\tilde{\mathbf{v}}, \tilde{p}, \tilde{\rho}, \tilde{T}$ are the transformed field variables of velocity, pressure, density, and temperature. c_p and β are the specific heat capacity of dry air at constant pressure and the thermal expansion coefficient.

From the velocity vector ($\bar{\mathbf{v}} = u\,\mathbf{i} + v\,\mathbf{j} + \bar{w}\,\mathbf{k}$) only the vertical component was affected by the transformation. $\boldsymbol{\tau}$ contains the viscous and turbulent stresses, $\mathbf{g} = -g\,\mathbf{k}$ is the gravitational force per unit mass, and g = 9.81[N kg^{-1}]. In the presented system the turbulent transport is modeled by the realizable k–ε turbulence model with full buoyancy effects (Eqs. (8) – (9)) developed by *Shih et al.* (1995). σ_k and σ_ε are the turbulent Prandtl numbers for k and ε, respectively. The turbulent viscosity μ_t and the turbulent heat conduction coefficient K_t are evaluated on the basis of turbulence kinetic energy (k) and dissipation rate (ε) fields (*Launder* and *Spalding,* 1972). The constant values of $C_{1\varepsilon}$, $C_{2\varepsilon}$, the expressions of C_1 and $C_{3\varepsilon}$, the turbulence production and buoyancy terms G_k and G_b, modulus of mean rate-of-strain tensor S can be referred either from CFD literature (*Shih et al.*, 1995) or from software documentation (*ANSYS Inc.,* 2012) of the applied simulation system. ρ_0 and T_0 are reference (sea level) values of density and temperature.

Volume sources S_T, S_k, and S_ε in Eqs. (7)–(9), as well as vector $\mathbf{F} = S_u\,\mathbf{i} + S_v\,\mathbf{j} + S_w\,\mathbf{k}$ in Eq. (6), are functions of local values of field (prognostic) variables, and used for adjusting the model to handle mesoscale effects. The components of the Coriolis force are included in **F** through S_u, S_v, and S_w.

Reynolds averaging introduces other unknowns into the equation system, the so-called Reynolds stresses. Since there is no existing general formula for the description of these stresses, large number of engineering turbulence models were developed applicable to certain flow features, but there are no turbulence models that would be generally applicable to all kind of turbulent flows. The modeling of these virtual stresses is still a major part of the today's turbulence modeling science. Different versions of two equation models are used in CFD for turbulence modeling. The most popular are versions of the k–ε model or other two equation models. These versions are denoted as linear eddy viscosity models, which adopt the Boussinesq approximation, implying an isotropic eddy viscosity. There were attempts using two equation models in NWP codes. An example is the implementation of a version of the k–ε model by *Hanjalic* and *Launder* (1972) in the MESO-NH meteorological code. It was not used extensively since, according to the authors, the current version did not give satisfactory results. The disadvantage of these eddy viscosity models is that they give an unrealistic representation of the normal turbulent stresses. This representation of the turbulent stresses produces fairly good results as long as only one of the turbulent stresses is dominant in the momentum equations. Further downside is that in more complicated flows, where more than one of the normal stresses is important, the ability of a turbulence model to predict normal stress anisotropy becomes significant. This motivates the development and application of nonlinear k–ε models (*Gatski* and *Jongen,* 2000) and other more advanced models, such as LES or hybrid RANS-LES models.

2.2.2. Stratification and turbulence models

One can find several works on the application of turbulence models in neutral conditions (*Richards and Hoxey,* 1993; *Blocken et al.,* 2007; *Hargreaves* and *Wright,* 2007). Stable stratification, however, causes drainage flows over uneven topography, intermittent turbulence, low-level jets, gravity waves, flow blocking, intrusions, and meandering, thus posing challenges in modeling of stable stratification (*Lee et al.,* 2006).

Several problems can be identified regarding the maintenance of turbulence profiles with distance (*Huser et al.,* 1997) dissipating turbulence early downstream of the obstacle (*Hanna et al.,* 2006). Treatment of these inconsistencies is the modification of the model constants of existing models (*Duynkerke,* 1988), adding source terms to the turbulent dissipation rate (TDR) equation for ε or a non-constant formulation for the $C_{1\varepsilon}$ parameter (*Freedman and Jacobson,* 2003; *Pontiggia et al.,* 2009). *Vendel et al.* (2010) proposed an inlet pressure profile and flux condition for the ground in order to define an appropriate downwind boundary condition for the stable or unstable cases.

Although CFD models are currently slow to be used for real-time emergency response, they can be used for planning purposes and to guide parameterizations of real-time wind flow models. A good example of a dispersion model that is parameterized based on the CFD results is the Quick Urban and Industrial Complex dispersion modeling system (*Williams et al.,* 2004). As computing power has become more affordable, CFD has become an increasingly valuable tool for studying urban flow. These models explicitly account for building geometry and require minimal parameterizations (*Balczó et al.,* 2011; *Balogh* and *Kristóf,* 2010). With the current model transformation, one can take into account mesoscale effects in the same numerical model with finely resolved topography.

2.2.3. System of transformations

The proper representation of Coriolis force, compressibility, and stratification effects is achieved by a system of transformations. These adjust the governing equations solved by the CFD solver through user defined volume source or sink terms. The CFD solver operates with transformed field variables (Eqs. (5)–(10)). Relations between untransformed physical quantities (T, p, ρ, z, w) and transformed ones $(\widetilde{T}, \widetilde{p}, \widetilde{\rho}, \widetilde{z}, \widetilde{w})$ are defined by Eqs. (11)–(15).

$$T = \widetilde{T} - T_0 + \overline{T}, \tag{11}$$

$$p = \frac{\overline{\rho}}{\rho_0}\,\widetilde{p} + \overline{p} = Ce^{-\zeta\, z}\,\widetilde{p} + \overline{p}, \tag{12}$$

$$\rho = \tilde{\rho} - \rho_0 + \bar{\rho}, \tag{13}$$

$$z = -\frac{1}{\zeta} \ln\left(e^{-\zeta z_{ref}} - \frac{\zeta}{C}\left(\tilde{z} - \tilde{z}_{ref}\right)\right), \tag{14}$$

$$w = \frac{\rho_0}{\bar{\rho}} \tilde{w} = \tilde{w} C^{-1} e^{\zeta z}, \tag{15}$$

where ζ is the density parameter described by Eq. (18) and z_{ref} is a reference altitude (Eq. (20)). Zero subscipt denotes values at ground level. The vertical extent of the atmosphere is "compressed" below a well-defined bound (C/ζ) described by Eq. (14), thus $\tilde{z} \to C/\zeta$, when $z \to \infty$, where C, described by Eq. (19), acts as a switch between the description of stratosphere and troposphere. The model utilizes an (x, y, z) Cartesian coordinate system. The Jacobian of the transformation of coordinate z can be calculated according to Eq. (16). $J \to 1$ when $\tilde{z} \to 0$, and therefore the geometrical transformation has a negligible effect close to ground.

$$J = \frac{dz}{d\tilde{z}} = C^{-1} \exp(\zeta z). \tag{16}$$

In this zone, the original form of the Cartesian equations existing in the CFD solver gives a good enough description for the flow close to the surface.

2.2.4. Reference profiles

The relationship between the absolute physical quantities and the field variables in the CFD solver are based on the reference profiles (distinguished by over-bars) Eqs. (21)–(29). It can be optimized to have the least possible deviation from the hydrostatic equilibrium and can simplify the specification of the initial conditions. These terms depend only on the vertical coordinate using approximation of the polytrophic atmosphere, as according to Eqs. (21)–(29). The original transformation expressions (*Kristóf et al.,* 2009) that were valid below an altitude of 11 km have been extended to incorporate the tropopause and the lower stratosphere up to an altitude of 25 km. For simplicity, the following double valued constants are introduced to describe these layers:

$$\gamma = \begin{Bmatrix} \gamma_t \text{ , when } z < z_{tp} \\ 0 \text{ , when } z \geq z_{tp} \end{Bmatrix}, \tag{17}$$

$$\zeta = \begin{Bmatrix} \zeta_t \text{ , when } z < z_{tp} \\ \zeta_s \text{ , when } z \geq z_{tp} \end{Bmatrix}, \tag{18}$$

$$C = \begin{Bmatrix} 1 \text{ , when } z < z_{tp} \\ e^{(\zeta_s - \zeta_t) z_{tp}} \text{ , when } z \geq z_{tp} \end{Bmatrix}, \tag{19}$$

where subscripts t and s denote values for the troposphere and stratosphere, and z_{tp} is the tropopause altitude. In the stratospheric region we use z_{tp} as a reference altitude, therefore:

$$z_{ref} = \begin{Bmatrix} 0 \text{ , when } z < z_{tp} \\ z_{tp} \text{ , when } z \geq z_{tp} \end{Bmatrix}. \tag{20}$$

Using the above notations, the reference profiles for the troposphere will read as:

$$\overline{T_t} = T_0 - \gamma_t \, z, \tag{21}$$

$$\overline{p_t} = p_0 \left(\frac{T_0 - \gamma_t \, z}{T_0} \right)^{\frac{g}{R \, \gamma_t}}, \tag{22}$$

$$\overline{\rho_t} = \rho_0 \, e^{-\zeta_t \, z}, \tag{23}$$

$$\zeta_t = -\left(\frac{g - R\gamma_t}{z \, R \, \gamma_t} \right) \ln\left(1 - \frac{\gamma_t \, z}{T_0} \right). \tag{24}$$

The reference profiles in the stratospheric region are based on an isothermal temperature profile, therefore:

$$\overline{T_s} = T_{tp}\,, \tag{25}$$

$$\overline{p_s} = p_{tp}\, e^{-\zeta_s\left(z - z_{tp}\right)}, \tag{26}$$

$$\overline{\rho_s} = \rho_{tp}\, e^{-\zeta_s\left(z - z_{tp}\right)}, \tag{27}$$

$$\zeta_s = \frac{g}{RT_{tp}}. \tag{28}$$

By using the above notations, the universal density profile reads:

$$\overline{\rho} = \rho_0 C\, e^{-\zeta\, z}\,. \tag{29}$$

The constant values in Eqs. (21)–(29) can be optimized for a given case, but the standard ICAO (*Manual of the ICAO Standard Atmosphere,* Doc 7488, 1993) temperature and pressure profiles, based on the following constants, have been found to be suitable references for simple applications: $\gamma_t = 0.0065\ ^{\circ}\mathrm{C\ m^{-1}}$, $T_0 = 15\ ^{\circ}\mathrm{C}$, $p_0 = 1.01325 \cdot 10^5$ Pa, $\rho_0 = 1.225\ \mathrm{kg\ m^{-3}}$, $R = 287.05\ \mathrm{J\ kg^{-1}\ K^{-1}}$, $\zeta_t = 10^{-4}\ .\ \mathrm{m^{-1}}$

2.2.5. Volume sources

The volume sources (Eqs. (30)–(35)) have been calculated according to Eqs. (20)–(25) by utilizing the UDF capability of the system.

$$S_u = \rho_0 fv - \rho_0 \ell\, \widetilde{w} J\,, \tag{30}$$

$$S_v = -\rho_0 fu\,, \tag{31}$$

$$S_w = \rho_0\left(J^2 - 1\right)\left(\ell\, u\, J^{-1} + \beta\left(\widetilde{T} - T_0\right)g\right) + \rho_0\, \ell\, u\, J^{-1} + \zeta\, J\left(\widetilde{p} - \rho_0 \widetilde{w}^2\right), \tag{32}$$

$$S_T = -\rho_0\, c_p\, \widetilde{w}(\Gamma - \gamma)\, J\,, \tag{33}$$

$$S_k = -\beta\, g\, \frac{\mu_t}{\mathrm{Pr}_t}(\Gamma - \gamma), \tag{34}$$

$$S_\varepsilon = -C_{1\varepsilon}\, C_{3\varepsilon} \frac{\varepsilon}{k} \beta\, g \frac{\mu_t}{\mathrm{Pr}_t} (\Gamma - \gamma) \,. \tag{35}$$

In the above expressions, μ_t and Pr_t are the turbulent viscosity and turbulent Prandtl number, $f = 2\,\Omega \sin\varphi$ and $1 = 2\Omega\cos\varphi$ are the Coriolis parameters, φ is the average latitude, and Ω is the angular velocity of Earth. Moisture transport is not taken into account in the mathematical model, therefore the dry adiabatic temperature gradient Γ, appearing in Eqs. (19)–(21), is calculated according to the assumption of a dry adiabatic process: $\Gamma = g/c_p = 0.00976\ ^{\circ}\mathrm{C\ m^{-1}}$.

2.2.6. A simplified model version for water-tank experiments

Validation against small scale water tank experiments requires the adjustment of the transformation expressions. The working medium is liquid and the vertical extent of the device is small, therefore the atmospheric pressure variation with the vertical coordinate is negligible. Compressibility is not taken into account consequently ($\Gamma = 0, z = \tilde{z}$, and $\zeta_t = 0$). The vertical reference profiles for pressure and density are $\overline{\rho_t} = \rho_0, \overline{p_t} = p_0$. Due to the very weak turbulence characterizing these experiments, a laminar approach or LES method should be used instead of the k–ε model. The Coriolis force usually has a negligible effect in such experiments, and therefore, $\Omega = 0$ can be assumed.

These assumptions will simplify the source term acting on the energy equation:

$$S_{T,\,incomp.} = \rho_0\, c_p\, \tilde{w}\, \gamma \,. \tag{36}$$

The values of $\gamma = -dT/dz$, c_p, β, and T_0 for water-tank simulations can be calculated according to the temperature or density gradient of the fluid, maintaining the same Brunt-Väisälä frequency and material properties of the experiment.

2.2.7. Nesting

In NWP models the simplest method is the "one-way" downward nesting, where the outer model provides 4D boundary conditions to the inner higher resolution domain. In some cases it can be provided, if the mesoscale model horizontal resolution is as fine as a few hundred meters. The one-way nesting technique, in the Advanced Regional Prediction System (ARPS), allows adjustments in vertical resolution between grids, which is important for LES mode, where the

grid aspect ratio should be kept close to unity. In more advanced "two-way" nesting, the nested finer domain and the outer coarser domain interact at every time step of the outer coarse grid and, the microscale model provides lower boundary-condition to the outer domain. "With current computer capacities, this can be done within small parts of the mesoscale domain, which creates inconsistencies with the remaining parts of that domain." (*Baklanov et al.,* 2011) The current implementation of two-way nesting schemes in WRF or MM5 does not allow higher vertical resolution in the inner nesting levels, because the number of vertical levels must be the same for all levels (*Michioka* and *Chow,* 2008). Another problem that also exists in the CFD field is the velocity and length scale changes across the boundaries of nesting levels. This is especially important when the complex high resolution topography generates nonlinear motions close to these boundaries. One may also expect the damping of low frequency motions passing through the boundary and as a consequence providing an improper upstream turbulence field for the inner microscale model.

The advantage of the CFD approach is that it allows arbitrary mesh refinements in the simulation domain, resulting a continuous change of field variables around the finely resolved region. The possibility of nesting also exists in the CFD solver allowing different mesh resolution either horizontally or vertically on both sides of the domain interface, but one can avoid it with the existing mesh refinement options (*ANSYS Inc.,* 2012). In the following case studies, structured quad meshes can be used (without additional interfaces) due to the simplicity of the underlying geometries.

3. Results and discussion

The application of the model transformation will be presented in this section. Results will be compared against the analytical solution of linear, hydrostatic mountain wave field. Nonlinear and non-hydrostatic simulation cases are then compared to small scale water-tank experiments, and finally, a full scale nonlinear and non-hydrostatic downslope windstorm case will be shown against an inter-comparison study of NWP models and field measurements.

3.1. Verification with analytic solution

The simulations were compared with the analytic solution of a linear hydrostatic wave field. A Witch of Agnesi curve was used for the relief geometry,

$$z(x) = h \frac{a}{x^2 + a^2}, \tag{37}$$

where h and a are the obstacle height and half width, respectively. This geometry has been used extensively in the literature (*Wurtele et al.,* 1996), as an analytic solution can be derived for this shape. In order to obtain comparable results with water-tank experiments, the following material properties and working conditions were used:

$\rho_0 = 998\ \mathrm{kgm^{-3}}$, $T_0 = 27\ ^{\circ}\mathrm{C}$, $\beta = 0.000207\ \mathrm{K^{-1}}$, $-\gamma = 832\ \mathrm{K\ m^{-1}}$, $\mathrm{U} = 0.25\ \mathrm{ms^{-1}}$.

The Reynolds number, based on the inlet flow speed (U) and the obstacle height (h), was about 2500; therefore a laminar model was used. Compressibility and the Coriolis force were not taken into account. Free-slip wall and symmetry boundary conditions were applied at the lower and upper boundaries. A constant velocity and static pressure profile were prescribed as inlet and outlet conditions. The model was initialized with constant $\tilde{T} = T_0$, $\tilde{p} = p_0$, and uniform horizontal velocity $\tilde{U} = U_0$.

Based on the linear wave theory (Eq. (38)), an analytic solution can be found for hydrostatic problems with a constant Scorer parameter (l). The Scorer parameter is usually a function of the vertical coordinate, and it is derived from the wave equation for atmospheric gravity waves with an assumption of a two-dimensional, non-viscous, adiabatic flow (*Smith,* 1979; *Durran,* 1990). This parameter is most often used to forecast the existence of trapped lee waves, which can be expected when l decreases strongly with height. This is especially true if l decreases suddenly in the mid-troposphere due to the presence of a stable layer dividing the troposphere into a highly and a weekly stable layer. The square root of the parameter l (Eq. (40)) has units of wave number. The wave number of the lee wave (l) lies between l_{upper} of the upper layer and l_{lower} of the lower layer. Wide mountain ranges generate vertically propagating waves of wave numbers less than l_{upper}. Small obstacles, that force wave numbers greater than l_{lower}, produce waves that will vanish with height.

For hydrostatic problems, the development of the full analytic solution has been summarized by several researchers (*Alaka,* 1960; *Smith,* 1979). The combined governing equations were resulted in the deep Boussinesq equation (Eq. (38)) for w. The Scorer parameter l is defined by Eq. (38) and Eq. (39):

$$\frac{\partial^2\left(\sqrt{\frac{\rho_0(z)}{\rho_0(z=0)}}w\right)}{\partial x^2}+\frac{\partial^2\left(\sqrt{\frac{\rho_0(z)}{\rho_0(z=0)}}w\right)}{\partial z^2}-l^2(z)\left(\sqrt{\frac{\rho_0(z)}{\rho_0(z=0)}}w\right)=0, \quad (38)$$

$$l^2(z)=\frac{N^2}{U^2}-\frac{1}{U}\frac{d^2U}{dz^2}-\frac{1}{U}\frac{d\ln\rho}{dz}\frac{dU}{dz}-\frac{1}{4}\left(\frac{d\ln\rho}{dz}\right)^2-\frac{1}{2}\left(\frac{d^2\ln\rho}{dz^2}\right), \quad (39)$$

where w is the perturbation vertical velocity, $N = \sqrt{-\frac{g}{\rho_0}\frac{\partial \rho(z)}{\partial z}}$ is the Brunt-Väisälä frequency, U is the inlet flow speed, ρ is the fluid density, and z is the vertical coordinate, respectively. For incompressible flow only the first two terms remain.

$$l^2(z) = \frac{N^2}{U^2} - \frac{1}{U}\frac{d^2U}{dz^2}. \tag{40}$$

The first term on the right-hand side dominates in our case, and additionally, if a uniform velocity profile ($U = U_0$) and Brunt-Väisälä frequency (N) are used, Eq. (40) simplifies to:

$$l = \frac{N}{U}. \tag{41}$$

With the help of the Scorer formula, flows can be categorized on the basis of the following two dimensionless quantities:

$$F_x = a\,l, \quad F_z = h\,l. \tag{42}$$

When $F_x >> 1$, the flow is essentially hydrostatic, while non-hydrostatic effects become important when $F_x \sim 1$ (*Schumann et al.,* 1987). Regarding the linearity, when $F_z << 1$, the flow is linear and nonlinear effects dominate, when the value approaches to $F_z \sim 1$. The borders are, however, not well-defined, and that is why one can find test cases marked as moderately hydrostatic or moderately nonlinear (*Thunis* and *Clappier,* 2000). Calculating these parameters using $a = 2$ m and $h = 0.01$ m, one can find that our setup is linear and hydrostatic with $l = 5.32\ \mathrm{m}^{-1}$, $F_x = 10.64$, and $F_z = 0.0532$. In the case of hydrostatic flow, an analytic solution exists (Eq. (43)) for the vertical velocity field w(x, z), based on Eq. (38):

$$w(x,z) = \sqrt{\frac{\rho_0(z=0)}{\rho_0(z)}}\,U\,h\,a\,\frac{(x^2 - a^2)\sin(l\cdot z) - 2\,x\,a\,\cos(l\cdot z)}{(a^2 + x^2)^2}. \tag{43}$$

The vertical velocity contours have been plotted against the corresponding analytic solution on *Fig. 1*. The agreement between the two solutions is very good, with the magnitude of the vertical velocity in the numerical solution being only slightly smaller. The locations of velocity maxima, in the case of the CFD results, are shifted only moderately downward in the vertical direction.

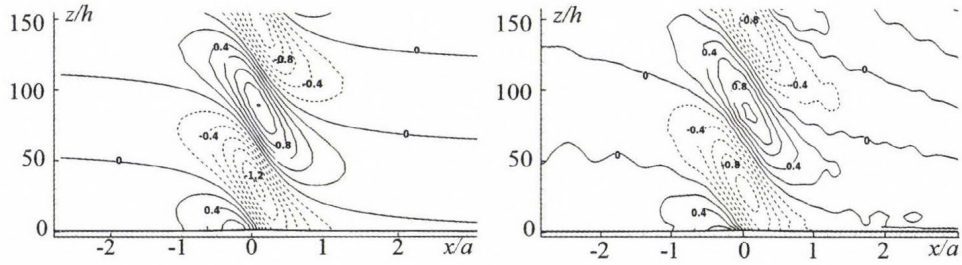

Fig. 1. Contour plots of the vertical velocity (w [mm s^{-1}]), obtained from the analytic solution based on Eq. (43) (left) and from CFD calculations (right). The solution is obtained for $U = 0.25$ m s^{-1}, $l = 5.32$ m^{-1}, $N = 1.3$ s^{-1}, $a = 2$ m, $h = 0.01$ m. The vertical and horizontal scales are normalized by the mountain height (h) and half width (a) respectively. Dashed lines represent negative values.

In the next section, a set of test cases have been prepared and the results are compared against experiments that cover a hydrostatic and nonlinear parameter range. The statistical performance measures applied for the comparison are also described briefly.

3.2. Statistical performance measures used during the evaluation

To quantitatively evaluate the output of the model with observations, *Hanna et al.* (1991, 1993) recommend the use of the following statistical performance measures (*Chang et al.,* 2005): the fractional bias (FB), the normalized mean-square error (NMSE), the fraction of predictions within a factor of 2 of observations (FAC2), and the hit rate (HR). *Chang* and *Hanna* (2004) suggest that a good model would be expected to have about 50% of the predictions within a factor of 2 of the observations (i.e., FAC2 > 0.5), a relative mean bias within 30% of the mean (i.e., –0.3 < FB < 0.3), a relative scatter of about a factor of 2 or 3 of the mean (i.e., NMSE < 4), and a hit rate above 66% (HR > 0.66) with an allowed deviation of D = 0.25. The absolute value of the model's fractional bias (FB) is reasonably good if it is less than 0.25. A tendency toward overprediction of wind speeds is seen, with the fractional bias regularly between 0 and –0.25 (*Lundquist* and *Chan,* 2006). The perfect model would have the following idealized performances: FAC2 = HR = 1 and FB = NMSE = 0. In air quality modeling, typical values of the above statistical

measures have been defined as acceptable for model evaluation and also correspond to a model acceptance criterion (*Chang* and *Hanna,* 2004).

3.3. Numerical model results compared to small scale water-tank experiments

Among the experiments focused on topography-induced gravity waves, one can find investigations dealing with symmetric and asymmetric obstacles, looking at the effect of asymmetry (*Gyüre* and *Jánosi,* 2003), determining surface drag by numerical simulations (*Klemp* and *Lilly,* 1975) and numerically examining the wave breaking characteristics (*Doyle et al.,* 2000; *Afanasyev* and *Peltier,* 2001). The common feature of the former experiments is the experimental apparatus. They use mainly the water as working medium, since in water it is relatively easy to generate and maintain stable stratification for a longer period of time. Usually, this is done by using layered salt water. The achievable range of Reynolds number is limited to approximately 10^3. In spite of this fact, these methods are widely used, since there is more control on the parameters and conditions, than in real atmosphere.

Two-dimensional simulations of internal gravity waves have been carried out by using symmetric and asymmetric obstacles, in correspondence with the experiments performed by *Gyüre* and *Jánosi* (2003). Obstacle shapes have been characterized by the following function:

$$z(x) = a \exp\left(-b \mid x \mid 2k\right) \tag{44}$$

where a, b, and k are shape parameters and x is the horizontal coordinate of the obstacle. Both the symmetric and asymmetric shapes can be described by Eq. (44), by prescribing different parameters for the upstream and downstream part of the mountain barrier. Measurements were performed in a narrow plexi glass tank of 2.4 m × 0.087 m × 0.4 m filled with linearly stratified salt water, by towing the obstacles along the bottom of the tank at a constant speed. The range of the experimental parameters (obstacle height h=0.02–0.04 m, towing velocity U=0.01–0.15 m s^{-1}, and Brunt-Väisälä frequency N=1.09–1.55 s^{-1}) corresponds to an atmospheric flow up to an elevation of 5–10 km for an obstacle height of 600 m and a wind speed of 10–70 m s^{-1} for a large range of hydrostatic state and linearity.

The flow was considered unsteady, incompressible, and two-dimensional in the simulation. Due to the low Reynolds number range, a laminar model was used. The domain was discretized with a structured quad grid, using 150 x 800 quad elements (*Fig. 2*). Second order time discretization, pressure staggering option (PRESTO) for pressure interpolation (*ANSYS Inc.,* 2012), and second order upwinding methods were used when solving the momentum and energy equations. Compressibility was turned off in this case by using the transformation described in Section 2.2.6.

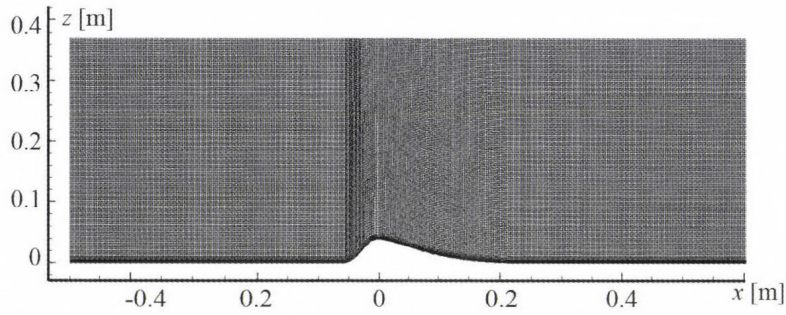

Fig. 2. Computational domain and numerical grid in the case of a gentle leeward side obstacle.

Typically for higher flow velocities, we observed flow separation during the simulation of symmetric steep lee-side obstacles. The separation induced bubble modified the shape of the leeward side in this case, quasi elongating the obstacle (*Fig. 3*), consequently changing the hydrodynamic characteristics of the barrier. Therefore, these cases were excluded from the comparison.

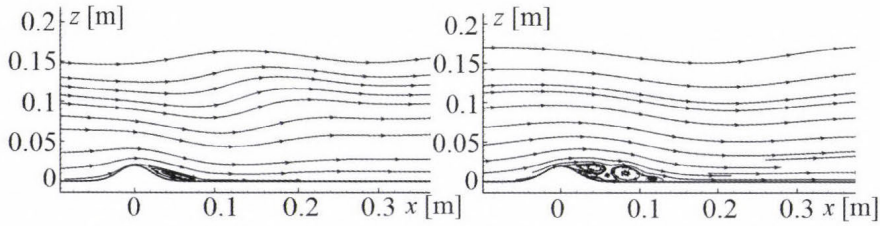

Fig. 3. Computed streamlines of the velocity field for $U/Nh = 0.7$ (left) and $U/Nh = 1$ (right) showing the elongation of the separation bubble and of the wave lengths for a symmetric obstacle.

In the numerical model, flow enters into the domain with a uniform inlet velocity profile. A moving bottom wall, for simulating the stationary bottom wall of the experiment was used. No visible disturbances were observed on the water surface, consequently a rigid lid (symmetry) with free slip boundary condition was applied in the simulation model. Avoiding the interaction between upward propagating and reflected wave fronts, data extraction was made after a short transient period, before interference could occur. This period was estimated from the vertical group velocity (*Gyüre* and *Jánosi,* 2003), which was proportional to the towing speed. In those cases where steepening and wave breaking occurred, samples were excluded from the averaging of amplitudes and wavelengths.

In *Table 1*, the simulations were categorized into four groups based on $F_x = Na/U$ and $F_z = Nh/U$ non-dimensional numbers as described by Eq. (42). These groups are nonlinear (NL), moderately nonlinear (M–NL), hydrostatic (H), and moderately non-hydrostatic (M–NH) cases. For all cases, the mountain height h, was 0.04 m, the leeward half width a, was 0.13 m, the Brunt-Väisälä frequency N, was 1.33 s^{-1} and U was the incoming flow velocity corresponding to the towing velocities of the obstacle in the survey.

Table 1. List of cases and parameters for the simulation of the gentle leeward side obstacle. Vertical structure and linearity categories are: H – hydrostatic, M-NH – moderately non-hydrostatic, NL – nonlinear, M–NL – moderately nonlinear

Case No.	U (m s^{-1})	Na/U	Nh/U	Vertical structure	Linearity
1	0.016	10.80	3.33	H	NL
2	0.032	5.31	1.64		
3	0.037	4.63	1.43		
4	0.041	4.15	1.28		
5	0.048	3.60	1.11		
6	0.053	3.24	1.00		
7	0.077	2.23	0.69	M–NH	M–NL
8	0.106	1.62	0.50		
9	0.160	1.08	0.33		

Wavelengths and amplitudes were measured in multiple positions above and downstream of the obstacle, by locating the wave fronts and measuring the distance between the fronts. The error bars in *Fig. 4* show the standard deviation of both the measured and simulated values. Circular wave fronts assumed in the case when lee waves are generated by a moving point source (*Voisin,* 1994). As shown from the upper part of *Fig. 5*, the shape of the wave fronts has been strongly affected by the obstacle shape, even in the M–NL cases. Here the centers of the wave fronts were gradually shifted toward negative coordinates, indicating strong wave dispersion. The large error bars of the measurements (*Fig. 4*) represent not only the limited resolution caused by the visualization technique (dying of different layers), but are also the consequence of the aforementioned strong dispersion of lee waves.

It was observed that our model performs well in the H–NL range for steeper lee-side obstacles, like the one presented in *Fig. 3*. However, close to the M–NH range with the same obstacle, results tend to differ from the experiments. This difference may be explained by boundary layer separation effects. At an increased velocity, the separation bubble that developed behind the obstacle elongated and caused the virtual mountain half width (mountain half width plus the horizontal size of the separation) and consequently the normalized wave length to almost double. (See the wave field in *Fig. 3*)

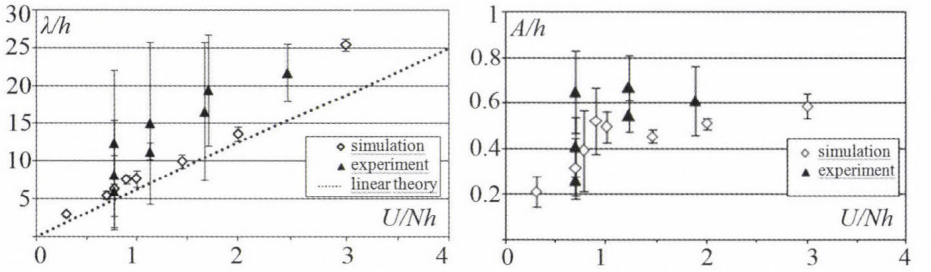

Fig. 4. Normalized averaged wave length (λ/h) (left) and normalized averaged wave amplitude (A/h) (right) as a function of non-dimensional horizontal flow velocity, in the case of the gentle leeward slope. The dotted line represents the wave length obtained from a linear theory, based on $\lambda = 2\pi U / N$ (*Scorer,* 1949). Filled symbols represent the measurements of *Gyüre* and *Jánosi* (2003). Error bars indicate the error originating from the data extraction technicque and wave dispersion.

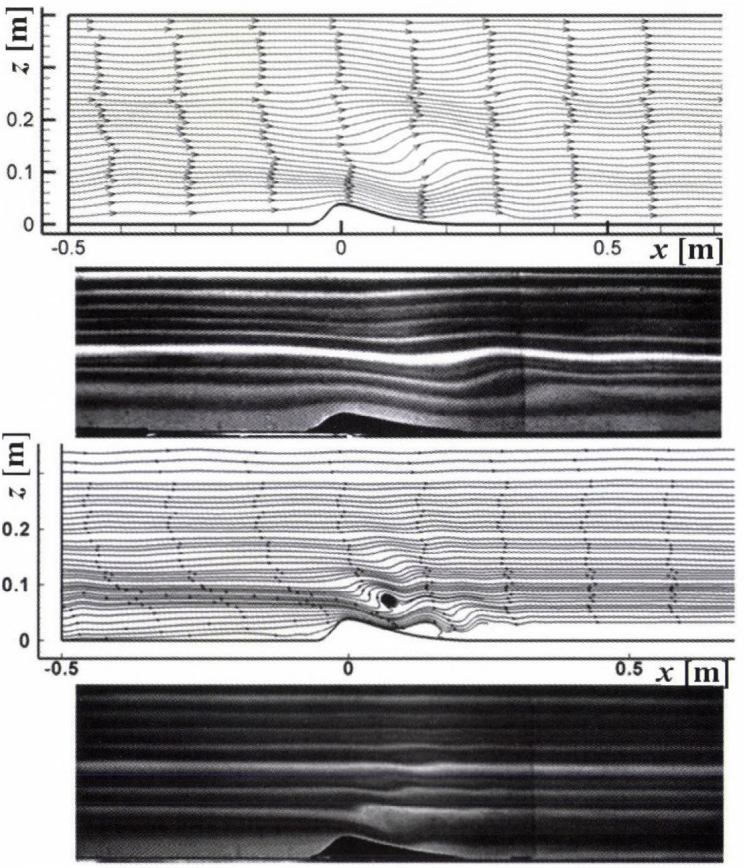

Fig. 5. Contours of computed streamlines and wave fields from the experiments (courtesy of *Gyüre* and *Jánosi,* 2003) at $Nh/U = 0.69$ (the upper two) and $Nh/U = 3.33$ (the lower two) non-dimensional flow velocities.

According to experimentalists (*Qiu* and *Xia,* 1998; *Gyüre* and *Jánosi,* 2003), the side walls have a negligible overall effect on the experimental results, however, the exact location and size of the separation were not captured properly, which can possibly be explained by the 3-D structure of the flow characterizing the laboratory experiments, due to the boundary layer on the side walls interacting with the separation bubble. In the case of a 3-D narrow obstacle, the separation bubbles were smaller, as the stratified flow tended to flow around the obstacle, instead of flowing over it. The prediction of the location of separation is currently a difficult topic, it requires the modeling of transitional turbulence and is beyond the scope of this investigation. Avoiding separation by using a gentle leeward side obstacle, however, gave both qualitative and quantitative agreements concerning the normalized amplitudes and wavelengths (*Fig. 4*). *Table 2* shows the performance measures, indicating good model performance. At low inlet velocities (bottom of *Fig. 5*), where wave breaking and rotors occurred, the flow structures, characterized by a high nonlinearity, were also captured properly.

Table 2. Statistic metrics of normalized wavelength *(λ/h)* and amplitude *(A/h)* for water-tank studies using CFD and experimental data of *Gyüre and Jánosi* (2003). Definition and the applied limits for the statistic metrics are described in *Chang et al.* (2005)

Validation metric	Abbreviation	Limit	*λ/h*	*A/h*	Classification
Correlation coefficient	R	>0.8	0.95	0.99	good
Fractional bias	FB	±0.3	0.317	0.21	good
Normalized mean square error	NMSE	0–4	0.12	0.05	good
Hit rate	HR	>0.66	0.75	1	good
Fraction of predictions within a factor of two of observations	FAC2	>0.5	1	1	good

3.4. Model comparison with a full scale event

3.4.1. Case study

A relatively well documented and studied event occurred during the winter of 1972 near Boulder, Colorado, where a severe wind storm, with a strong descent of air originating from the higher atmosphere, caused significant damage to the environment (*Lilly* and *Zipser,* 1972; *Brinkman,* 1974). The strong tropospheric descent is well reflected in the potential temperature contours in *Fig. 6a*, where the contours become denser close to the ground. The accompanying near ground downwind was also reported as being especially severe. A hydraulic jump and waves also developed behind the mountain (*Fig. 6a*).

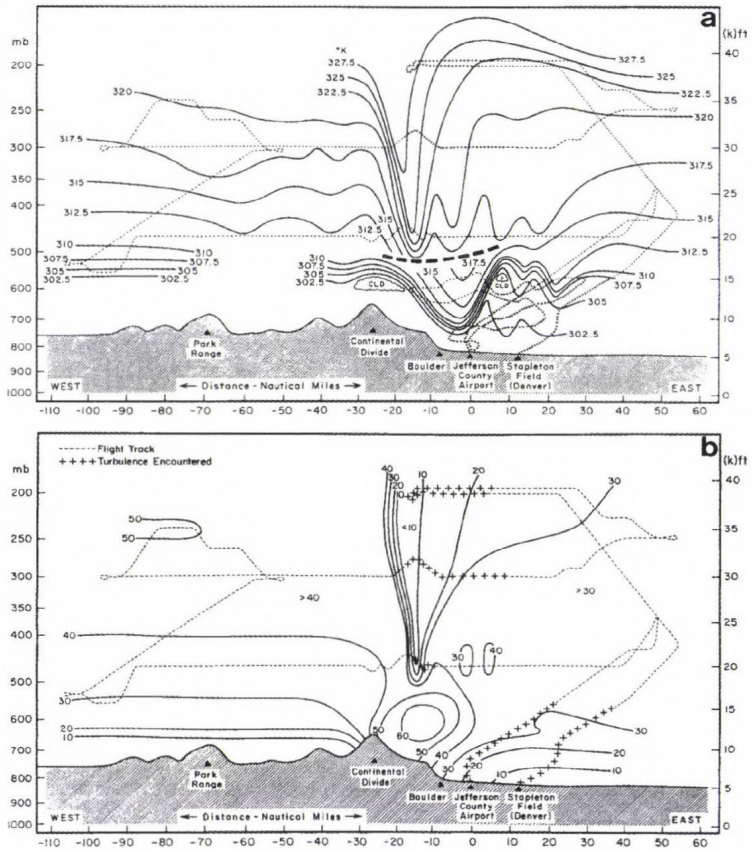

Fig. 6. Analysis of the potential temperature (a) and the horizontal velocity component (b) from aircraft flight data and sondes taken on January 11, 1972. Aircraft tracks are shown by dashed lines with the locations of significant turbulence indicated by plus signs (*Klemp* and *Lilly,* 1975).

The purpose of the present simulation is to show that the model is able to capture the main features and nonlinearities of such flows, for example the existence of the mentioned nonlinearities. This event became a standard test case of researchers (see ,e.g., *Xue et al.,* 2000) for developing simulation models, or to reproduce and understand the related mechanisms of such phenomena. A recent study dealt with the development of a severe thunderstorm in Budapest. With high resolution numerical modeling using MM5, they were able to reproduce the main features of the severe convective storm (*Horváth et al.,* 2007).

Different assumptions are made during similar case studies, in order to reduce computational cost, taking the advantage of the quasi two-dimensionality of the flow, or simply investigating each flow phenomena separately. Although mountain flows are generally three-dimensional, two-dimensionality can be a

good assumption for the downslope windstorm case, as the continental divide is long compared to its cross section. This is acceptable only if the large scale flow is being investigated and the microstructure has only negligible influence on the main flow. In some cases these structures have an effect, e.g., by modifying the horizontal position of the hydraulic jump. This is due to the increased surface friction resulting from a non-slip boundary. In spite these differences in the treatment of the lower boundary, the main features of the flow will still remain.

The elevation of the realistic terrain of the E–W oriented section was derived from a 3 arc second resolution SRTM (Shuttle Radar Topographic Mission) database. The section was then interpolated for the latitude of 40.015 N. The longitudinal coordinates were between 107.100 W and 103.900 W, giving an approximately 270 km wide section. The new coordinates were transformed onto the Universal Transverse Mercator (UTM) coordinates and were interpolated onto an approximately 1.5 arc second grid using a bicubic spline method.

Test cases using an idealized geometry have also been examined, where a simplified two-dimensional model has been used. In spite of the fact, that the real mountain has a plateau-like shape, due to the upstream influence and partial blocking, the upstream mountain profile does not affect significantly the upstream flow. Due to this fact, a symmetric mountain profile was used in several works (*Klemp* and *Lilly,* 1975), as well as in this study. The profile described by Eq. (37) was used for modeling both the upstream and downstream sections of the geometry. Here $a = 10$ km and $h = 2$ km are the mountain half width and height, respectively. The initial temperature and velocity profiles were based on the intercomparison study of *Doyle et al.* (2000). They found that these initial conditions were more appropriate for wave breaking tests, and more realistic than the conditions used in earlier studies (*Peltier* and *Clark,* 1979). Conditions favorable for downslope windstorms are usually characterized by strong cross mountain winds, and by the presence of a stable layer at the appropriate height (*Durran,* 1986). Both of these conditions were present in the studied situation.

The solution was found to be sensitive to the grid resolution (*Doyle et al.* 2000), therefore, in this study a relatively higher resolution grid was used. An equidistant grid was applied with a size of 1000 m and adapted to 250 m in two steps in the vicinity of the mountain. In the vertical direction the mesh size decreased down to 10 m resolution close to the ground. The domain extended from 2 to 25 km in the vertical and – 115 to 120 km in the horizontal direction, with the mountain crest positioned at $x = 0$ km. The top boundary was defined as symmetry with zero normal velocity, and the bottom was defined as a free-slip wall. A standard non-reflective boundary condition (outflow) was applied as an outlet. This means that the internal pressure field has been extrapolated to the outlet surface, and therefore, no further information on the outlet velocity and pressure profiles were required by the system.

Second order time discretization, pressure staggering option (PRESTO) for pressure interpolation (*ANSYS Inc.*, 2012), and second order upwinding methods were used in the momentum and energy equations. Compressibility was introduced with the help of the transformation used for model adaption. Moist effect and the Coriolis force were not considered during the calculations.

By using the ANSYS–FLUENT 13 simulation system, the model was integrated for a non-dimensional period of time of $t^* = \overline{U}t / a = 43.2$, based on an average inlet flow speed of 30 $m s^{-1}$, which corresponds to a 4-hour flow time. The results shown in this section are obtained at $t^* = 32.4$ time instant. Results were quantitatively compared to several mesoscale meteorological codes using statistical performance measures described in Section 3.2. The summary of the comparison can be seen in *Table 3.* Based on FB, NMSE, and FAC2, the idealized model can be considered acceptable. Negative FB values indicate lower predicted overall horizontal velocity. The correlation coefficient and hit rate, however, show values under the limit. The hit rate was calculated with 5 $m s^{-1}$ absolute and 10% relative deviation for the velocity and 1 K and 5% for the temperature, respectively, since large deviations with a factor of 2 differences were realized among the different intercomparision cases presented by *Doyle et al.* (2000). *Chang* and *Hanna* (2004) suggest that the model performance should not be judged based only on the performance measures but together with the comparison of flow patterns or the time evolution of the flow field.

Table 3. Statistic metrics calculated for horizontal velocity (U) and potential temperature (Θ) for the Boulder windstorm case study comparing CFD and NWP (*Doyle et al.*, 2000) model results

Validation metric	Abbreviation	Limit	U	Θ	Classification
Correlation coefficient	R	>0.8	0.154	0.96	not sufficient
Fractional bias	FB	±0.3	–0.07	–0.056	good
Normalized mean square error	NMSE	0–4	0.396	0.01	good
Hit rate	HR	>0.66	0.29	0.56	not sufficient
Fraction of predictions within a factor of two of observations	FAC2	>0.5	0.7	1	good

According to the experiments of *Doyle et al.* (2000), the results were highly time dependent, and therefore, unsteady simulations were executed and time-averaging was applied on the results. An averaging interval varying from 10 to 60 minutes was applied during the simulation, and it was found that the value and location of the maximum velocity were not affected. The horizontal position of the upstream edge of the hydraulic jump however changed significantly. The lee-slope wind magnitude varied considerably among the model simulations

presented by *Doyle et al.* (2000), and these differences were also reflected in the horizontal position of the hydraulic jump. The location of the upstream edge in some models, e.g., the *Durran* and *Klemp* (1983) model (DK83) or the Eulerian/semi-Lagrangian model (EULAG) was positioned immediately after the lee slope, similarly to our results, while in other cases it was positioned 10 – 25 km downstream of that (e.g., MESONH, RAMS, or RIMS models of the same intercomparison). This partially explains the lower HR and R values due to the horizontal shift in the flow pattern. Regarding the downslope wind, a higher value of maximum horizontal velocity was realized by the simulation than that of the onsite measurements. At $t^* = 32.4$, the location of the maximum velocity peak was found at approximately 8.5 km downstream of the mountain crest at a height of 7 km (*Fig. 7*). With further integration, the locations of the maxima were shifted downstream to approximately 16 km beyond the crest and to a lower height of 4 km (bottom of *Fig. 7*). The magnitudes were not changed considerably, stabilizing at around 66 m s^{-1}. Regarding the wind speed close to the ground, within the lowest 50 m, 51 – 59 m s^{-1} was realized, depending on the position along the mountain lee side. The near ground values of velocity magnitude were in fair agreement both with the observations and the meteorological models. The high instantaneous velocity peaks at higher altitudes obtained from the simulation could be partly caused by the lack of moisture transport and phase change processes. According to *Durran* and *Klemp* (1983), the wave response could be even 50% lower if a proper treatment for moist air flow is applied. This could significantly affect the properties of wave breaking, and consequently the development of a low level jet.

Several mesoscale codes simulated multiple breaking regions with the strongest ones located above the hydraulic jump at an altitude of 12 km and above (see the model results of RAMS, MESONH models presented by *Doyle et al.* (2000)). Wave steepening regions were obtained by CFD for the ideal and real mountain profiles at a similar altitude (between 10 and 15 km). Using the idealized geometry (*Fig. 7*), this region was weaker. The altitude of the maximum steepness above the hydraulic jump in the breaking region was at about 12 km with the highest amplitude waves being of 2–2.5 km.

The present results show smooth downstream isolines. In some of the cases of *Doyle et al.* (2000), the downstream part of the hydraulic jump was oscillatory, while in other cases the isolines were smooth. Among the results of different mesoscale meteorological solvers, depending on the amount of applied eddy diffusivity (K_d), different flow structures were obtained. Smaller K_d values usually resulted in smaller wave structures.

The stratospheric air descent reached the altitude of 5–6 km using the real topography which correlates well with the non-hydrostatic mesoscale vorticity (TVM) model solution of *Thunis* and *Clappier* (2000), or the model comparisons presented by *Doyle et al.* (2000) (CUMM, RAMS, RIMS). The descent was even stronger and propagated to lower altitudes in the case of the

simplified geometry accompanied by high TKE values (see *Fig. 7*) . The highest peaks, even reaching 117 $m^2 s^{-2}$, can be found around the upstream edge of the hydraulic jump and at the wave steepening regions at higher altitudes. The maximum value of TKE is reported approximately 15–20 $m^2 s^{-2}$ in atmospheric rotors (*Doyle et al.,* 2002) and even reaches higher values in the case of extremely severe turbulence.

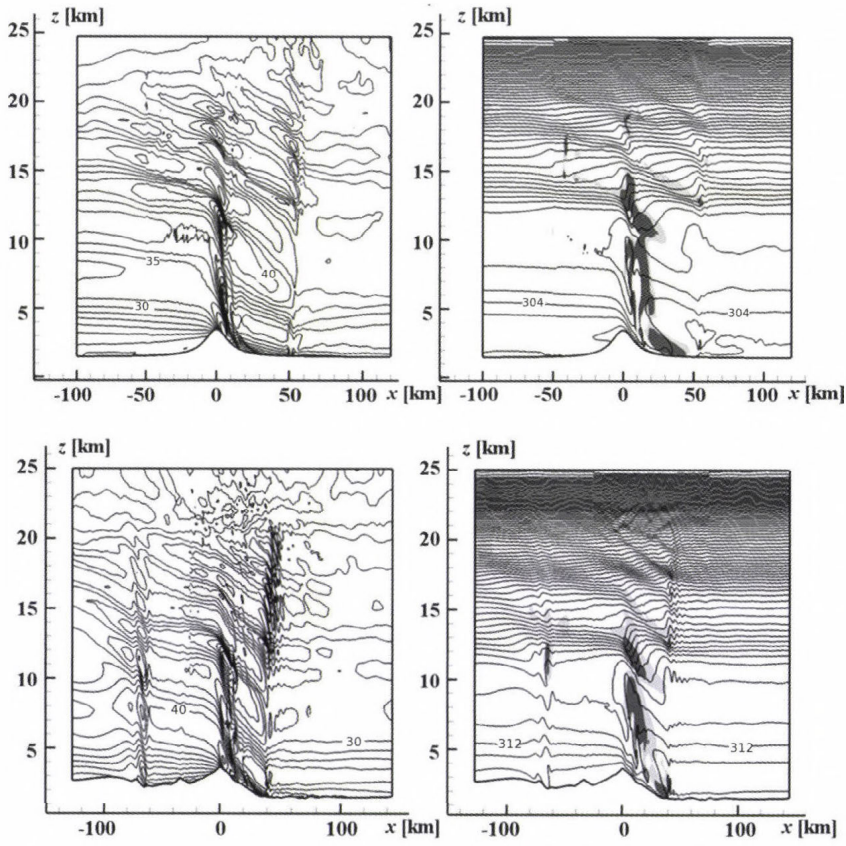

Fig. 7. Contours of horizontal velocity component (left panel) and potential temperature (right panel) for an idealized (top) and a real (bottom) mountain shape. The pictures show the results at $t^* = 32.4$ non-dimensional flow time. Vertical coordinates were magnified by a factor of 12 for better visualization. Potential temperature and velocity contour intervals are 8°C and 5 m s^{-1}, respectively. Light and dark grey areas indicate regions characterized by turbulent kinetic energy higher than 5 $m^2 s^{-2}$ and between 5–25 $m^2 s^{-2}$.

Differences in the magnitude of the horizontal velocity may also be related to the two-dimensional treatment of the topography if compared to the real situation. In three spatial dimensions, the flow can pass around the obstacle,

while in 2-D it is forced over it. The test results of *Doyle et al.* (2000) confirmed that a significant reduction in wave breaking could be found for the 3-D case. Some of the studies dealing with gravity wave evolution used a frictionless lower boundary (*Richard et al.,* 1989). Concerning the bottom boundary condition, a more realistic treatment of the ground surface could result in a slower movement and different horizontal location of the hydraulic jump.

4. Summary and conclusions

We briefly presented an adaptation method applicable to general purpose CFD solvers for atmospheric flow simulations, which was based on the application of an incompressible fluid model. Mesoscale effects, such as thermal stratification, adiabatic cooling caused by hydrostatic pressure driven expansion, compressibility, and Coriolis force were taken into account with the help of a transformation system and customized volume sources.

In this paper, simulations were presented around more complex geometrical features, idealized barriers, and real terrain, demonstrating the capabilities of the CFD based approach.

Simulations of linear hydrostatic waves were compared to an analytical solution, and it was stated that for this regime the code behaved well, and an excellent agreement was found.

Secondly, the simulation results were compared to water-tank experiments of two-dimensional mountain waves with different degrees of nonlinearity and hydrostacity. A good agreement was found based on the statistical performance measures and flow pattern comparison concerning the measured and simulated wavelengths and amplitudes. The model evaluation for λ/h gave a correlation coefficient of 0.95, fractional bias 0.317, normalized mean square error of 0.12, a hitrate value of 0.75 and 100% of predictions within a factor of two of observations. The equivalent results for A/h were 0.99 (R), 0.21 (FB), 0.05 (NMSE), 1 (HR), and 100% (FAC2). The model was also able to capture well the location and size of the appearing nonlinear structures, such as the rotor that was formed behind the obstacle.

Simulation of the Boulder windstorm case is ideal for testing and evaluating mesoscale numerical models, therefore it was chosen as the third object of analysis. The simulation results were compared to the on-site observations and a series of modeling experiments that were presented by *Doyle et al.* (2000). Model evaluation has demonstrated reasonable agreement with measurements for potential temperature (Θ). The model evaluation statistics gave a correlation coefficient of 0.96 and fractional bias –0.056, normalized mean square error of 0.01, a hit rate value of 0.56, and 100% of predictions within a factor of two of observations. The equivalent results for horizontal velocity (U) were 0.154 (R), –0.07 (FB), 0.396 (NMSE), 0.29 (HR) and

0.7 (FAC2). Results obtained from our simulations are encouraging with regard to the predictability of a low level, highly accelerated channel flow, and upper level wave breaking. Close to the ground a very strong lee-side wind was realized, accompanied by a well-defined hydraulic jump downstream.

Using only one single unstructured grid and a uniform physical description for close- and far-field flow, one can take the advantage of the model adaption in the simulation of mesoscale atmospheric phenomena. In the same model, one can investigate the finely structured microscale flow around complex geometrical features, such as flow around buildings with pollution dispersion or to study the close- and far-field of cooling towers and its effects to the environment.

The implementation and evaluation of non-reflective boundaries is planned through a 3-D mountain wave and associated downslope windstorm case study and the inclusion of moisture transport and phase change processes is also an important further step towards the practical application of the method.

Acknowledgments–This work has been supported by the Hungarian Research Fund under contract number OTKA T049573, the National Research and Development Program under contract number NKFP 3A/088/2004, and the TÁMOP-4.2.1.B-11/2/KMR-2011-0001 program. The authors are thankful for the data support from the SRTM.

References

Afanasyev, Y.D. and *Peltier, W.R.*, 2001: Numerical simulations of internal gravity wave breaking in the middle atmosphere: the influence of dispersion and three-dimensionalization. *J. Atmos. Sci. 58*, 132–153.

Alaka, M.A., Ed., 1960: The airflow over mountains. *WMO Tech. Note* 34, [Available from World Meteorological Organization, Case Postale 2300, CH-1211 Geneva 2, Switzerland.]

Almut, G. and *Herzog, H.J.*, 2007: A consistent time-split numerical scheme applied to the nonhydrostatic compressible equations. *Mon. Weather Rev. 135*, 20–36.

Andre, J.C., DeMoor, G., Lacarrere, P., Therry, G., and *Du Vachat, R.*, 1978: Modelling the 24-hour evolution of the mean and turbulent structures of the planetary boundary layer. *J Atmos Sci 35*, 1861–1883.

ANSYS Inc., 2012: FLUENT 13 documentation. In: Fluent User Services Center. [Available online at http://www.fluentusers.com/fluent/doc/doc_f.htm., Cited 26. September 2012.]

Baklanov, A.A., Grisogono, B., Bornstein, R., Mahrt, L., Zilitinkevich, S.S., Taylor, P., Larsen, S.E., Rotach, M.W., and *Fernando, H.J.S.*, 2011: The nature, theory, and modeling of atmospheric planetary boundary layers. *B. Am. Meteorol. Soc. 92*, 123–128.

Balczó, M., Balogh, M., Goricsán, I., Nagel, T., Suda, J.M., and *Lajos, T.*, 2011: Air quality around motorway tunnels in complex terrain - Computational Fluid Dynamics modeling and comparison to wind tunnel data. *Időjárás 115*, 179–204.

Balogh, M. and Krisróf, G., 2010: Fine scale simulation of turbulent flows in urban canopy layers. *Időjárás 114*, 135–148.

Belušič, D. and *Klaič, Z.B.*, 2004: Estimation of bora wind gusts using a limited area model. *Tellus A 56*, 296–307.

Berg, L.K. and *Zhong, S.*, 2005: Sensitivity of MM5-Simulated Boundary Layer Characteristics to Turbulence Parameterizations. *J. Appl. Meteorol.* 44, 1467–1483.

Blackadar, A.K., 1976: Modeling the nocturnal boundary layer. Preprints of the Third Symposium on Atmospheric Turbulence and Air Quality, Rayleigh, NC, 19–22 October 1976, Amer. Meteor. Soc., Boston, 46–49.

Blocken, B., Stathopoulos, T. and *Carmeliet, J.,* 2007: CFD simulation of the atmospheric boundary layer: wall function problems. *Atmos. Environ. 41*, 238–252.

Brinkman, W.A.R., 1974: Strong downslope winds at Boulder, Colorado. *Mon. Weather Rev. 102*, 592–602.

Castro, F.A., Santos, C.S. and *Palma, J.M.L.M.,* 2008: Parallelisation of the CFD Code of a CFD-NWP Coupled System for the Simulation of Atmospheric Flows over Complex Terrain. *High Performance Computing for Computational Science - VECPAR* 2008, 27–38.

Cenedese, A. and *Monti, P.,* 2003: Interaction between an urban heat island and a sea-breeze flow. A laboratory study. *J. Appl. Meteorol. 42*, 1569–1583.

Chang, J.C. and *Hanna, S.R.,* 2004: Air quality model performance evaluation. *Meteorol. Atmos. Phys. 87*, 167–196.

Chang, J.C., Hanna, S.R., Boybeyi, Z. and *Franzese, P.,* 2005: Use of Salt Lake City URBAN 2000 Field Data to Evaluate the Urban Hazard Prediction Assessment Capability (HPAC) Dispersion Model. *J. Appl. Meteorol. 44*, 485–501.

Colle, B.A. and *Mass, C.F.,* 2000: High resolution observation and numerical simulation of easterly gap flow through the strait of Juan de Fuca on 9–10 December 1995. *Mon. Weather Rev. 128*, 2398–2422.

Corrsin, S., 1975: Limitation of gradient transport models in random walks and in turbulence. *Adv. Geophys. 18A*, 25–60.

Deardorff, J.W., 1974a: Three-dimensional numerical study of the height and mean structure of a heated planetary boundary layer. *Bound.-Lay. Meteorol. 7*, 81–106.

Deardorff, J.W., 1974b: Three-dimensional numerical study of turbulence in an entraining mixed layer. *Bound.-Lay. Meteorol.* 7, 199–226.

Deardorff, J.W., 1980: Stratocumulus-capped mixed layers derived from a three-dimensional model. *Bound.-Lay. Meteorol.* 18, 495–527.

Doyle, J.D., Durran, D.R., Chen, C., Colle, B.A., Georgelin, M., Grubisic, V., Hsu, W.R., Huang ,C.Y., Landau, D., Lin, Y.L., Poulus, G.S., Sun, W.Y., Weber, D.B., Wurtele, M.G., and *Xue, M.,* 2000: An intercomparison of model-predicted wave breaking for the 11 January 1972 boulder windstorm. *Mon. Weather. Rev. 128*, 901–914.

Doyle, J.D. and *Durran, D.R.,* 2002: The Dynamics of mountain–wave induced rotors. *J. Atmos. Sci. 59*, 186–201.

Dudhia, J., 1993: A nonhydrostatic version of the Penn State / NCAR mesoscale model: Validation tests and simulations of an Atlantic cyclone and cold front. *Mon. Weather Rev. 121*, 1493–1513.

Durran, D.R. and *Klemp, J.B.,* 1983: A Compressible model for the simulation of moist mountain waves. *Mon. Weather. Rev 111*, 2341–2361.

Durran, D.R., 1986: Another look at downslope windstorms. Part I: The development of analogs to supercritical flow in an infinitely deep, continuously stratified fluid. *J. Atmos. Sci.* 43, 2527–2543.

Durran, D.R., 1990: Mountain waves and downslope winds. Atmospheric Processes over Complex Terrain. *Meteorol. Monog. 45*, 59–81.

Duynkerke, P.G., 1988: Application of the E–ε turbulence closure model to the neutral and stable atmospheric boundary layer. *J. Atmos. Sci. 45*, 865–880.

Faragó, I., 2006: Application of the operator splitting method for real-life problems. *Időjárás 110*, 379-395.

Freedman, F.R. and Jacobson, M.Z., 2003: Modification of the Standard ε equation for the stable ABL through enforced consistency with Monin-Obukhov similarity theory. *Bound-Lay Meteorol* 106, 384–410.

Gatski, T.B. and *Jongen, T.,* 2000: Nonlinear eddy viscosity and algebraic stress models for solving complex turbulent flows. *Prog. Aerosp. Sci. 36*, 655–682.

Geiser, J., 2008: Iterative operator-splitting methods with higher-order time integration methods and applications for parabolic partial differential equations. *J. Comput. Appl. Math. 217*, 227–242.

Grell, G.A., Dudhia, J. and *Stauffier, D.R.,* 1995: A description of the fifth-generation Penn State/NCAR mesoscale model. *NCAR Tech. Note, NCAR/TN-398-398+ST.*

Gyüre, B. and *Jánosi, I.M.*, 2003: Stratified flow over asymmetric and double bell-shaped obstacles. *Dynam. Atmo.s Oceans 37*, 155–170.

Hanjalic, K. and *Launder, B.E.*, 1972: A Reynolds stress model of turbulence and its application to thin shear flows. *J. Fluid Mech. 52*, 609–638.

Hanna, S.R., Strimaitis, D.G. and *Chang, J.C.*, 1991: Evaluation of commonly-used hazardous gas dispersion models. Vol. II, Hazard Response Modeling Uncertainty (A Quantitative Method). *Rep. A119/A120 prepared by Earth Tech, Inc., for Engineering and Services Laboratory, Air Force Engineering and Services Center, and for the American Petroleum Institute,* 334 pp.

Hanna, S.R., Chang, J.C. and *Strimaitis, D.G.*, 1993: Hazardous gas model evaluation with field observations. *Atmos. Environ.* 27A, 2265–2285.

Hanna, S.R., Brown, M.J., Camelli, F.E., Chan, S.T., Coirier, W.J., Kim, S. and *Reynolds, R.M.*, 2006: Detailed Simulations of Atmospheric Flow and Dispersion in Downtown Manhattan: An Application of Five Computational Fluid Dynamics Models. *B. Am. Meteorol. Soc. 87*, 1713–1726.

Hargreaves, D.M. and *Wright, N.G.*, 2007: On the use of the k–ε model in commercial CFD software to model the neutral atmospheric boundary layer. *J. Wind Eng. Ind. Aerod. 95*, 355–369.

Havasi, Á., Bartholy, J., and *Faragó, I.*, 2001: Splitting method and its application in air pollution modeling. *Időjárás 105*, 39–58.

Holton, J.R., 2004: An Introduction to Dynamic Meteorology. 4th Edition, Academic Press, 192–212

Holtslag, A.A.M. and *Moeng, C.-H.*, 1991: Eddy diffusivity and countergradient transport in the convective atmospheric boundary layer. *J. Atmos. Sci. 48*, 1690–1698.

Hong, S.-Y., 2010: A new stable boundary-layer mixing scheme and its impact on the simulated East Asian summer monsoon. *Q. J. Roy. Meteorol. Soc. 136*, 1481–1496.

Hong, S.-Y. and *Pan, H.-L.*, 1996: Nonlocal boundary layer vertical diffusion in a medium-range forecast model. *Mon. Weather Rev. 124*, 2322–2339.

Hong, S.-Y., Noh, Y, and *Dudhia, J.*, 2006: A new vertical diffusion package with an explicit treatment of entrainment processes. *Mon. Weather Rev. 134*, 2318–2341.

Horváth, Á., Geresdi, I., Németh, P. and *Dombai, F.*, 2007: The Constitution Day storm in Budapest: Case study of the August 20, 2006 severe storm. *Időjárás 111*, 41–63.

Huser, A., Nilsen, P.J. and *Skatun, H.*, 1997: Application of k-ε model to the stable ABL: pollution in complex terrain. *J. Wind Eng. Ind. Aerod. 67–68*, 425–436.

Janjic, Z.I., 1990: The step–mountain coordinates: physical package. *Mon. Weather Rev. 118*, 1429–1443.

Janjic, Z.I., 1996: The Mellor-Yamada level 2.5 scheme in the NCEP Eta Model. 11th Conference on Numerical Weather Prediction, Norfolk, VA, 19-23 August 1996; Amer Meteor Soc, Boston, MA, 333–334.

Janjic, Z.I., 2002: Nonsingular Implementation of the Mellor-Yamada Level 2.5 Scheme in the NCEP Meso model. *NCEP Office Note 437*.

Kasahara, A., 1974: Various vertical coordinate systems used for numerical weather prediction. *Mon. Weather Rev. 102*, 509–522.

Klemp, J.B. and *Lilly, D.K.*, 1975: The dynamics of wave-induced downslope winds. *J. Atmos. Sci. 32*, 320–339.

Klemp, J.B. and *Wilhelmson, R.B.*, 1978: The simulation of three-dimensional convective storm dynamics. *J. Atmos. Sci. 35*, 1070–1096.

Klemp, J.B., Skamarock, W.C., and *Dudhia, J.*, 2007: Conservative Split-Explicit Time Integration Methods for the Compressible Nonhydrostatic Equations. *Mon. Weather Rev. 135*, 2897–2913.

Knievel, J.C., Bryan, G.H. and *Hacker, J.P.*, 2007: Explicit Numerical Diffusion in the WRF Model. *Mon. Weather Rev. 135*, 3808–3824.

Kristóf, G., Rácz, N., and *Balogh, M.*, 2009: Adaptation of Pressure Based CFD Solvers for Mesoscale Atmospheric Problems. *Bound.-Lay. Meteorol. 131*, 85–103.

Launder, B.E. and *Spalding, D.B.*, 1972: Lectures in mathematical models of turbulence. Academic Press, London, England 1972. 169 pp.

Lee, S.-M., Giori, W., Princevac, M., and *Fernando, H.J.S.*, 2006: Implementation of a Stable PBL Turbulence Parameterization for the Mesoscale Model MM5: Nocturnal Flow in Complex Terrain. *Bound.-Lay. Meteorol. 119*, 109–134.

Lesieur, M., 2008: Turbulence in Fluids. Fourth edition, Springer, ISBN: 9781402064340.

Lilly, D.K. and *Zipser, E.J.*, 1972: The front range windstorm of 11 January 1972 – a meteorological narrative. *Weatherwise 25*, 56–63.

Lin, Y-L., 2007: Mesoscale dynamics. Cambridge University Press, ISBN 9780521808750.

Long, R.R., 1953: Some aspects of the flow of stratified fluids. I. A theoretical investigation. *Tellus 5*, 42–58.

Lopes da Costa, J.C., Castro, F.A., Palma, J.M.L.M., and *Stuart, P.*, 2006: Computer simulation of atmospheric flows over real forests for wind energy resource evaluation. *J. Wind Eng. Ind. Aerod.* 94, 603–620.

Lu, J., Arya, S.P., Snyder, W.H. and *Lawson Jr., R.E.*, 1997: A laboratory study of the urban heat island in a calm and stably stratified environment. Part I: Temperature field. *J. Appl. Meteorol. 36*, 1377–1391.

Lundquist, J.K. and *Chan, S.T.*, 2006: Consequences of urban stability conditions for computational fluid dynamics simulations of urban dispersion. *J. Appl. Meteorol. Clim. 46*, 1080–1097.

Lynch, P., 2006: The Emergence of Numerical Weather Prediction: Richardson's Dream. Cambridge University Press, Cambridge, ISBN: 0521857295.

Madala, R.V., 1981: Efficient time integration schemes for atmosphere and ocean models. In (Book, D.L. Ed.) Fine-difference techniques for vectorized fluid dynamics calculations. Springer-Verlag, New York, 56–74.

Manual of the ICAO Standard Atmosphere, 1993: Doc 7488-CD, Third Edition, ISBN: 92-9194-004-6.

Mellor, G.L. and *Yamada, T.*, 1974: A hierarchy of turbulence closure models for planetary boundary layers. *J. Atmos. Sci. 31*, 1791–1806.

Mellor, G.L. and *Yamada, T.*, 1982: Development of a turbulence closure model for geophysical fluid problems. *Rev. Geophys. 20*, 851–875.

Michioka, T. and *Chow, F.K.*, 2008: High-resolution large-eddy simulations of scalar transport in atmospheric boundary layer flow over complex terrain. *J. Appl. Meteorol. Climatol. 47*, 3150–3169.

Montavon C., 1998: Simulation of atmospheric flow over complex terrain for wind power potential assessment. Doctoral thesis, EPFL, Lausanne, doi: 10.5075/epfl-thesis-1855.

Nagy, A., 2010: Application of WRF model for the meso-g scale processes. MSc Thesis Eötvös Loránd University, Departmernt of Meteorology. (In Hungarian)

Nakanishi, M. and *Niino, H.*, 2009: Development of an Improved Turbulence Closure Model for the Atmospheric Boundary Layer. *J. Meteorol. Soc. JPN* 87, 895–912.

National Research Council, 1983. Low-Altitude Wind Shear and Its Hazard to Aviation. Washington, DC: The National Academies Press, Washington, DC, 1. Print.

Noto, K., 1996: Dependence of heat-island phenomena on stable stratification and heat quantity in a calm environment. *Atmos. Environ. 30*, 475–485.

Palma, J.M.L.M., Castro, F.A., Ribeiro, L.F., Rodrigues, A.H.. and *Pintod, A.P.*, 2008: Linear and nonlinear models in wind resource assessment and wind turbine micro-siting in complex terrain. *J. Wind Eng. Ind. Aerod. 96*, 2308–2326.

Peltier, W.R. and *Clark, T.L.*, 1979: The evolution and stability of finite-amplitude mountain waves. Part II: Surface wave drag and severe downslope windstorms. *J. Atmos. Sci. 36*, 1498–1529.

Pleim, J.E., 2007: A combined local and nonlocal closure model for the atmospheric boundary layer. Part II: Application and evaluation in a mesoscale meteorological model. *J. Appl. Meteorol. Climatol. 46*, 1396–1409.

Pleim, J.E. and *Chang, J.S.*, 1992: A non-local closure model for vertical mixing in the convective boundary layer. *Atmos. Environ. 26A*, 965–981.

Pontiggia, M., Derudi, M., Busini, V., and *Rota, R.*, 2009: Hazardous gas dispersion: A CFD model accounting for atmospheric stability classes. *J. Hazard Mater. 171*, 739–747.

Qiu, X.-L. and Xia, K.-Q., 1998: Viscous boundary layers at the sidewall of a convection cell. *Phys. Rev. E 58*, 486–491.

Richard, E., Mascart, P. and *Nickerson, E.C.*, 1989: The role of surface friction in downslope wind storms. *J. Appl. Meteorol. 28*, 241–251.

Richards, P.J. and *Hoxey, R.P.*, 1993: Appropriate boundary conditions for computational wind engineering models using the k–ε turbulence model. *J. Wind Eng. Ind. Aerod. 46–47*, 145–153.

Saito, K., Ishida, J., Aranami, K., Hara, T., Segawa, T., Narita, M., and *Honda, Y.,* 2007: Nonhydrostatic atmospheric models and operational development at JMA. *J. Meteorol. Soc. JPN 85B*, 271–304.

Schumann, U., Hauf, T., Holler, H., Schmidt, H,. and *Volkert, H.,* 1987: A mesoscale model for the simulation of turbulence, clouds and flow over mountains: Formulation and validation examples. *Beitr. Phys. Atmos. 60*, 413–446.

Scorer, R.S., 1949: Theory of waves in the lee of mountains. *Q. J. Roy. Meteor. Soc.* 75, 41–56.

Shafran, P.C., Seaman, N.L., and *Gayno, G.A.,* 2000: Evaluation of numerical predictions of boundary layer structure during the Lake Michigan Ozone Study (LMOS). *J. Appl. Meteorol. 39* 412–426.

Shih, T.-H., Liou, W.W., Shabbir, A., Yang, Z., and *Zhu, J.,* 1995: A new k–ε eddy-viscosity model for high Reynolds number turbulent flows – model development and validation. *Comput. Fluids 24*, 227–238.

Simon, A., Horváth, Á., and *Vivoda, J.,* 2006: Case study and numerical simulations of the November 19, 2004 severe windstorm in central Europe. *Időjárás 110*, 91–123.

Skamarock, W.C., Klemp, J.B., Dudhia, J., Gill, D.O., Barker, D.M., Wang, W., and *Powers, J.G.,* 2005: A Description of the Advanced Research WRF Version 2. *NCAR/TN–468+STR NCAR Technical Note.*

Smith, R.B., 1979: The influence of mountains on the atmosphere. Adv Geophys, Academic Press 21, 87–230.

Smith, R.B., 2002: Stratified airflow over mountains. In (Grimshaw, R., Ed.) Environmental Stratified Flows, Kluwer Publishing, 119–159.

Smith, R.B., Skubis, S., Doyle, J.D., Broad, A.S., Kiemle, C. and *Volkert, H.*, 2002: Mountain waves over Mont Blanc: Influence of stagnant boundary layer. *J. Atmos. Sci. 59*, 2073–2092.

Stull, R.B., 1993: Review of non-local mixing in turbulent atmospheres: Transilient turbulence theory. *Bound.-Lay. Meteorol. 62*, 21–96.

Sušelj, K. and *Sood, A,* 2010: Improving the Mellor–Yamada–Janjic parameterization for wind conditions in the marine planetary boundary layer. *Bound.-Lay. Meteorol. 136*, 301–324

Thunis, P. and *Clappier, A.,* 2000: Formulation and evaluation of a Nonhydrostatic Mesoscale Vorticity Model (TVM). *Mon. Weather Rev. 128*, 3236–3251.

Townsend, A.A., 1980: The response of sheared turbulence to additional distortion. *J. Fluid. Mech. 98*, 171–191.

Troen, I. and *Mahrt, L.,* 1986: A simple model of the atmospheric boundary layer; sensitivity to surface evaporation. *Bound.-Lay. Meteorol. 37*, 129–148.

Vendel, F., Lamaison, G., Soulhac, L., Volta, P., Donnat, L., Duclaux, O., and *Puel, C.,* 2010: Modelling diabatic atmospheric boundary layer using a RANS CFD code with k-epsilon turbulence closure. *HARMO13 – 1–4 June 2010, Paris, France – 13th Conference on Harmonisation within Atmospheric Dispersion Modelling for Regulatory Purposes* H13-124, 652–656.

Voisin, B., 1994: Internal wave generation in uniformly stratified fluids. Part 2. Moving point sources. *J. Fluid. Mech. 261*, 333–374.

Weigel, A.P., Chow, F.K., and *Rotach, M.W.,* 2007: On the nature of turbulent kinetic energy in a steep and narrow Alpine valley. *Bound.-Lay. Meteorol. 123*, 177–199.

Wicker, L.J. and *Skamarock, W.C.,* 2002: Time splitting methods for elastic models using forward time schemes. *Mon. Weather Rev. 130*, 2088–2097.

Wilhelmson, R. and *Klemp, J.B.,* 1978: A numerical study of storm splitting that leads to long-lived storms. *J. Atmos. Sci. 35*, 1974–1986.

Williams, M.D., Brown, M.J., Singh, B., and *Boswell, D.,* 2004: QUIC-Plume Theory Guide. LANL Report: LA-UR-04-0561.

Wyngaard, J.C., Cote, O.R., and *Rao, K.S.,* 1974: Modeling of the atmospheric boundary layer. *Adv. Geophys. 18(A),* 193–212.

Wyngaard, J.C. and *Brost, R.A.,* 1984: Top-down and bottom-up diffusion of a scalar in the convective boundary layer. *J. Atmos. Sci. 41*, 102–112.

Wurtele, M.G., Sharman, R.D., and *Datta, A.,* 1996: Atmospheric lee waves. *Annu. Rev. Fluid. Mech. 28*, 429–476.

Xue, M., Zong, J., and *Drogemeier, K.K.,* 1996: Parameterization of PBL turbulence in a multi-scale nonhydrostatic model. Preprints, 11th Conf. on Numerical Weather Prediction, Norfolk, VA, Amer Meteor Soc, P2.5.

Xue, M., Droegemeier, K.K., and *Wong, V.,* 2000: The Advanced Regional Prediction System (ARPS). A multi-scale nonhydrostatic atmospheric simulation and prediction model. Part I: Model dynamics and verification. *Meteorol. Atmos. Phys. 75*, 161–193.

Yang, X., 1993: A nonhydrostatic model for simulation of airflow over mesoscale bell-shaped ridges. *Bound.-Lay. Meteorol.* 65, 401–424.

Zhang, D.-L. and *Anthes, R.A.,* 1982: A high-resolution model of the planetary boundary layer-sensitivity tests and comparisons with SESAME-79 data. *J. Appl. Meteorol.* 21, 1594–1609.

Zhong, S., In, H., and *Clements, C.,* 2007: Impact of turbulence, land surface, and radiation parameterizations on simulated boundary layer properties in a coastal environment. *J. Geophys. Res. 112*, D13110, doi:10.1029/2006JD008274.

Zilitinkevich, S.S., 1995: Non-local turbulent transport: pollution dispersion aspects of coherent structure of convective flows. In (Power, H., Moussiopoulos, N., and Brebbia, C.A., Eds.) Air Pollution III—Volume I. Air Pollution Theory and Simulation, Computational Mechanics Publications, Southampton Boston, 53–60.

IDŐJÁRÁS

Quarterly Journal of the Hungarian Meteorological Service
Vol. 117, No. 31, July–September 2013, pp. 277–294

Performance of the Asymmetric Convective Model Version 2, in the Unified EMEP Model

Zorica Podrascanin[1]* and **Dragutin T. Mihailovic**[2]

[1]*Faculty of Sciences, Department of Physics, University of Novi Sad, Dositej Obradovic Sq. 4, 21000 Novi Sad, Serbia*

[2]*Faculty of Agriculture, Department of Field and Vegetable Crops, University of Novi Sad, Dositej Obradovic Sq. 8, 21000 Novi Sad, Serbia, guto@polj.uns.ac.rs*

**Corresponding author E-mail: zorica.podrascanin@gmail.com*

(Manuscript received in final form March 6, 2013)

Abstract–We have investigated the performance of the Asymmetric Convective Model Version 2 (ACM2), a planetary boundary layer (PBL) vertical turbulent mixing scheme, that is a combination of local and non-local closures, in a complex system such as a chemical transport model, the Unified EMEP (European Monitoring and Evaluation Program) Model. For this purpose, we modified the local part of the ACM2 scheme to take into account the level of turbulent kinetic energy, and then incorporated this scheme in the Unified EMEP model. After incorporation, the scheme was validated under all stability conditions and for several compounds. Comparisons were made against the K-scheme currently used in the Unified EMEP model, and surface nitrogen dioxide (NO_2), sulfur dioxide (SO_2), and sulphate (SO_4^{2-}) concentrations were observed at different EMEP stations during the year 2005. In most cases, the model better simulated the NO_2, SO_2, and SO_4^{2-} concentrations when the ACM2 scheme was used, especially for NO_2 during the summer months, when the non-local mixing is presumably dominant.

Key-words: non-local convective mixing, local scheme, turbulent kinetic energy, chemical modeling, vertical turbulent mixing

1. Introduction

The Unified EMEP model (*Simpson et al.,* 2003) was developed as a part of the European Monitoring and Evaluation Programme (EMEP) under the Convention on Long-Range Transboundary Air Pollution (LRTAP). This and previous versions of this model have been used over the last 30 years to simulate the transboundary transport of air pollution on the European scale. The surface concentrations of pollutants are strongly related to the turbulent vertical mixing, and thus, a good representation of vertical mixing in the planetary boundary layer (PBL) is very important for every chemical transport model, including the Unified EMEP model. During the past 30–50 years, various turbulent vertical mixing schemes for use in the PBL were developed and tested in 1D and 3D simulations in both meteorological and air quality models. All of the suggested vertical mixing schemes can be categorized as diffusion schemes, K-schemes (e.g., *O'Brien*, 1970; *Deardorff*, 1972; *Louis,* 1979; *Holtslag* and *Moeng*, 1991; *Holtslag* and *Boville*, 1993; *Alapaty* and *Alapaty*, 2001), second and higher-order closure models (e.g., *Mellor* and *Yamada*, 1974; *Janjic*, 1990, 1994, etc.), non-local schemes (e.g., *Blackadar*, 1976; *Stull,* 1984; *Pleim* and *Chang*, 1992; *Hong* and *Pan*, 1996), and combinations of local (diffusion) and non-local schemes (e.g., *Pleim*, 2007a). Most of these schemes have been intensively tested and compared with each other and against measurements in many studies (e.g., *Zhang* and *Zheng*, 2004; *Berg* and *Zhong*, 2005; *Hu et al.*, 2010). The most important conclusions from those studies are as follows: 1) the model is sensitive to the turbulent vertical mixing scheme in the PBL; 2) the non-local aspect of these schemes is important for realistically representing the convective boundary layer (CBL); and 3) the realistic apportionment of fluxes between local and non-local components is critical for satisfactorily representing the mixing in a CBL.

The Unified EMEP model is an off-line chemical transport model, which means that the model is driven with outputs from meteorological weather prediction models without feedback between chemical and meteorological models. The advantage of this approach is the possibility of independent parameterizations, a more flexible grid construction, and that it is easier to use for the inverse modeling, among others (*Baklanov* and *Korsholm,* 2007). The Unified EMEP model uses K-schemes for parameterizing the vertical mixing: the O'Brien (*O'Brien*, 1970) scheme is used in the CBL, and the Blackadar scheme (*Blackadar*, 1979) is used in the stable boundary layer (SBL). During the past several years, some other vertical mixing schemes have been proposed for use in this model. *Mihailovic* and *Alapaty* (2007) proposed a closure based on turbulent kinetic energy (TKE) as an improvement of the vertical diffusion scheme by *Alapaty* (2003). They examined the performance of the scheme comparing simulated and measured NO_2 gas concentrations for the years 1999, 2001, and 2002. In 2008, the non-local convective mixing scheme with varying

upward mixing rates (VUR) was proposed for use in the Unified EMEP model (*Mihailovic et al.*, 2008) and was later combined with TKE vertical diffusion scheme (*Mihailovic et al.*, 2009). This combination of the two previous schemes uses the VUR scheme for convective conditions and the TKE scheme for stable conditions. The disadvantage of this approach is an abrupt change from one scheme to another in the transition from convective to stable conditions. Additionally, in the VUR schemes, bottom-up fluxes originated in the first layer are distributed to the layers above; this is not realistic, because there is clearly an additional mixing between adjacent layers. The scheme that avoids the aforementioned drawback of the previous schemes used in the EMEP model has a realistic apportionment of fluxes between the local and non-local components as a result of combined local and non-local closures; this scheme is called the Asymmetric Convective Model Version 2 (ACM2) (*Pleim*, 2007a). The ACM2 scheme is built on the original Asymmetric Convective Model (ACM) (*Pleim* and *Chang*, 1992), a non-local convective mixing scheme, by adding an eddy diffusion component. The main advantage of this scheme in comparison to the ACM scheme (which is applicable only in convective conditions) is its applicability for all stability conditions. Mixing between a non-local and local diffusion scheme, in the case of convection, is governed by a pre-specified weighting factor that depends on the PBL height and Monin-Obukhov length. In stable conditions, stratification mixing is reduced to local diffusion. The ACM2 scheme has been tested in its 1D form against large-eddy simulations (LES) (*Pleim*, 2007a) and has been implemented in the meteorological model (fifth-generation Pennsylvania State University–NCAR Mesoscale Model (MM5)) (*Pleim*, 2007b). The profiles obtained with the ACM2 scheme in the 1D test have shapes that are more similar to the shapes of the LES profiles than those obtained with the ACM scheme. The MM5 model with the ACM2 scheme is evaluated with surface meteorological measurements, rawinsonde profile measurements, and the observed PBL height. The MM5 model with ACM2 performed as well or better than similar MM5 model studies.

We have incorporated the ACM2 scheme into the Unified EMEP model because of its previously mentioned properties to test its ability to work in a complex system that depends on a large number of processes: horizontal advection, emissions, vertical mixing, chemical reactions, dry and wet deposition, among others. For this purpose, we modified the local part of ACM2 to account for the level of turbulent kinetic energy and then incorporated it in the Unified EMEP model. The goal of this study was to demonstrate the possibility of applying the ACM2 scheme in the Unified EMEP model on the most important air pollutants from an environmental standpoint: NO_2, SO_2, and SO_4^{2-} (*Jericevic et al.*, 2010). The validation has been performed for all stability conditions, and the modeled surface nitrogen dioxide (NO_2), sulfur dioxide (SO_2), and sulphate (SO_4^{2-}) concentrations were compared with observations at different EMEP measurement stations during the year 2005. Descriptions of the

standard Unified EMEP schemes and the ACM2 scheme are given in Section 2. The comparison results between the currently used scheme in the Unified EMEP model, the ACM2 scheme, and the measured concentrations are given in Section 3, while Section 4 summarizes the study and presents the concluding remarks.

2. *Materials and methods*

2.1. *Formulation of the vertical diffusion currently used in the Unified EMEP chemical model*

The vertical sub-grid transport is modeled using the K-scheme in the Unified EMEP chemical model as well as in many other chemical transport models. K is determined in the unstable conditions as

$$K(z)=\begin{cases} K(h)+\left(\dfrac{h-z}{h-h_s}\right)^2\left\{\left[K(h_s)-K(h)\right]+\right. \\ \qquad \left.(z-h_s)\left[\dfrac{\delta}{\delta_s}K(h_s)+2\dfrac{K(h_s)-K(h)}{h-h_s}\right]\right\}, & h_s \le z < h \\ \dfrac{u_* kz}{\phi\left(\dfrac{z}{L}\right)}, & z < h_s \end{cases} \tag{1}$$

where z is the model layer height, h is the PBL height, h_s is the surface boundary layer height, u_* is friction velocity, ϕ is the atmospheric stability function for temperature, and k is the von Karman constant. In the model calculation, h_s is equal to 4% of the PBL height (*O'Brien*, 1970). The atmospheric stability function for temperature in convective conditions is

$$\phi=\left(1-16\frac{z}{L}\right) \tag{2}$$

and for stable conditions is

$$\phi=1+5\frac{z}{L}. \tag{3}$$

Accordingly, K is calculated in stable conditions and above the PBL (*Blackadar*, 1979) as

$$K(z)=\begin{cases}0.001 & R_i > R_{ic} \\ 1.1(R_{ic}-R_i)l^2\left|\Delta V_H/\Delta z\right| R_{ic} & R_i \le R_{ic}\end{cases}, \tag{4}$$

where l is the turbulent mixing length, ΔV_H represents the difference in wind-speed between two grid-cell centers separated by distance Δz, R_i is the Richardson number and R_{ic} is the critical Richardson number. The turbulent mixing length is parameterized according to:

$$\begin{aligned} l &= kz, \quad z \le z_m \\ l &= kz_m, \quad z > z_m \end{aligned} \tag{5}$$

where k is the von Karman constant, z is the height above the ground, and $z_m = 200$ m. Hereafter, the currently used scheme in the Unified EMEP model will be called the OLD scheme.

2.2. Formulation of the ACM2 scheme for use in the Unified EMEP model

According to the ACM2 scheme, the quantity φ in the model layer i is calculated as

$$\frac{\partial \varphi_i}{\partial t} = Mu'\varphi_1 - Md'_i\varphi_i + Md'_{i+1}\varphi_{i+1}\frac{\Delta z_{i+1}}{\Delta z_i} + \frac{1}{\Delta z_i}\left[\frac{K'_{i+1/2}(\varphi_{i+1}-\varphi_i)}{\Delta z_{i+1/2}} - \frac{K'_{i-1/2}(\varphi_i-\varphi_{i-1})}{\Delta z_{i-1/2}}\right], \tag{6}$$

where Mu' and K' are the upward convective mixing rate and a diffusion coefficient, respectively, weighted by the factor f_{conv}, and Δz_i is the thickness of layer i. This factor f_{conv} controls the degree of local versus non-local behavior. The scheme reverts to either the non-local or local scheme for $f_{conv} = 1$ or $f_{conv} = 0$, respectively. The f_{conv} is estimated as

$$f_{conv} = \left[1 + \frac{k^{-2/3}}{0.1a}\left(-\frac{h}{L}\right)^{-1/3}\right]^{-1}, \tag{7}$$

where k is the von Karman constant, h is the PBL height, L is the Monin-Obukhov length, and a is set to 7.2. The Mu', Md' and K' were calculated as

$$Mu' = \frac{f_{conv}K(z_{1+1/2})}{\Delta z_{1+1/2}(h - z_{1+1/2})}, \tag{8}$$

$$Md_i' = \frac{Mu'(h - z_{i-1/2})}{\Delta z_i} \tag{9}$$

and

$$K'(z) = K(z)(1 - f_{conv}), \tag{10}$$

where z is the height of the model layer and h is the PBL height. The diffusion coefficient K is calculated as in *Mihailovic* and *Alapaty* (2007). This method was chosen because it takes into account the level of TKE, which is a decisive parameter in the vertical mixing within the PBL. In the PBL, K is calculated as

$$K(z) = \frac{\overline{e}_* kz\left(1 - \frac{z}{h}\right)^2}{\phi}, \tag{11}$$

where $\overline{e}_*$ is the mean turbulent velocity scale within the PBL, k is the von Karman constant, z is the vertical coordinate, h is the PBL height, and ϕ is the atmospheric stability function for temperature (Eqs. (2-3)). The mean turbulent velocity scale within the PBL is calculated as

$$\overline{e_*} = \frac{1}{h}\int_0^h \sqrt{e(z)}\Psi(z)dz, \tag{12}$$

where Ψ is the vertical profile function (see *Mihailovic* and *Alapaty* (2007) for details about this function) and e is TKE.

The TKE vertical profile, $e(z)$, for near neutral to free convection conditions (*Zhang et al.*, 1996) is expressed as

$$e(z) = \frac{1}{2}\left(\frac{L_E}{h}\right)^{\frac{2}{3}}\left(0.4w_*^3 + u_*^3(h - z)\frac{\phi}{kz}\right)^{\frac{2}{3}}, \tag{13}$$

where h is the PBL height, $L_E = 2.6h$, w_* is the convective velocity scale, u_* is the friction velocity scale, k is the von Karman constant, and ϕ is a non-dimensional function of heat. For the stable atmospheric boundary layer, we modeled the TKE profile using an empirical function (*Lenschow et al.*, 1988) based on aircraft observations:

$$e(z) = 6u_*\left(1 - \frac{z}{h}\right)^{1.75}, \tag{14}$$

where h is the PBL height, z is the height of the model layer, and u_* is the friction velocity scale. Above the PBL, the diffusion coefficient K is calculated using Eq. (4).

2.3. Short description and model setups

The EMEP chemical model is designed to describe the transboundary acidification, eutrophication, and ground level ozone in Europe and has influenced European air quality policies since the late 1970s. Since the 1990s, this model has provided the reference inputs for the integrated assessment modeling atmospheric dispersion calculations. The Unified EMEP chemical model was developed at the Norwegian Meteorological Institute. In this work, tests were performed using the rv3.0 version of this model (*Simpson et al.*, 2003). The model advection is designed using a scheme by *Bott* (1989a, 1989b); the diffusion scheme, which is described in Section 2.1, is used for the turbulent vertical mixing. The Unified EMEP chemical model emissions inputs are provided for 10 anthropogenic source sectors and consist of gridded annual national emissions of sulfur dioxide (SO2), nitrogen oxides (NOx= NO + NO2), ammonia (NH3), non-ethane volatile organic compounds (NMVOC), carbon monoxide (CO), and particulates (PM2.5, PM10). The meteorological fields used in the model are provided every 3 hours from PARLAM-PS, which is a dedicated version of the HIRLAM (High Resolution Limited Area Model) Numerical Weather Prediction (NWP) model with parallel architecture (*Bjorge* and *Skalin*, 1995; *Berge* and *Jakobsen*, 1998; *Lenschow* and *Tsyro*, 2000). The linearly interpolated 3-hour meteorological fields, wind components, temperature and humidity, cloudiness, precipitation, and momentum and energy fluxes between the surface and atmosphere are then used to calculate the velocity scales, PBL height, and Monin-Obukhov length in every model time step. Note that we calculate new mixing levels using meteorological parameters from the meteorological model that has its own mixing. The parameters imported from PARLAM-PC are the friction velocity and energy fluxes. These parameters come from the Monin-Obukhov theory, that has been widely accepted as the best theory for the surface layer with the implicit assumption that the rest of the PBL mixing should be improved. The Unified EMEP model uses a polar-stereographic projection, true at 60° N, with a grid size of 50×50 km^2 and a vertical σ coordinate with 20 levels. The horizontal grid of the model is the Arakawa C grid. All other model details can be found in *Simpson et al.* (2003). The domain with (131, 100) points is used in the simulations with a 1200 s time step and with the 3-hour resolution meteorological data from the PARLAM-PS model.

2.4. EMEP measurement network

The EMEP measurement network was one of the first international environmental measurement networks established in Europe. The data sets from that network are

well documented, quality controlled, and suitable for comparing with model results. All details on measurement techniques, location of stations, and data sets can be found at http://www.nilu.no/projects/ccc/emepdata.html. The observed values from the EMEP measurement network have already been used in many papers for testing various mixing schemes as well as for other chemical transport studies (*Topçu et al.*, 2002; *Mihailovic* and *Alapaty*, 2007; *Mihailovic et al.*, 2009; *Calvo et al.*, 2010). In this study, we analyze the influence of the ACM2 scheme for vertical mixing in the PBL on the quality of the model's performance. For comparison, we have chosen the year 2005 and compared our results against surface concentration measurements of NO_2 ($\mu g\, N\, m^{-3}$), SO_2 ($\mu g\, S\, m^{-3}$), and SO_4^{2-} ($\mu g\, S\, m^{-3}$) from the EMEP stations because of their good spatial and temporal resolutions. Furthermore, these three compounds were chosen because they are important acidifying and atrophying pollutants and play a significant role in air pollution in Europe. Nitrogen contributes to the formation of photochemical smog, which can have significant impacts on human health. Sulphate, an oxidant of SO_2, is a secondary pollutant that contributes to acid rain formation. Mixing in the lower part of the PBL will influence mostly those tracers that have sources on the ground. This is not the case with ozone, the daytime concentration of which is primarily controlled by photochemistry and transport rather than the vertical mixing; therefore, the interpretation of the influence of vertical mixing on ozone concentrations is much more difficult (*Pleim*, 1992). Note that the Unified EMEP chemical model outputs cannot be always compared with observations in this network because of the coarse horizontal model resolution, which is especially pronounced at high altitudes. Additionally, a problem is encountered with the shipping emission path, because the high concentrations are horizontally diffused over a large area. The differences between the observed and modeled concentrations might be due to other reasons, such as stations can be affected by local sources, emissions, meteorology, and chemistry, among others. Some mountain stations (e.g., SK002R, DE003R, PL003R, and DE008) and some stations in the North Sea shipping area (e.g., DK005R, DE008R, and EE011R) with the highest discrepancies were excluded from the comparison (*Jericevic et al.*, 2010).

3. The results and discussion

The Unified EMEP model Version rv3.0 was first run with the OLD scheme with the setup described in Section 2.3. Whenever a new scheme is introduced into a model, the first step in the analysis usually concerns the differences between the new and the old vertical mixing schemes, especially for the chemical species that originate in the ground. At this moment, the full importance of comparing with the OLD scheme becomes evident. If just one aspect of the model is changed and the result improves, then it is very likely that the introduced change was the

reason for the improvement. Clearly, this may not be always true in a complex meteorological-chemistry model. Then, if there is some sensitivity to introducing a new scheme, the model results are compared with the measurements if they are available. Eventually, better results with the new scheme suggest that it should be used in the Unified EMEP model. In our analysis, we will concentrate on the monthly averaged value of concentrations for the four aforementioned compounds. However, to be absolutely sure that a scheme is stable and that the monthly averaged value of concentrations is not a consequence of very low or very high peaks in daily concentrations, it is necessary to evaluate the daily concentrations in this scheme.

In addition to monthly averages, we will also present some diurnal variations as well as annual averages. For that purpose, we will use a few stations from the EMEP measurement network that are at different locations and altitudes. Station AT0002R is a measurement site located in Illmitz, Austria, at 47° 46'N, 16° 46'E and at an altitude of 117 m above sea level; station DE0001R is a measurement site located in Westerland, Germany, at 54° 56'N, 08° 19'E and at an altitude of 10 m above sea level; the station CZ0001R is a measurement site located in Svratouch, Czech Republic, at 49° 44'N, 16° 02'E and at an altitude of 737 m above sea level; station FR0012R is a measurement site located in Iraty, France, at 43° 02'N, 01° 05'W and at an altitude of 1300 m above sea level; and station DE0007R is a measurement site located in Neuglobsow, Germany, at 53° 09'N, 13° 02'E and at an altitude of 62 m above sea level. The annual time series of daily NO_2 and SO_2 concentrations at the stations AT0002R, DE0001R, and CZ0001R are depicted in *Fig. 1* and *2*, respectively, while the daily SO_4^{2-} concentrations at the stations FR0012R, DE0007R, and CZ0001R are shown in *Fig. 3*. The surface concentrations of NO_2 obtained by the ACM2 scheme at all stations are higher than those obtained with the OLD scheme. The differences between the concentrations of SO_2 and SO_4^{2-} obtained with the ACM2 and OLD schemes are not as pronounced as with the NO_2 concentrations. The root mean square error (RMSE) and mean annual concentration (MAC) for the above-mentioned stations are shown in *Tables 1-3* for the concentrations of NO_2, SO_2, and SO_4^{2-}, respectively. The RMSE values for the NO_2 concentrations are lower when the ACM2 scheme was used at the stations AT0002R and CZ0001R and higher for station DE0001R. The mean annual concentrations of NO_2 obtained by the ACM2 scheme at all stations are closer to the measured mean annual concentrations. The RMSE and MAC values obtained with the OLD and ACM2 schemes are very similar for the concentrations of SO_2 and SO_4^{2-}. The scatter plot diagrams with coefficient of determination (R^2) between measured and modeled concentrations with the OLD and ACM2 schemes for NO_2, SO_2, and SO_4^{2-} at mentioned stations are showed in *Fig. 4*. The R^2 between daily measured and modeled data is slightly higher when the ACM2 scheme is used than the OLD scheme for the concentrations of NO_2 and SO_2 and opposite for the concentration of SO_4^{2-}.

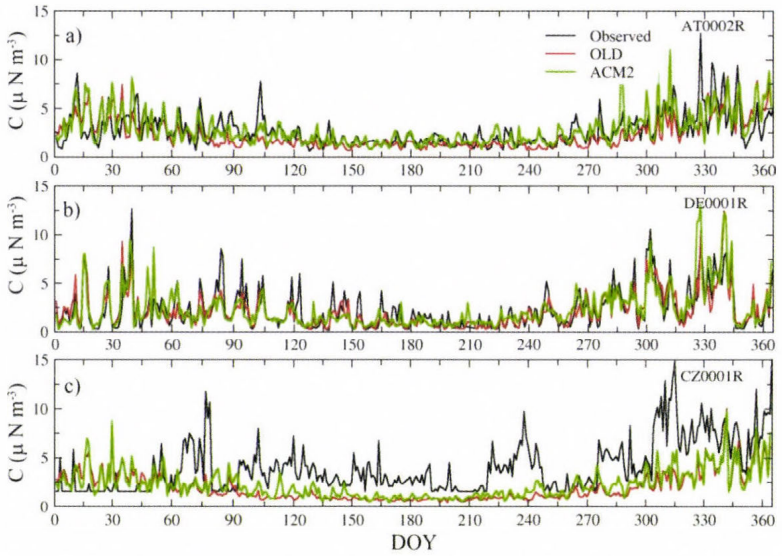

Fig. 1. Time series of the measured and modeled daily surface NO2 concentrations for a) AT0002R, b) DE0001R, and c) CZ0001R in the year 2005. Modeled results are obtained with two vertical diffusion schemes: OLD and ACM2. The time is shown on the x-axis as the day of the year (DOY).

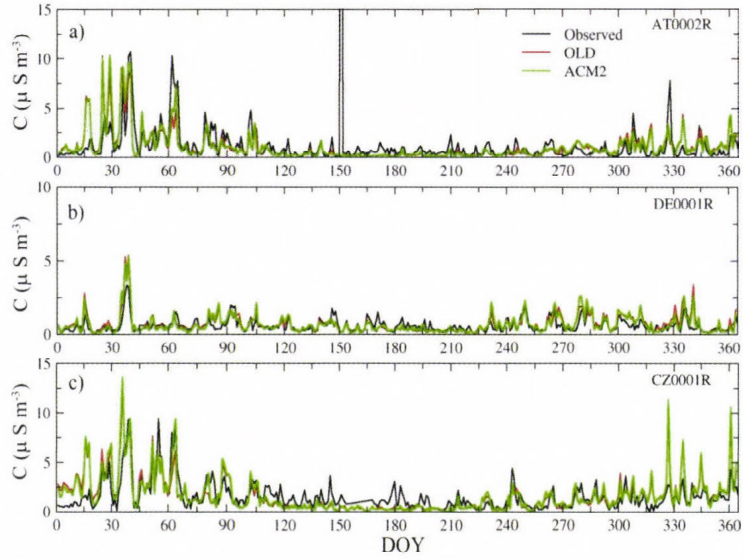

Fig. 2. Time series of the measured and modeled daily surface SO2 concentrations for a) AT0002R, b) DE0001R, and c) CZ0001R in the year 2005. The modeled results are obtained with two vertical diffusion schemes: OLD and ACM2. The time is shown on the x-axis as the day of the year (DOY).

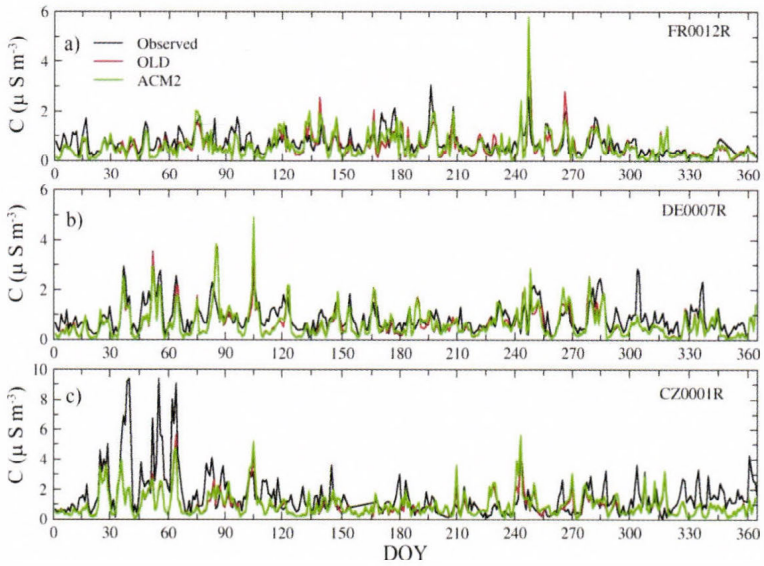

Fig. 3. Time series of the measured and modeled daily surface SO_4^{2-} concentrations for a) FR0012R, b) DE0007R, and c) CZ0001R in the year 2005. Modeled results are obtained with two different vertical diffusion schemes: OLD and ACM2. The time is shown on the x-axis as the day of the year (DOY).

Table 1. RMSE and mean annual concentration of NO_2

Station	RMSE (OLD)	RMSE (ACM2)	MAC(OLD) (μg N m^{-3})	MAC(ACM2) (μg N m^{-3})	MAC (observed) (μg N m^{-3})
AT0002R	1.66	1.59	2.26	2.82	2.69
DE0001R	1.30	1.52	2.16	2.33	2.33
CZ0001R	3.21	2.96	1.91	2.23	4.00

Table 2. RMSE and mean annual concentration of SO_2

Station	RMSE (OLD)	RMSE (ACM2)	MAC(OLD) (μg S m^{-3})	MAC(ACM2) (μg S m^{-3})	MAC(observed) (μg S m^{-3})
AT0002R	3.45	3.45	1.05	1.09	1.25
DE0001R	0.45	0.44	0.70	0.67	0.59
CZ0001R	1.43	1.47	1.56	1.67	1.72

Table 3. RMSE and mean annual concentration of SO_4^{2-}

Station	RMSE (OLD)	RMSE (ACM2)	MAC(OLD) (μg S m^{-3})	MAC(ACM2) (μg S m^{-3})	MAC (observed) (μg S m^{-3})
FR0012R	0.43	0.43	0.56	0.58	0.70
DE0007R	0.49	0.52	0.62	0.63	0.88
CZ0001R	1.37	1.39	0.92	1.00	1.56

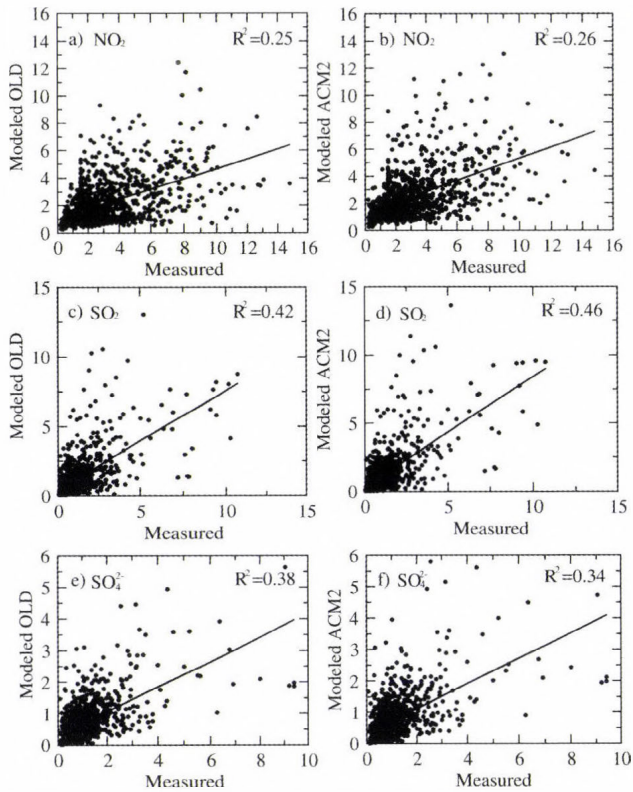

Fig. 4. Scatter plot diagrams of modeled against measured daily concentrations with corresponding coefficients of determination. Panels are: concentration of NO2 modeled by a) OLD and b) ACM2; concentration of SO2 modeled by c) OLD and d) ACM2, and concentration of SO_4^{2-} modeled by e) OLD and f) ACM2.

After the analysis of the daily concentrations showed that there are no peaks in this concentration, we compared the average monthly concentrations at the stations from the EMEP network, except those mentioned in Section 2.4 with the model results obtained using the OLD and ACM2 schemes. The scatter plot

diagrams with R^2 between monthly concentrations of NO_2, SO_2, and SO_4^{2-} calculated using the OLD and ACM2 scheme and corresponding measured concentrations are depicted in *Fig. 5*. The R^2 between monthly measured and modeled data using the OLD and ACM2 scheme are very similar for all compounds. To compare the results, we calculated the following statistical quantities: (i) RMSE, (ii) BIAS, and (iii) standard deviations of the simulations (SDS) and observations (SDO). These quantities are given by the following equations:

$$\mathrm{RMSE} = [\sum_{i=1}^{N_s} (M_i - O_i)^2 / N_s]^{1/2} , \tag{15}$$

$$\mathrm{BIAS} = \left(\frac{\overline{M} - \overline{O}}{\overline{O}} \right) \cdot 100\% , \tag{16}$$

$$\mathrm{SDS} = [\sum_{i=1}^{N_s} (M_i - \overline{M})^2 / N_s]^{1/2} , \tag{17}$$

$$\mathrm{SDO} = [\sum_{i=1}^{N_s} (O_i - \overline{O})^2 / N_s]^{1/2} , \tag{18}$$

where M_i and O_i denote the modeled and observed average monthly concentrations, respectively, and N_s is the number of stations, while an over bar indicates an average monthly concentration for all stations.

Biases for the measured and modeled average monthly NO_2, SO_2, and SO_4^{2-} concentrations for both schemes are shown in *Fig. 6*. In the upper panel of this figure, the BIAS of the ACM2 scheme is observed to be lower than that of the OLD scheme. Both schemes underestimate the observations during the warmer months, but the ACM2 scheme overestimates the observed NO_2 concentration in the colder months. Inspecting the BIAS for SO_2 (middle panels of the same figure) does not show larger differences in the BIAS for the OLD and ACM2 schemes. Both schemes underestimate the SO_2 observations during the warmer months and overestimate them during the colder months. The BIAS of the ACM2 scheme for SO_4^{2-} (lower panels of the same figure) is lower than for the OLD schemes. Both schemes underestimate the SO_4^{2-} observations except for September, when the ACM2 scheme overestimates the observations. The higher BIAS obtained for SO_4^{2-} may be due to many complicated processes, including microphysics and aqueous phase reactions, connected with this particular compound. Our understanding of *Fig. 6* is as follows: in the colder part of the year, the atmosphere is basically stable; therefore, the diffusive part of the ACM2 scheme has a greater contribution to its

performance. In contrast to the colder months, the warmer months are more influenced by the non-local part of the ACM2 scheme. The smaller BIAS between the modeled and observed concentrations for the ACM2 scheme indicates that the average estimated concentrations are closer to the average observed concentrations.

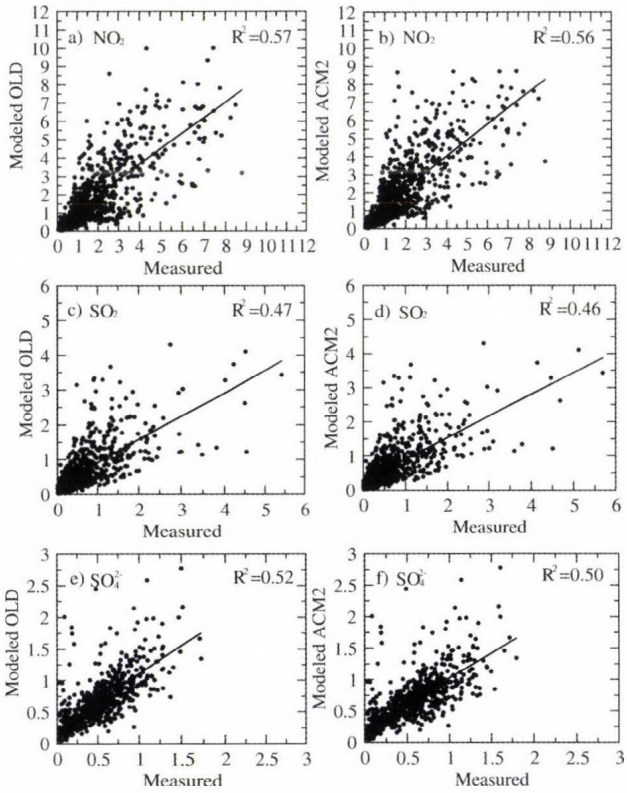

Fig. 5. Scatter plot diagrams of modeled against measured monthly concentrations with corresponding coefficients of determination. Panels are: concentration of NO2 modeled by a) OLD and b) ACM2; concentration of SO2 modeled by c) OLD and d) ACM2, and concentration of SO_4^{2-} modeled by e) OLD and f) ACM2.

The RMSE is a good measure in this type of comparison, and *Fig. 7* shows the RMSE for the measured and modeled average monthly NO_2, SO_2, and SO_4^{2-} concentrations for both schemes. In the upper panel of this figure, the RMSE of the ACM2 scheme is shown to be slightly lower than that for the OLD scheme, except January and December. A further inspection of the RMSE for SO_2 and SO_4^{2-} (middle and lower panels of the same figure) shows that the non-local scheme and the OLD scheme show similar behavior, i.e., SO_2 and SO_4^{2-} are very similar.

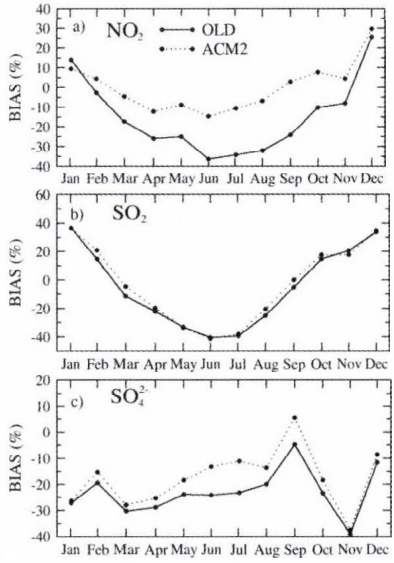

Fig. 6. Average monthly BIAS (%) for the observed and modeled (a) NO_2, (b) SO_2 and (c) SO_4^{2-} concentrations for the ACM2 and OLD schemes used in the Unified EMEP chemical model for 2005.

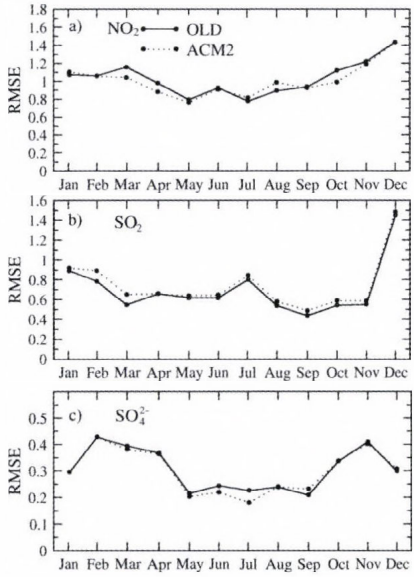

Fig. 7. Average monthly RMSE values for the observed and modeled concentrations of (a) NO2, (b) SO2, and (c) SO_4^{2-} for the ACM2 and OLD schemes used in the Unified EMEP chemical model for 2005.

The final statistics compared are the standard deviations of the observed and modeled concentrations. The standard deviations of the average monthly observed and modeled concentrations (SDS and SDO), given by Eqs. (17)–(18), are depicted in *Fig. 8*. The scheme is considered to give better results if its SDS is closer to its SDO. It can be concluded from this figure that (i) the SDS for both schemes are higher for colder months except for SO_4^{2-}, and that (ii) the SDS for the ACM2 scheme is much closer to the SO_4^{2-} SDO. For both schemes, the SDS values are similar for some months, indicating that they have the same yearly pattern.

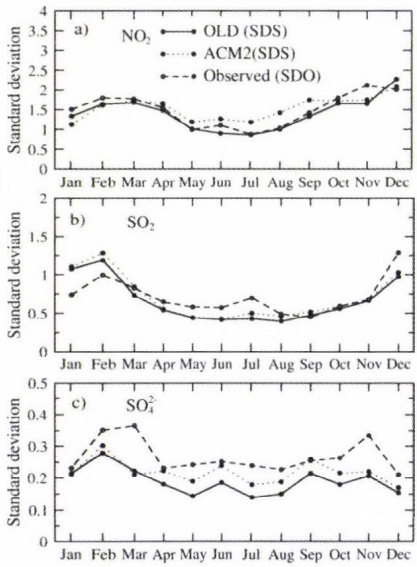

Fig. 8. Average monthly SDO and SDS values of (a) NO_2, (b) SO_2, and (c) SO_4^{2-} for the ACM2 and OLD schemes used in the Unified EMEP chemical model for 2005.

4. Conclusions

The ACM2 scheme was incorporated into a Unified EMEP model. Comparisons between the already present scheme and the new one were made, and sensitivity was demonstrated. Furthermore, the outputs of NO_2, SO_2, and SO_4^{2-} surface concentrations for both schemes were compared with the measured values. In most cases, it was shown that the Unified EMEP chemical model slightly better simulates the concentrations of NO_2, SO_2, and SO_4^{2-} when the ACM2 scheme is used. The sensitivity of the NO_2 concentrations to the choice of vertical scheme is much higher than for the other analyzed compounds. The lifetime of NO_2 in troposphere is short and has a seasonal variability. It is the shortest during the

summer months. Additionally, during the summer months the mixing driven by bouncy is fast. Those are the reasons why the sensitivity of the NO_2 concentrations to the choice of vertical scheme is much higher than for the other analyzed compounds, and it is particularly emphasized for their concentrations during the summer months. Let us note that the lifetime of both compounds, SO_2 and SO_4^{2-} is longer than that of NO_2, so it is more influenced by the horizontal advection than by vertical mixing. Overall, the agreement with the measured values is reasonably good, such that the ACM2 scheme could be used in the Unified EMEP model. Furthermore, as the ACM2 scheme possesses a higher level of sophistication, it is expected that its influence will be higher with the increased horizontal resolution of the Unified EMEP model.

Acknowledgements–This paper was realized as a part of the project "Studying climate change and its influence on the environment: impacts, adaptation and mitigation" (No. III43007), which is financed by the Ministry of Education and Science of the Republic of Serbia within the framework of integrated and interdisciplinary research over the period 2011-2014. The authors would like to thank the Norwegian Meteorological Institute for giving us the meteorology inputs for the Unified EMEP chemical model for 2005.

References

Alapaty, K., 2003: Development of two CBL schemes using the turbulence velocity scale. Proceedings of 4thWRF Users' workshop, Boulder (http://www.wrf-model.org/wrfadmin/presentations.php).

Alapaty, K. and *Alapaty, M.*, 2001: Evaluation of a nonlocal-closure K-scheme using the MM5. Workshop Program for the Eleventh PSU/NCAR MM5 Users' Workshop, Foothills Laboratory, NCAR (http://www.mmm.ucar.edu/mm5/workshop/).

Baklanov, A. and *Korsholm, U.*, 2007: On-line integrated meteorological and chemical transport modeling: Advantages and Prospectives. In (Eds.: *Borrego, C.* and *Miranda, A.I.*) Proceedings of the 29th NATO/CCMS International Technical Meeting on Air pollution Modelling and its Application, 24–28 September 2007, Aveiro.

Berg, L.K. and *Zhong, S.*, 2005: Sensitivity of MM5-simulated boundary layer characteristics to turbulence parameterizations. *J. Appl. Meteor. 44*, 1467–1483.

Berge, E. and *Jakobsen, H.A.*, 1998: A regional scale multi-layer model for the calculation of long-term transport and deposition of air pollution in Europe. *Tellus 50*, 205–223.

Bjorge, D. and *Skalin, R.*, 1995: PARLAM – the parallel HIRLAM version at DNMI. Research Report, No.27, Norwegian Meteorological Institute, Oslo.

Blackadar, A.K., 1976: Modeling the nocturnal boundary layer. Preprints, 3rd Symposium on Atmospheric Turbulence, Diffusion and Air Quality, Raleigh, NC, 19–22 October 1976, *Amer. Meteor. Soc.*, 46–49.

Blackadar, A.K., 1979: High resolution models of the planetary boundary layer. In (Eds. Pfaffin, J.R., and Ziegler, E.N.) Advances in environment and scientific engineering, Vol. 1, Gordon and Breach, Newark, 50–85.

Bott, A., 1989a: A positive definite advection scheme obtained by non-linear re-normalization of the advection uses. *Mon. Weather Rev. 117*, 1006–1015.

Bott, A., 1989b: Reply. *Mon. Weather Rev. 117*, 2633–2636.

Calvo, A.I., Olmo, F.J., Lyamani, H., Alados-Arboledas, L., Castro, A., Fernández-Raga, M., and *Fraile, R.*, 2010: Chemical composition of wet precipitation at the background EMEP station in Víznar (Granada, Spain) (2002–2006). *Atmos. Res. 96*, 408–420.

Deardorff, J.W., 1972: Theoretical expression for the countergradient vertical heat flux, *J. Geophys. Res. 77(30)*, 5900–5904.

Holtslag, A.A.M., and *Boville, B.A.*, 1993: Local versus nonlocal boundary-layer diffusion in a global climate model. *J. Climate 6*, 1825–1842.

Holtslag, A.A.M., and *Moeng, C.-H.*, 1991: Eddy diffusivity and countergradient transport in the convective atmospheric boundary layer. *J. Atmos. Sci. 48*, 1690–1698.

Hong, S.Y., and *Pan, H.L.*, 1996: Nonlocal boundary layer vertical diffusion in a Medium-Range Forecast model. *Mon. Weather Rev. 124*, 2322–2339.

Hu, X.-M., Nielsen-Gammon, J.W., and *Zhang, F.*, 2010: Evaluation of three planetary boundary layer schemes in the WRF model. *J. Appl. Meteor. Climatol. 49*, 1831–1844.

Janjic, Z.I., 1990: The step-mountain coordinate: Physical package. *Mon. Weather Rev. 118*, 1429–1443.

Janjic, Z.I., 1994: The step-mountain Eta coordinate model: Further development of the convection, viscous sublayer and turbulent closure schemes. *Mon. Weather Rev. 122*, 927–945.

Jericevic, A., Kraljevic, L., Grisogono, B., Fagerli, H., and *Vecenaj, Z.*, 2010: Parameterization of vertical diffusion and the atmospheric boundary layer height determination in the EMEP model. *Atmos. Chem. Phy. 10*, 341–364.

Lenschow, D.H., Li, X.S., and *Zhu, C.J.*, 1988: Stably stratified boundary layer over the Great Plains. Part I: Mean and turbulent structure. *Bound.-Layer Meteor. 42*, 95–121.

Lenschow, S., and *Tsyro, S.*, 2000: Meteorological input data for EMEP/MSC-W air pollution models. EMEP MSC-W Note 2/2000.

Louis, J., 1979: A parametric model of vertical eddy fluxes in the atmosphere. *Bound.-Layer Meteor. 17*, 187–202.

Mellor, G.L., and *Yamada, T.*, 1974: A hierarchy of turbulence closure models for planetary boundary layers. *J. Atmos. Sci. 31*, 1791–1806.

Mihailovic, D.T., and *Alapaty, K.*, 2007: Intercomparison of two K-schemes: local versus non-local in calculating concentrations of pollutants in chemical and air-quality models. *Environ. Model. Softw. 22*, 1685–1689

Mihailovic, D.T., Alalapaty, K., and *Sakradzija, M.*, 2008: Development of a non-local convective mixing scheme with varying upward mixing rates for use in air quality and chemical transport models. *Environ. Sci. Pollut. Res. 15*, 296–302.

Mihailovic, D.T., Alapaty, K., and *Podrascanin, Z.*, 2009: The combined non-local diffusion and mixing schemes, and calculation of in-canopy resistance for dry deposition fluxes. *Environ. Sci. Pollut. Res. 16*, 144–151.

O'Brien, J.J., 1970: A note on the vertical structure of the eddy exchange coefficient in the planetary boundary layer. *J. Atmos. Sci. 27*, 1213–1215.

Pleim, J.E., and *Chang, J.S.*, 1992: A non-local closure model for vertical mixing in the convective boundary layer. *Atmos. Environ. 26A*, 965–981.

Pleim, J.E., 2007a: A combined local and nonlocal closure model for the atmospheric boundary layer. Part I: Model description and testing. *J. Appl. Meteorol. Clim. 46*, 1383–1395.

Pleim, J.E., 2007b: A combined local and non-local closure model for the atmospheric boundary layer. Part 2: Application and evaluation in a mesoscale model, *J. Appl. Meteor. Clim. 46*, 1396–1409.

Simpson, D., Fagerli, H., Jonson, J.E., Tsyro, S., Wind, P., and *Tuovinen, J.-P.*, 2003: Transboundary acidification and eutrophication and ground level ozone in Europe: Unified EMEP Model Description, EMEP Status Report 1/2003 Part I, EMEP/MSC-W Report, The Norwegian Meteorological Institute, Oslo.

Stull, R.B., 1984: Transilient turbulence theory. Part I: The concept of eddy mixing across finite distances. *J. Atmos. Sci. 41*, 3351–3367.

Topçu, S., Incecik, S., and *Atimtay, A.T.*, 2002: Chemical composition of rainwater at EMEP station in Ankara, Turkey. *Atmos. Res. 65*, 77–92.

Zhang, D.L., and *Zheng, W.Z.*, 2004: Diurnal cycles of surface winds and temperatures as simulated by five boundary layer parameterizations. *J. Appl. Meteor. 43*, 157–169.

Zhang, C., Randall, D.A., Moeng, C.-H., Branson, M., Moyer, M., and *Wang, Q.*, 1996: A surface parameterization based on vertically averaged turbulence kinetic energy. *Mon. Weather Rev. 124*, 2521–2536.

IDŐJÁRÁS

Quarterly Journal of the Hungarian Meteorological Service
Vol. 117, No. 3, July–September 2013, pp. 295–314

Lightning behavior during the lifetime of severe hail-producing thunderstorms

Tsvetelina Dimitrova [1], **Rumjana Mitzeva** [2*], **Hans D. Betz** [3, 4], **Hristo Zhelev** [1, 2], and **Sebastian Diebel** [4]

[1] *Agency Hail Suppression, 17 Hristo Botev Blvd., 1606 Sofia, Bulgaria, E-mail: dimitrova_tsvetelina@abv.com*

[2] *Faculty of Physics, University of Sofia, 5 J. Bourchier Blvd.1164 Sofia, Bulgaria,*

[3] *University of Munich, Department of Physics, D-85748 Garching Germany, E-mail:hans-dieter.betz@physik.uni-muenchen.de*

[4] *Nowcast GmbH, Sauerbruchstraße 48, 81377 Munich, Germany, E-mail: sebastian.diebel@nowcast.de*

**Corresponding author; E-mail address: rumypm@phys.uni-sofia.bg*

(Manuscript received in final form November 6, 2012)

Abstract– Results from an analysis of total lightning (cloud-to-ground and intracloud) behavior during the lifetime of severe hail-producing thunderstorms are presented. The analysis was carried out for different types of storms: multicell, supercell, and multicell which evolved into supercell storms. The study reveals: (1) There is a positive time lag between the jumps of both multiplicity and flash rate and the beginning of large hail in the three analyzed thunderstorms. (2) The mean and maximum values of total flash rate, as well as the multiplicity of negative total strokes in the multicell and supercell storms are remarkably lower than for the multicell that became supercell storm. (3) Significant numbers of positive total strokes are detected in both supercell and multicell which evolved into supercell storms. The highest percentage of positive strokes is observed during the period of large hail falls on the ground. (4) The jump of lightning density is observed before large hail fall in the three storms, following a dramatic decrease of the lightning rate during the beginning of the hail fall. In the supercell storm the lightning "hole" occurred, associated with an existence of bounded weak-echo region of the cell.

Key-words: total lightning; flash rate; multiplicity; lightning density; hail; radar reflectivity

1. Introduction

The relationship between lightning and thunderstorm severity (large hail, heavy rain leading to flash flooding, strong wind, and tornado) has been subject of studies for more than 50 years. One of the purposes of these studies has been to evaluate whether lightning characteristics could be used to improve nowcasting of severe thunderstorm events. However, the results related to lightning characteristics during the lifetime of severe thunderstorms are often contradictory in the numerous studies.

In previous studies it is noted that severe storms are characterized by higher total flash rates than ordinary non-severe storms. The more intense the storm the more lightning is produced (*Maier* and *Krider*, 1982; *Taylor*, 1973; *Turman* and *Tettelbach*, 1980). *Williams* (1985) explained this link with the intensification of the updrafts. The correlation between updraft and flash rate is also established by *Deierling* and *Petersen* (2008), *Goodman et al.* (2005), and *Wiens et al.* (2005).

However, there are severe storms that are characterized by low cloud-to-ground flash rates. Low CG flash rates are observed when hail was produced in two thunderstorms studied by *Lang et al.* (2000). In both studied storms, radar reflectivity and the production of hail were anti-correlated with the production of significant negative cloud-to-ground lightning. The authors explained this with the elevation charge hypothesis (*MacGorman et al.*, 1989) and suggested that low production of negative CGs can be explained by the production of significant quantities of hail, high IC flash rates, and strong updrafts. In hail - bearing storms, studied by *Soula et al.* (2004), the CG rate does not exceed 2 min^{-1} when the cells produce hail, while it can reach up to 12 min^{-1} for heavy precipitating storms.

According to some studies, the cloud-to-ground (CG) lightning frequency decreases when hail forms in the cloud (*Lang et al.*, 2000; *Soula et al.*, 2004). *Williams et al.* (1999) found that peak flash rate precedes severe weather at the ground by 5–20 min. Their analysis showed that "A distinguished feature of severe storms is the presence of lightning "jumps"– abrupt increases in flash rate in advance of the maximum rate for the storm". *Kane* (1991) obtained similar results – tornadoes and large hail occurred about 10–15 min after the peak of the 5-min cloud-to-ground lightning rate.

Additionally, a change in the polarity ratio is apparent in cases of severe weather: positive CGs are more prevalent than negative ones, resulting in a decrease of negative CG lightning frequency. Some authors (e.g., *Carey* and *Rutledge*, 1998; *Lang et al.*, 2004; *Reap* and *MacGorman*, 1989; *Seimon*, 1993; *Stolzenburg*, 1994; *Wiens et al.*, 2005) reported a relationship between large hail and positive CG lightning. They showed that hailstorms usually produce large hailstones in the active period of positive CG flashes. For example, *MacGorman* and *Burgess* (1994) analyzed the characteristics of CG flashes in 15 severe

storms with large hailstones or tornadoes and found that the large hail occurred during the period when positive ground flashes dominated. In 11 tornadic storms, tornadoes occurred either during or after the period when positive ground flashes dominated. The strongest tornado usually begins after the positive ground flash rate decreases from its maximum value. *Montanya et al.* (2007, 2009) and *Soula et al.* (2004) revealed a reversal of the dominant polarity of the CG flashes from negative to positive during the period when cells produced hail.

Other studies showed that severe weather often occurs without dominating positive strokes. *Bluestein* and *MacGorman* (1998) and *Curran* and *Rust* (1992) reported that within the hailstorms they had studied, the negative cloud-to-ground flashes dominated.

Carey et al. (2003) analyzed severe storms for a period of 10 years (1989–1998) and came to the conclusion that there was a significant regional variability in the percentage of positive CG lightning produced by severe storms during the warm season. It is assumed that the geographical preference of positive storms is linked to specific meteorological conditions of the region. For this reason, some authors (*Gilmore* and *Wicker*, 2002; *MacGorman* and *Burgess*, 1994; *Smith et al., 2000*; *Williams et al.*, 2005) explored the relationships between the environmental conditions and CG lightning. Based on the hypothesis that mesoscale environment indirectly influences lightning polarity of the storms by directly controlling storm structure, dynamics, and microphysics which in turn control storm electrification, the analysis of *Carey* and *Buffalo* (2007) demonstrated significant and systematic differences in environmental conditions of positive and negative storms.

Lang and *Rutledge* (2002) analyzing 11 thunderstorms came to the conclusion that "The only significant differences between intense storms that produced predominately positive cloud-to-ground (CG) lightning for a significant portion of their lifetimes (PPCG storms) and intense storms that produced little CG lightning of any polarity (low-CG storms) was that PPCG storms featured much larger volumes of significant updrafts and produced greater amounts of precipitation (both rain and hail)".

Different authors reported various values of multiplicity. For example: *Soula et al.* (2004) obtained values from 1.9 to 2.6 for the negative CG flashes and from 1.0 to 1.2 for the positive ones, while *Carey et al.* (2003) obtained similar values of mean positive and negative CG multiplicity (1.2 and 1.1, respectively) for the analyzed supercell.

The interesting feature of lightning behavior during the lifetime of a severe storm is the presence of a lightning "hole" (areas of week or even zero total lightning density surrounded by larger values). The existence of a hole is reported by many authors (*Goodman et al.*, 2005; *Lang et al.*, 2004; *MacGorman et al.*, 2005; *McKinney et al.*, 2008; *Murphy* and *Demetriades*, 2005; *Steiger et al.*, 2007; *Wiens et al.*, 2005). *Lang et al.* (2004) found that the

lightning hole is associated with extremely strong updrafts in the bounded weak echo region of the supercell. This hypothesis is supported by different observations (for example, *Goodman et al.*, 2005; *Steiger et al.*, 2007). However, *Murphy* and *Demetriades* (2005) analyzing two hail-producing supercells reported that the lightning "hole" was not linked to the bounded weak echo region but rather was a manifestation of a more complicated radar structure.

It is clear that conclusions based on the investigations conducted in different geographical regions are often contradictory, because the variability of lightning parameters is linked to several factors, especially latitude, season, location, and climatic conditions (e.g., *Orville*, 2002; *Sheridan*, 1997; *Soriano et al.*, 2001; *Soula et al.*, 2004;). Different types of thunderstorms were studied by *Lang et al.* (2000) and *Ray et al.* (1987) in order to analyze the reasons for the differences in lightning behavior.

Bulgaria is situated in southeast Europe. Within a relatively small area (111 000 km^2), the Bulgarian landscape exhibits a striking topographic variety – large plains and lowlands, valleys and gorges, low and high mountains (up to 2–3 km). The mountains are important factor for the intensification of convection.

From April to September the frequency of thunderstorms in Bulgaria is high. In more than 60% of the days there are thunderstorms and half of them produce hail.

The analyses in *Dimitrova et al.,* (2009) revealed that most of lightning features of the studied severe and non-severe thunderstorms developed over Bulgaria were similar to those in other geographical regions. However, there are some differences in lightning behavior in severe storms that stimulated the analysis of lightning characteristics in different types of severe storms.

The goal of the present paper is to study the lightning behavior in three different types of severe storms produced large hail (diameter more than 2 cm) over Bulgaria. The evolution of lightning characteristics of a multicell, a supercell, and a multicell that evolved into a supercell storm is analyzed together with the radar characteristics.

2. Data

The lightning and volume radar data over the territory of Bulgaria have been available since 2008. Lightning data are taken from the LINET network (*Betz et al.*, 2008). Radar information is obtained from radar network of Hail Suppression Agency in Bulgaria.

The main information about the hail precipitation is regularly obtained using data from the rain gauge network with distance between the gauges of

about 10–12 km. Additional information is given by voluntary observers in towns and villages situated between the rain gauges.

2.1. Radar data

Data from two S-band Doppler radars were used (*Fig. 1*). The one is in North Bulgaria (Bardarski geran village, Vratsa district) and the other is in South Bulgaria (Golyam Chardak village, Plovdiv district).

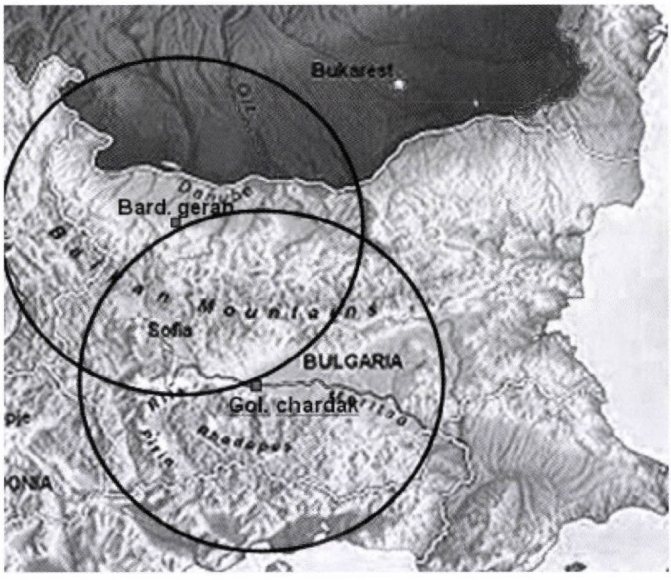

Fig. 1. Range of radar observation. Both radar stations (in Bardarski geran village – North Bulgaria and Golyam Chardak – South Bulgaria) are part of radar network of Hail Suppression Agency in Bulgaria.

Radar data were used to produce horizontal and vertical cross sections of thunderstorm cell structures. These profiles are estimated from volumetric data generated by an automatic scanning at 14 elevation angles. The elevation of the successive scan was increased from 0.2° to 85° with an irregular step while spinning around 360° of azimuth. The full volume scan was performed for 4 minutes in a range of 150 km. IRIS (Interactive Radar Information System) generates products based on this volume scan.

Data for the vertical profile of reflectivity for the storms' cells - maximum reflectivity, height of maximum reflectivity, Hzmax, maximum heights of 15 dBZ, and 45 dBZ contour (H15 and H45 respectively) were analyzed to investigate storm's structure and evolutions.

2.2. Lightning data

The analyzed information for lightning characteristics was taken from the European LINET (Betz et al., 2008).

LINET is a VLF/LF lightning detection network developed at the University of Munich, which provides continuous data for both research and operational purposes. During international co-operations, LINET has been deployed in four continents. LINET covers a wide area approximately from a longitude of –10° to 25° and from latitude of 35° to 66° (*Betz et al.*, 2009). The LINET data set provides information on stroke time, geographical location, height of intra-cloud (IC) events, peak current (PC), and polarity. The discrimination between CG and IC lightning in LINET relies on a TOA (times of arrival) analysis. The corresponding differences in travel time from high- and low-lying emission centers are exploited within the TOA locating algorithm (*Betz et al.*, 2004; *Betz at al.*, 2009). This 3D discrimination method is reliable when the sensor baseline does not exceed ~250 km. Thus, while the sensor geometry in the central part of the network allows locating very weak lightning events with the inclusion of large numbers of IC and reliable discrimination between CG and IC, in the surrounding areas the network reports predominantly the stronger events, which are mainly return strokes (CG) (*Betz et al.*, 2009). Bulgaria is in the edge of the LINET network geometry. To avoid inaccuracies in the separation of IC and CG strokes, total lightning is studied in the present paper.

The lightning characteristics – flash rate (FR), peak current (PC), multiplicity (number of strokes in one flash) Mn, and polarity of total lightning (intra-cloud and cloud-to-ground) were analyzed. The flash rate was calculated per 4 minutes in accordance with the period of radar volume scan.

3. Case studies

Three severe thunderstorms with a different development were studied. One of them was a multi-cellular storm (MC) which developed on August 8, 2010 (*Fig. 2a*). The other one occurred on May 30, 2009 and was an isolated developed supercell (SC) (*Fig. 2c*), while the third one, developed on August 6, 2010, was multicellular and evolved into a supercell storm (MSC) (*Fig. 2b*).

Maximum values of some radar characteristics together with the corresponding temperature given in *Table 1* show that the three thunderstorms had a strong vertical development (the top echo, H15 of thunderstorms reached at altitude of 16–17 km) and intense radar reflectivity echo – 60–65 dBZ. The other similarity between the studied thunderstorms is the long life time (longer than 2 hours) and the registration of large hail (diameter larger than 2 cm) at the ground.

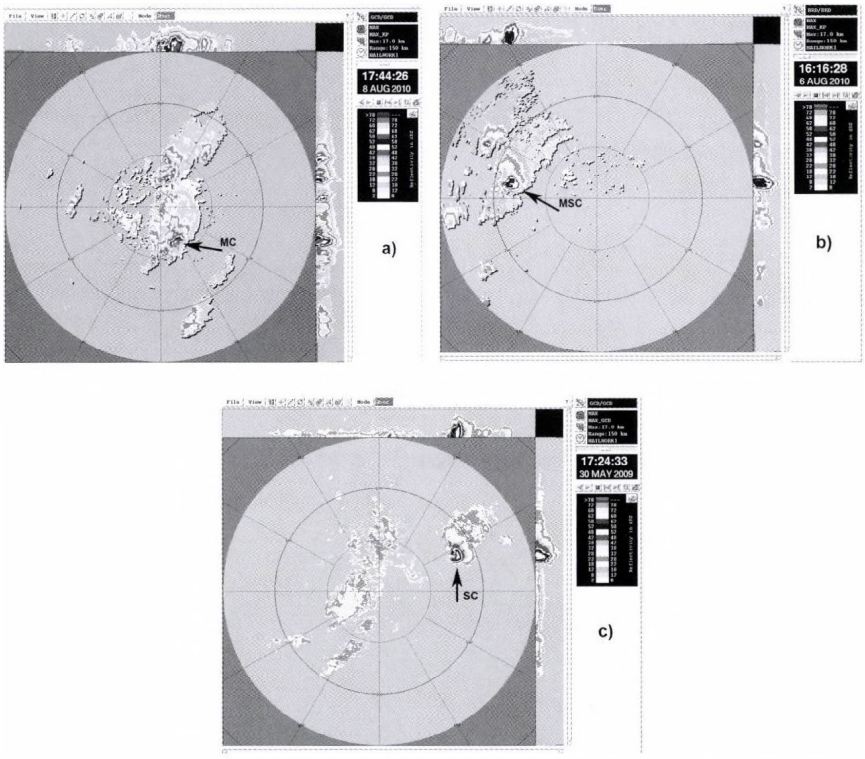

Fig. 2. Radar display of the maximum radar reflectivity [dBZ] obtained by S-band radar in the moment of maximum development of: a) multicell thunderstorm, MC on August 8, 2010 at 1444 UTC (1744 local time); b) multicell evolving into a supercell thunderstorm, MSC on August 6, 2010 at 1316 UTC (16:16 local time); c) supercell storm, SC on May 30, 2009 at 1424 UTC (1724 local time). The range markers identify 50 km separations.

Table 1. Maximum values of some radar characteristics and corresponding temperature in the three studied thunderstorms: multicell thunderstorm, MC; evolved from multicell into supercell thunderstorm, MSC; supercell storm, SC

Max values	**MC**	**MSC**	**SC**
H15 [km]	16.1	16.5	16.9
T_{H15} [°C]	–60.7	–59.2	–60.1
H45 [km]	11.8	13.5	10.9
T_{H45} [°C]	–42.2	–51.0	–54.3
Zmax [dBZ]	65.0	60.0	63.5
Hzmax [km]	8.8	7.9	8.0
T_{Hzmax} [°C]	–28.4	–24.6	–33.1

However, the studied storms had differences in the development and radar structure. From the beginning the SC storm developed as an individual super cell with a rapid vertical development. In 10 minutes the height of 15 dBZ radar echo increased from 7.6 km to 10 km and the maximum reflectivity increased from 35 dBZ to 53.5 dBZ. In the next 10 minutes the maximum reflectivity reached 60 dBZ keeping up these high values (60–65 dBZ) during the next 90 min.

Unlike this storm, both MSC and MC storms started as ordinary non-severe multicell storms. MSC storm underwent a transition from a weak multicellular storm into an intense supercellular storm in the period 1236 UTC – 1300 UTC. The development of MC storm intensified after 1416 UTC. The maximum measured radar reflectivity in MSC storm was 60 dBZ and in MC storm – 65 dBZ.

There is a well pronounced pulse in the vertical development of MC storm and two pulses in MSC storm. These pulses are associated with a sharp increase of H15 and H45 centered around 1416 UTC in the MC storm and around 1236 UTC and 1304 UTC in the MSC storm. The maximum values of H45 in the three studied storms are significantly different (Table 1). In MSC storm, H45 reached 13.5 km and in SC and MC storms – 10.9 and 11.8 km, respectively. Another significant difference between MSC storm and MC and SC storms is the location of region with high radar reflectivity $\geq$ 60 dBZ. The duration of an existence of high radar reflectivity above zero isotherm, H0, in MC storm and in SC storm was about 3 times longer than for MSC storm. (*Fig. 3a, b, c*)

The MC and SC thunderstorms produced hailstones with diameter up to 3 cm and MSC storm up to 6 cm. There is also a significant difference in the duration of large hail falling on the ground from the three thunderstorms – 60 min from MC storm (with interruptions due to the multi-cellular development), 15 min from SC storm, and 26 min from MSC storm.

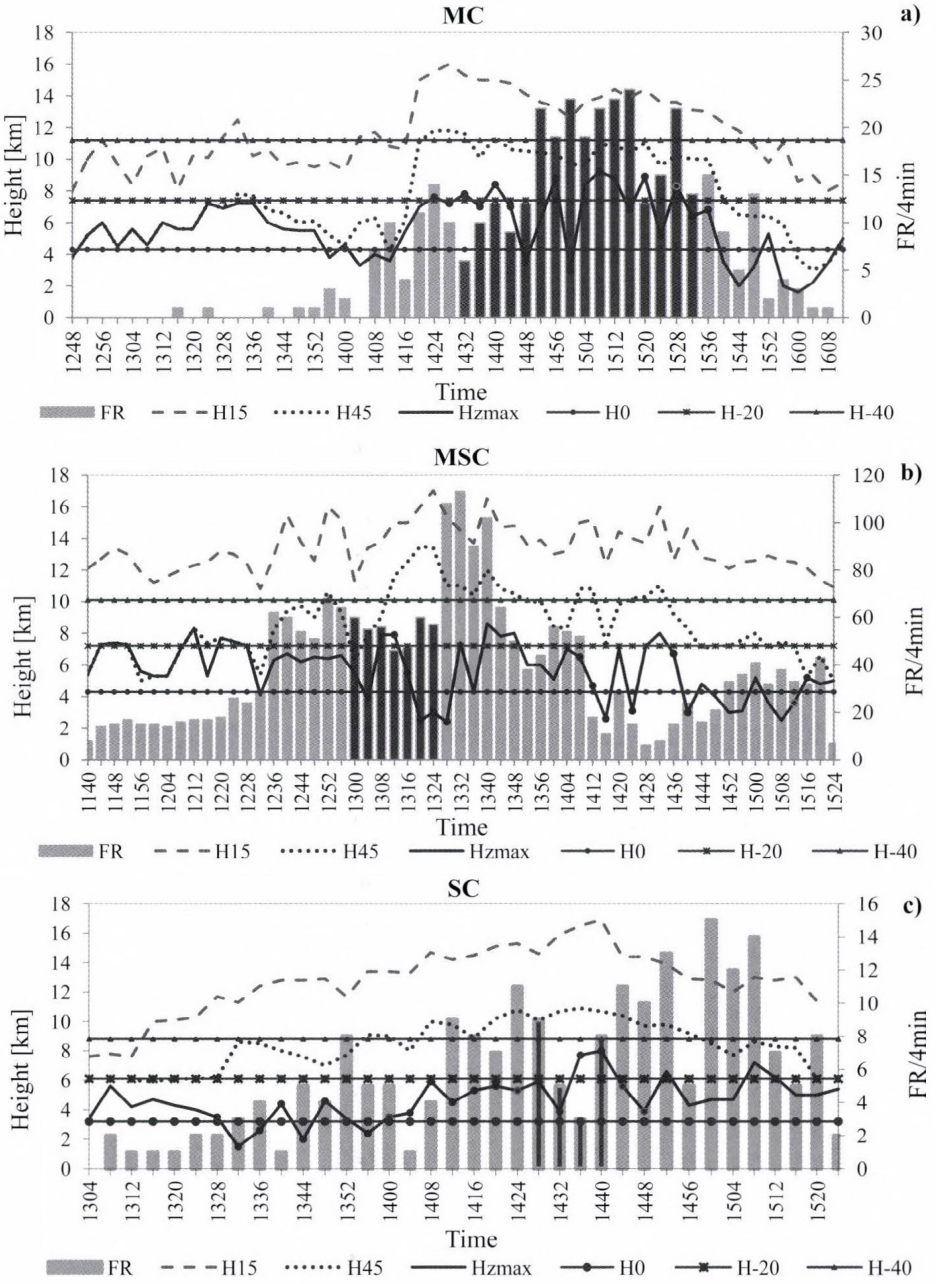

Fig. 3. Number of total flashes per 4 min, FR and radar information, as a function of time for the studied thunderstorms: a) multicell thunderstorm, MC; b) multicell evolving into a supercell thunderstorm, MSC; c) supercell storm, SC

4. Lightning behavior

Evolution of flash rate (FR), polarity, peak current (PC), and multiplicity (Mn), during the lifetime of the three severe storms were analyzed together with radar characteristics of the storms.

The flash rate of total lightning in MSC storm (*Fig. 3b*) is remarkably higher than in MC and SC storms (*Fig. 3a* and *Fig. 3c*, correspondingly). The mean and maximum values of both negative and positive flash rates in the MSC storm are also considerably higher than the corresponding characteristics in MC and SC storms (*Table 2*).

Table 2. Mean and maximum values of flash rate per 4 minutes during the lifetime of studied thunderstorms: multicell thunderstorm, MC; evolved from multicell into supercell thunderstorm, MSC; supercell storm, SC

	Flash rate per 4 minutes					
	Positive		Negative		Total	
	mean	max	mean	max	mean	max
MC	1.2	2	9.9	23	10.1	24
SC	2.1	5	4.9	15	6.0	15
MSC	11.2	38	27.8	80	38.8	113

During the non-severe stage of MC storm (from 1248 UTC till 1412 UTC) and MSC storm (from 1140 UTC till 1232 UTC), the flash rate is significantly lower in comparison with the severe stage (see *Fig. 3a*, *Fig. 3b*). In the non-severe stage, the time duration of H15 and H45 above –40 °C and –20 °C isotherms, respectively, is longer for MSC storm in comparison with MC storm. Thus, the vertical profile of radar reflectivity indicates that MSC storm has a stronger updraft than MC storm. One can speculate (see *Carey* and *Rutledge*, 1996) that the stronger updraft in MSC storm is responsible for the greater number of graupel than in MC storm and thus for higher flash rate via the non-inductive mechanism of thunderstorm electrification (*Saunders et al.*, 1991).

In the three thunderstorms there is a jump in the flash rate before the occurrence of large hail on the ground. The flash rate $FR \geq 1$ min^{-1} sharply increases more than 2 times 12 min before the hail fall in MC storm, 20 min in SC storm, and 24 min in the MSC storm (see *Fig.3a, b, c*). The increase is more pronounced in MSC and MC storms. It is just before the transition of non-severe to severe stage of both thunderstorms, when a pulse in the vertical development of the cells (sharp increase of H15 and H45) is abrupt.

The maximum values of flash rate in the three storms are detected after the maximum vertical development of the storms (see *Fig 3*). In MC and MSC storms

these values are reached after a second jump of flash rate, which occurs after the lowering of the height of radar reflectivity ≥ 60 dBZ below the 0°C isotherm.

A small decrease of the flash rate is observed in MSC storm during the large hail falls, while the corresponding decrease by a factor of 4 is significant in SC storm. However, the flash rate reached maximum values in MC storm during the occurrence of large hail.

The plot of lightning density (number of strokes for 10 minutes in a grid cell 5 km × 5 km) is shown in *Fig. 4*. The lightning density reached its maximum values before the falling of large hail on the ground and decreased in the beginning of this period in all three thunderstorms. While the lightning density reached its maximum, there was a convective vertical development, when a reflectivity of 45 dBZ extended up to –40°C isotherm and the maximum radar reflectivity (≥60 dBZ) – extended up to the –20 °C isotherm.

During the large hail fall (the period of time is denoted by red color in *Fig. 4*), the decrease of lightning density was observed, although the radar reflectivity was very high. The lower panel in *Fig. 4* shows that a lightning "hole" is observed in SC storm during the hail fall (from 1430 UTC till 1440 UTC). The more detailed analysis revealed that the presence of a lightning "hole" is accompanied by an occurrence of bounded weak-echo region (BWER) of the SC storm (*Fig. 5*).

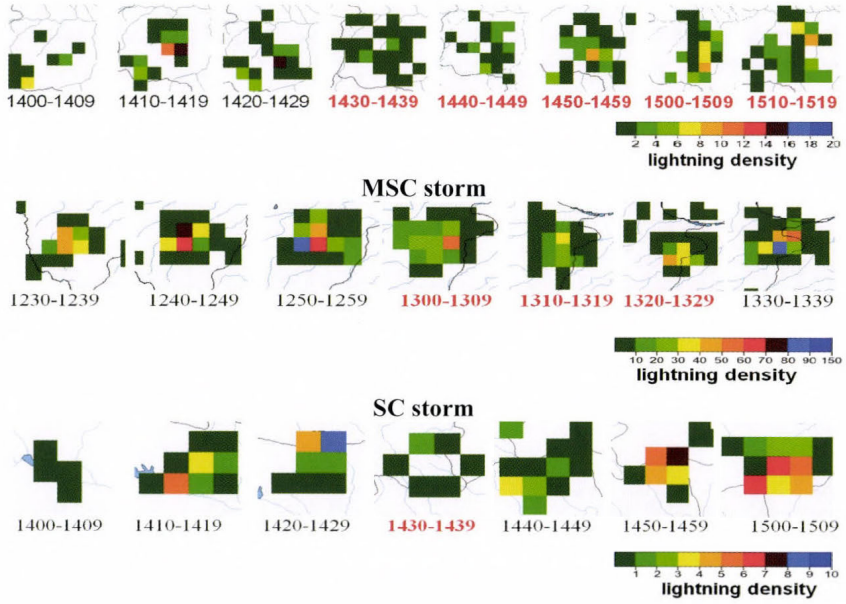

Fig. 4. Lightning density (number of strokes for 10 minutes in a grid cell 5 km x 5 km) during the part of lifetime of a multicell thunderstorm, MC (upper panel); multicell evolving into supercell thunderstorm, MSC (middle panel); a supercell storm, SC (lower panel). The period of large hail is denoted in red.

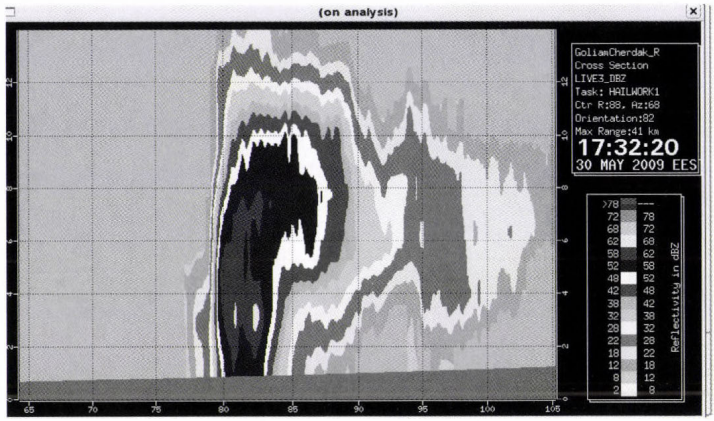

Fig. 5. Vertical cross-section of the supercell storm, SC on May 30, 2009 at 1432 UTC (17:32 in local time).

There is no direct correlation between flash rate, FR, and radar characteristics. However, a statistically significant (α=0.05) correlation is established between H45 and FR averaged in 1 km bin (see *Fig. 6*). Based on the assumption that the radar volume fraction for graupel correlates with the volume with reflectivity of 45 dBZ, one can speculate that these results are consistent with the non-inductive charging mechanism (*Saunders et al.*, 1991; *Sanders*, 1993), which relies on the rebounding collisions between graupel and ice crystals in the presence of the super-cooled liquid water.

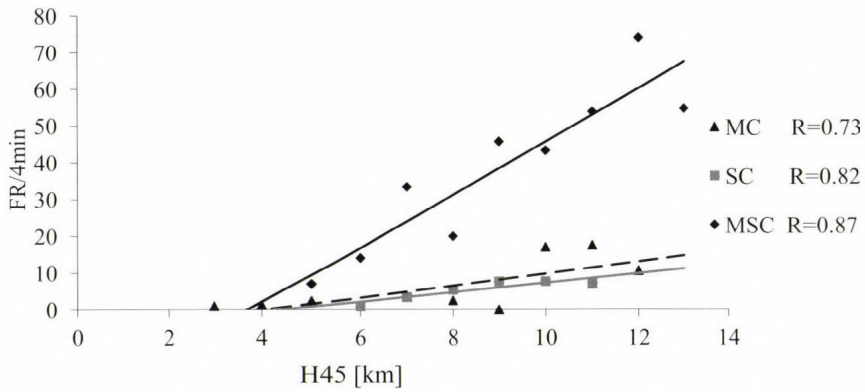

Fig. 6. Flash rate FR (averaged in 1 km bin), as a function of H45.

The analysis of strokes polarity showed that positive strokes were detected in all three studied cases (*Fig. 7*). However, the percentage in MC storm is very low (≈1%), while in SC and MSC storms it is approximately 20%. The number of positive strokes is highest during the period of large hail detected on the ground (*Fig. 8*). In SC storm, the FR of positive flashes predominated and was 2.5 times higher than FR of negative ones 8 minutes before large hail on the ground (*Fig. 7c*).

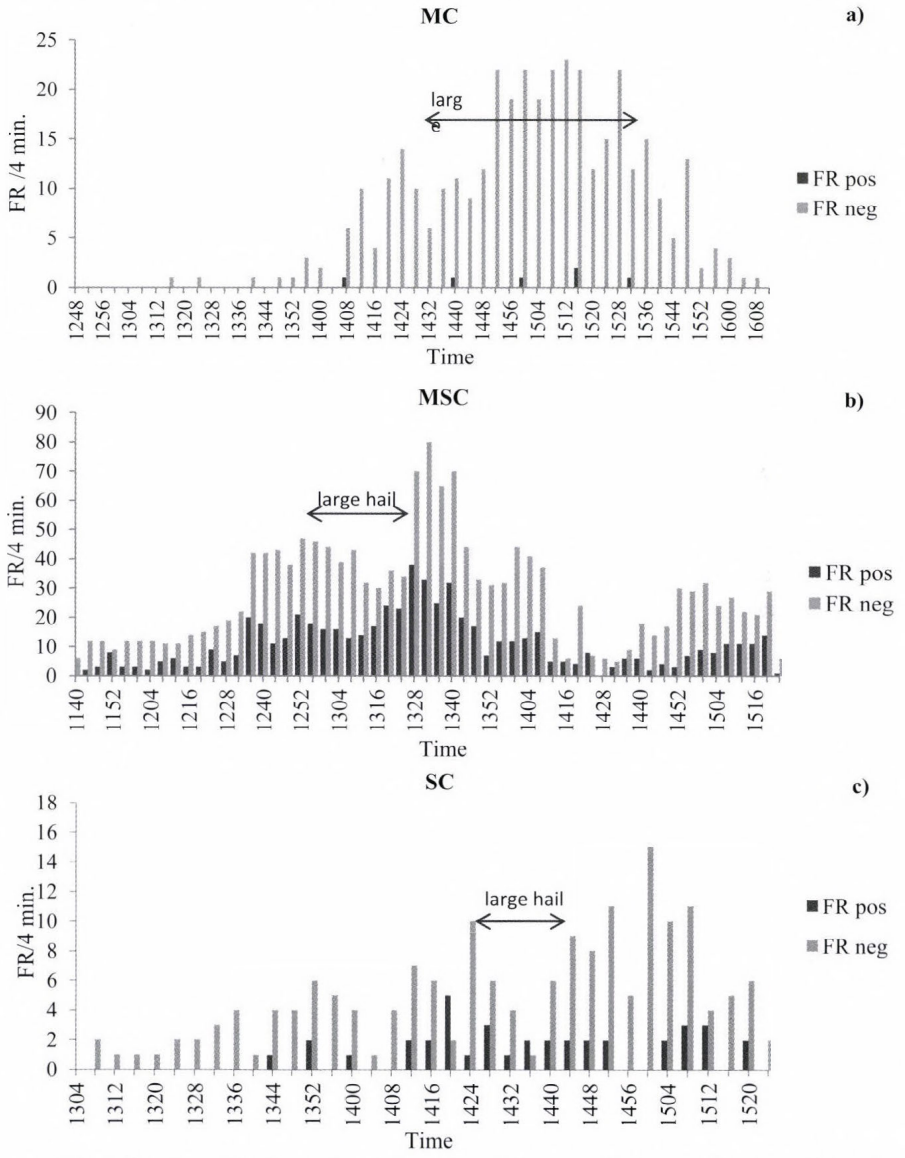

Fig. 7. Number of total negative and positive flashes per 4 min. as a function of time for the studied thunderstorms: a) multicell thunderstorm, MC; b) multicell that evolved into a supercell thunderstorm, MSC; c) supercell storm, SC.

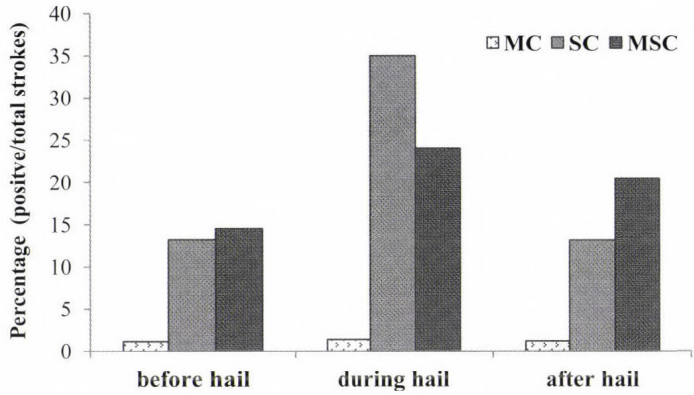

Fig. 8. Percentage of positive strokes before, during, and after large hail falling on the ground.

The mean and maximum values of multiplicity of negative flashes in MC and SC storms are similar (*Table 3*). Their maximum values are significantly lower than the ones in MSC storm.The maximum values of multiplicity in the three storms were before the falling of large hail on the ground (*Table 4*).The highest value of 16 is registered in MSC storm, while maximum values in MC and SC storms are 6 and 7, respectively. In the three thunderstorms, there is a pronounced jump in multiplicity before the time of detection of large hail on the ground – 18 min in MC storm, 8 min in SC storm, and 68 min in MSC storm (*Fig. 9 a, b, c*).

Table 3. Mean and maximum values of multiplicity and peak current (absolute value), PC, of the studied thunderstorms

	Multiplicity				PC			
	Positive		Negative		Positive		Negative (absolute values)	
	mean	max	mean	max	mean	max	mean	max
MC	1.0	1.0	1.2	6.0	22.8	48.2	21.4	67.6
SC	1.0	1.0	1.3	7.0	21.2	70.3	17.4	64.5
MSC	1.1	3.0	1.8	16.0	10.8	37.3	16.4	104.7

Table 4. Mean and max values of multiplicity, Mn during different periods of the studied thunderstorms development: before the first severe hail fall on the ground; during a severe hail fall on the ground; after the last registration of severe hail on the ground

	MC				MSC				SC			
	mean		max		mean		max		mean		max	
	Neg	Pos	Neg	Pos	Neg	Pos	Neg	Pos	Neg	Pos	Neg	Pos
before	1.4	1.0	6.0	1.0	2.3	1.1	16	2.0	1.3	1.0	7.0	1.0
during	1.2	1.0	4.0	1.0	2.0	1.1	11	2.0	1.1	1.0	2.0	1.0
after	1.2	1.0	3.0	1.0	1.5	1.1	10	3.0	1.3	1.0	5.0	1.0

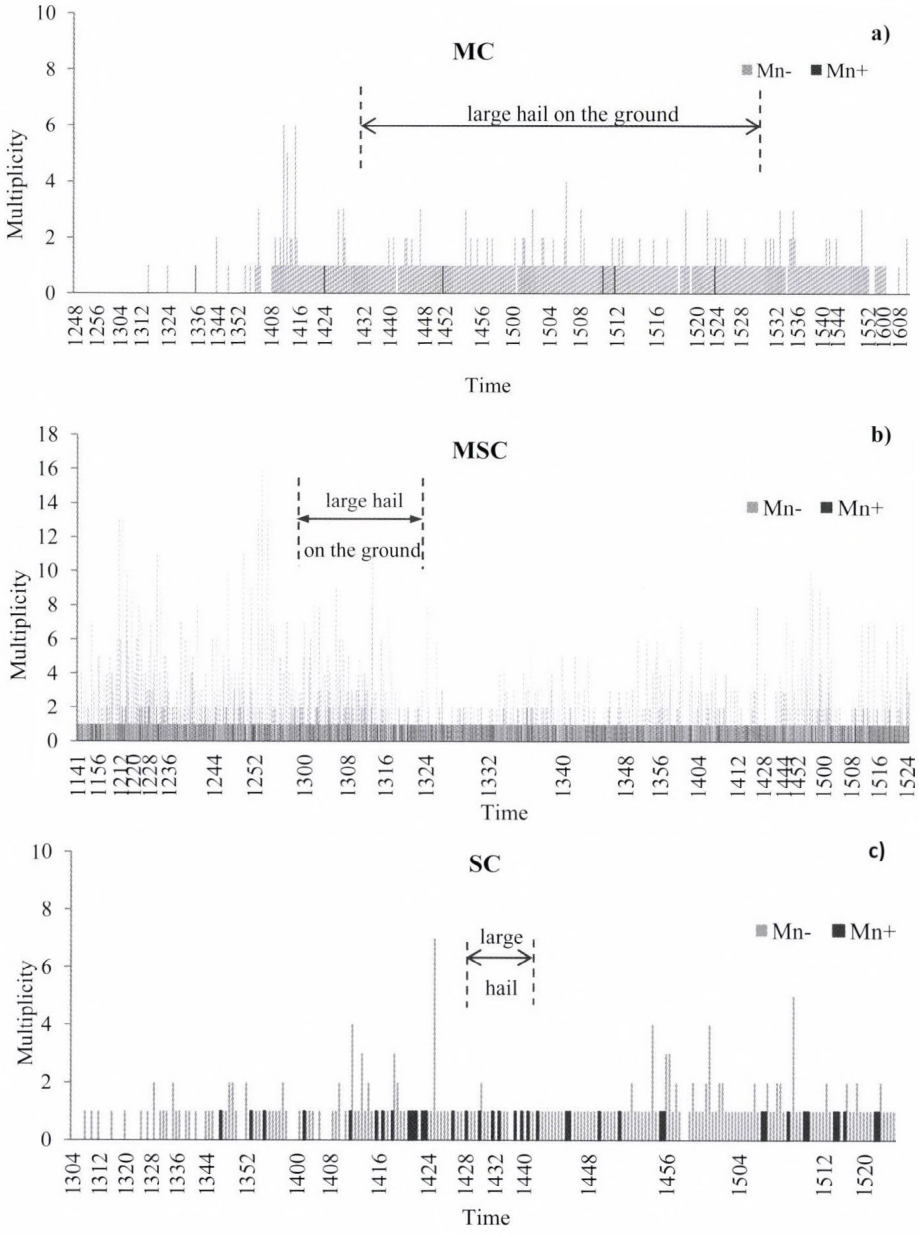

Fig. 9. Multiplicity of positive flashes, Mn+ and negative flashes, Mn−, as a function of time for a) multicell thunderstorm, MC; b) multicell that evolved into a supercell thunderstorm, MSC; c) supercell storm, SC.

The analysis of negative peak current shows that there are no significant differences in their mean absolute values for the three storms (*Table 3*). The mean values of positive peak current in MC and SC storms are 2 times higher than in MSC storm, and the highest value of 70.3 kA was registered in SC, while the highest absolute values of negative peak current was detected in MSC (105 kA). Additional analyses showed that in MC and SC storms all detected strokes had absolute values of peak current above 10 kA, and in MSC storms there was a great number of strokes (14% for negative and 46% for positive) with absolute values of peak currents less than 10 kA.

5. Discussion and conclusion

An analysis was carried out on total lightning behavior during the lifetime of different types of severe thunderstorms (a multicell, a supercell, and a multicell that evolved into a supercell) producing large hail over Bulgaria.

Significant number of positive strokes was detected in both supercell SC and MSC storms with the highest percentage during the period of large hail falls on the ground. In the supercell of the SC storm, the positive strokes even dominated over negative ones 8 minutes before the beginning of large hail fall. The detected significant number of positive strokes is in agreement with the results obtained by other authors (e.g., *Carey* and *Rutledge*, 1998; *Lang et al.*, 2004; *MacGorman* and *Burgess*, 1994; *Stolzenburg*, 1994; *Wiens et al.*, 2005). There are two "main" hypotheses for explaining the large number of positive CG lightning in some thunderstorms – the tilted-dipole charge structure or the formation of inverted dipole (*MacGorman* and *Nielsen,* 1991, *MacGorman* and *Burgess,* 1994). Since a high number of negative flashes together with the positive ones were detected in SC and MSC, one can assume that tilted dipole structure of supercell storm can explain the high number of positive CG flashed. The analyses reveal that the top of the updraft core in SC and MSC is displaced sufficiently far horizontally from the reflectivity core, which supports the assumption that the tilted dipole structure is responsible for the large positive flashes in SC and MSC.

The jump of lightning density is observed before large hail fall in the three thunderstorms, associated with a dramatic decrease in the beginning of the hail fall. There is a positive time lag between the jumps of both multiplicity and flash rate and start of large hail falls in the three studied thunderstorms. The established jump in the flash rate before the large hail fall corresponds to the results reported by *Kane* (1991), *Soula et al.* (2004), and *Williams et al.* (1999). Laboratory results in *Brooks et al.*, 1997 show that the magnitude of separated charge is higher at higher liquid water content and velocity of interacting particles. Based on that one can assume that the flash rate increases sharply at the increase of supercooled water and updraft velocity which also lead to the

growth of large hail. Thus, an increase in the CG lightning rate may consider as an indication of the subsequent falling of damage hail on the grounds. One possible reason for the decrease of flash rate at the beginning of intensive hail fall is the diminution of charge density due to the fall out of charged particles from thunderstorm cloud.

The mean and maximum values of total flash rate, as well as of the multiplicity of negative strokes in MC and SC storms are remarkably lower than in MSC storm. In the frame of the present study, the reason for the dramatically higher values of flash rates in MSC storm in comparison to those for MC and SC storms is not clear. One can speculate that this results from the more intensive vertical development during the severe stage of MC and SC storms in comparison with MSC storm. *Lang et al.*, 2000, obtained similar results and suggested that a possible explanation could be the elevation charge hypothesis (*MacGorman et al.*, 1989), namely that strong updraft prevents the formation of dipole structure due to the elevation of interacting ice particles (ice crystals and graupel) at higher level. In the supercell storm, SC, the lightning "hole" in the flash density is observed. The hole is associated with a bounded weak-echo region (BWER) of the cell, respectively with a strong updraft in this region (*Lang et al.*, 2000, *MacGorman et al.,* 2005, 2008, *Wiens,* 2005). We supposed that two processes are responsible for the lack of lightning in this region – the elevation of the interacting ice particles by very strong updraft (*MacGorman et al.,* 2005, 2008) and reduction of the amount of charge separation by rebounding collisions of ice particles in regions where hail is in a regime of wet growth (*MacGorman* et al., 2012; *Murphy* and *Demetriades,* 2005).

The present study reveals that most of the lightning signatures in the studied severe thunderstorms developed over Bulgaria are similar to those in other geographical regions, and the results are promising that lightning activity information can be used as an indicator for the occurrence of large hail on the ground over Bulgaria. One can speculate that the significant difference in some lightning characteristics of the three types of thunderstorms supports the conclusion by *Fehr et al.* (2005) that the convective organization plays a crucial role in lightning development. Due to the limited number of the studied cases, the results presented here have to be considered only as a first step to the study of lightning behavior from severe thunderstorms over Bulgaria. For firm conclusions, the analysis of lightning characteristics of more severe thunderstorms producing damaging hail has to be carried out in order to establish a broader statistical basis.

Acknowledgements–The authors are grateful to Hail Suppression Agency in Bulgaria for radar information and LINET for reliable lightning data. The present work is partially supported by the Science Foundation of Sofia University (Grant 170/2011)

References

Betz, H.-D., Schmidt, K., and *Oettinger, W.P.*, 2008: LINET – An International VLF/LF Lightning Detection Network in Europe. In (Eds. *H.-D. Betz, U. Schumann, and P. Laroche*) Lightning: Principles, Instruments and Applications, ch. 5, Dordrecht (NL), Springer.

Betz, H.-D., Schmidt, K., Oettinger, P., and *Wirz, M.*, 2004: Lightning detection with 3D-discrimination of intracloud and cloud-to-ground discharges. *J.Geophys. Res. Lett. 31*, L11108. doi:10.1029/2004GL019821.

Betz, H.D., Schmidt, K., Laroche, P., Blanchet, P., Oettinger, W.P., Defer, E., Dziewit, Z., and *Konarski, J.*, 2009: LINET— An international lightning detection network in Europe. *Atmos. Res. 91*, 564–573.

Bluestein, H.B. and *MacGorman, D.R.*, 1998: Evolution of cloud-to-ground lightning characteristics and storm structure in Spearman, Texas, tornadic supercells of 31 May 1990. *Mon. Weather Rev. 126*, 1451–1467.

Brooks, M., Saunders, C.P.R., Mitzeva, R., and *Peck, S.L.*, 1997: The effect on thunderstorm charging of the rate of rime accretion by graupel. *J. Atmos. Res. 43*, 277–295.

Carey, L.D. and *Buffalo, K.M.*, 2007: Environmental control of cloud-to ground lightning polarity in severe storm. *Mon. Weather. Rev. 135*, 1327–1353.

Carey, L.D. and *Rutledge, S.A.*, 1996: A multiparameter radar case study of the microphysical and kinematic evolution of a lightning producing storm. *Meteor. Atmos. Phys. 59*, 33–64.

Carey, L.D. and *Rutledge, S.A.*, 1998: Electrical and multiparameter radar observations of a severe hailstorm. *J. Geophys. Res. 103*, 13979–14000.

Carey, L.D., Rutledge, S.A., and *Petersen, W.A.*, 2003: The Relationship between Severe Storm Reports and Cloud-to-Ground Lightning Polarity in the Contiguous United States from 1989 to 1998. *Mon. Weather Rev. 131*, 1211–1228.

Curran, E.B., and *Rust, W.D.*, 1992: Positive ground flashes produced by low-precipitation thunderstorms in Oklahoma on 26 April 1984. *Mon. Weather. Rev. 120*, 544–553.

Deierling, W. and *Petersen W.*, 2008: Total lightning activity as an indicator of updraft characteristics. J. *Geophys. Res. 113*, D16210, doi: 10.1029/2007JD009598.

Dimitrova, Ts., Mitzeva, R., and *Todorova, A.*, 2009: Lightning activity in rain and hail bearing thunderstorms over Bulgaria. Preprints 5th European Conference on Severe Storms, Landshut, Germany, 12–16 October 2009, 239–240

*Fehr, Th., Dotzek, N.,*and *Höller, H.*, 2005: Comparison of lightning activity and radar-retrieved microphysical properties in EULINOX storms. *Atmos. Res. 76*, 167–189.

Gilmore, M.S. and *Wicker, L.J.*, 2002: Influences of the local environment of supercell cloud-to-ground lightning, radar characteristics, and severe weather on 2 June 1995. *Mon. Weather. Rev. 130*, 2349–2372.

Goodman, S.J. , Blakeslee T.R., Christian, H., Koshak, W., Bailey, J., Hall, J., McCaul, E., Buechler, D., Darden, C., Burks, J., Bradshaw, T., and *Gatlin, P.*,2005: The North Alabama Lightning Mapping Array: Recent severe storm observations and future prospects. *Atmos. Res. 76*, 423–437

Kane, R.J., 1991: Correlating lightning to severe local storms in the northeastern United States. *Weather Forecast. 6*, 3–12.

Lang, T.J. and *Rutledge, S.A.*, 2002: Relationships between convective storm kinematics, precipitation, and lightning. *Mon. Weather. Rev. 130*, 2492–2506.

Lang, T.J., Rutledge, S.A., Dye, J., Venticinque, M., Laroche, P., and *Defer, E.*, 2000: Anomalously low negative Cloud-to-ground lightning flash rates in intense convective storms observed during STERAO-A. *Mon. Weather Rev. 128*, 160–173.

Lang, T.J, Miller, L.J, Weissman, M., Rutledge S.A., Barker III, L.J., Chandrasekar, V., Detwiler, A., Doesken, N., Helsdon, J., Knight, C., Krehbe, P, Lyons, W.A., MacGorman, D., Rasmussen, E., Rison, W., Rust, W., and *Thomas, R. J.*, 2004: The severe thunderstorm electrification and precipitation study. *B. Am. Meteorol. Soc. 85*, 1107–1125.

MacGorman, D.R. and *Burgess, D. W.*, 1994: Positive cloud-to-ground lightning in tornadic storms and hailstorms. *Mon. Weather Rev. 122*, 1671–1697.

MacGorman, D. R., and *Nielsen, K. E.*, 1991: Cloud-to-ground lightning in a tornadic storm on 8 May 1986. *Mon. Weather Rev. 119*, 1557–1574.

MacGorman, D.R., Emerisc, C., and *Heinselman P.L.*, 2012: Lightning activity in a hail-producing storm observed with phased-array radar. 22nd International lightning detection conference, Broomfield Colorado, USA, 2–3 April 2012.

MacGorman, D.R., Burgess, D.W., Mazur, V., Rust, W.D., Taylor, W.L., and *Johnson, B.C.*, 1989: Lightning rates relative to tornadic storm evolution on 22 May 1981. *J. Atmos. Sci. 46*, 221–250.

MacGorman D.R., Rust, W.D., Krehbiel, P., Rison, W., Bruning, E., and *Wiens, K.*, 2005: The electrical structure of two supercell storms during STEPS. *Mon. Weather Rev. 133*, 2583–2607.

MacGorman, D.R., Rust, W.D., Schuur, T.J., Biggerstaff, M.I., Straka, J.M., Ziegler, C.L., Mansell, E.R., Bruning, E.C., Kuhlman, K. ., Lund, N.R., Biermann, N.S., Payne, C., Carey, L.D., Krehbiel, P.R., Rison, W., Eack, K.B., and *Beasley, W.H.*, 2008: TELEX: The Thunderstorm Electrification and Lightning Experiment. *B. Am. Meteor. Soc. 89*, 997–1013.

Maier, M. W., Krider, E. P., 1982: A comparative study of cloud-to-ground lightning characteristics in Florida and Oklahoma thunderstorms. Twelfth Conference on Severe Local Storms, San Antonio, *Am. Meteor. Soc*, 363–367.

McKinney, C.M., Carey, L.D., and *Patrick, G.R.*, 2008: Total lightning observations of supercells over north central Texas. *Electron. J. Severe Storms Meteor. 4(2)*, 1–25.

Montanya, J., Soula, S., and *Pineda, N.*, 2007: A study of the total lightning activity in two hailstorms. *J. Geophys. Res. 112(D13)118*, doi:10.1029/2006JD007203.

Montanya, J., Soula, S., Pineda, N., Van der Velde, O., Clapers, P., Sola, G., Bech, J., and *Romero, D.*, 2009: A study of the total lightning activity in a hailstorm. *Atmos. Res. 91*, 430–437.

Murphy, M. J. and *Demetriades, N.W.S.*, 2005: An analysis of lightning holes in a DFW supercell storm using total lightning and radar information. Extended Abstracts, Conf. on Meteorological Applications of Lightning Data, San Diego, CA, Amer. Meteor. Soc.

Orville, R. E., Huffines, G. R., Burrows, W. R., Holle, R. L., and *Cummins, K.*, 2002: The North American Lightning Detection Network (NALDN)- First results: 1998–2000. *Mon. Weather Rev. 130*, 2098–2109.

Ray, P.S., MacGorman, D.R., Rust, W.D., Taylor, W.L., and *Rasmussen, L.W.*, 1987: Lightning location relative to storm structure in a supercell storm and a multicell storm. *J. Geophys. Res. 92*, 5713–5724.

Reap, R.M. and *MacGorman, D.R.*, 1989: Cloud-to-ground lightning: Climatological characteristics and relationships to model fields, radar observations, and severe local storms, *Mon. Weather Rev. 117*, 518–535.

Saunders, C.P.R., 1993: A review of thunderstorm electrification processes. *J. Appl. Meteorol. 32*, 642–655.

Saunders, C.P.R., Keith, W.D., and *Mitzeva, R.P.*, 1991: The effect of liquid water on thunderstorm charging. *J. Geophys. Res. 96*, 11007–11017.

Seimon, A., 1993: Anomalous cloud-to-ground lightning in an F5-tornado producing supercell thunderstorm on 28 August 1990. *B. Am. Meteor. Soc. 74*, 189–203.

Sheridan, S.C., Griffiths, J.H., and *Orville, R.E.*, 1997: Warm season cloud-to-ground lightning – precipitation relationship in the South-Central United States. *Weather Forecast. 12*, 449–458.

Smith, S.B., LaDue, J.G., and *MacGorman, D.R.*, 2000: The relationship between cloud-to-ground lightning polarity and surface equivalent potential temperature during three tornadic outbreaks. *Mon. Weather Rev. 128*, 3320–3328.

Sorriano, L.R., De Pablo, F., and *Diez, E.G.*, 2001: Relationship between convective precipitation and cloud-to-ground lightning in the Iberian Peninsula. *Mon. Weather. Rev. 129*, 2998–3003.

Soula, S., Seity, Y., Feral, L., and *Sauvageot, H.*, 2004: Cloud-to-ground lightning activity in hail-bearing storms. *J. Geophys. Res. 109*, D02101, 1–13.

Steiger, S.M., Orville, R., and *Carey, L.D*, 2007: Total lightning signatures of thunderstorm intensity over North Texas, Part I: Supercell. *Mon. Weather Rev. 135*, 3281–3302.

Stolzenburg, M., 1994: Observations of high ground flash densities of positive lightning in summertime thunderstorms. *Mon. Weather Rev. 122*, 1740–1750.

Taylor, W.L., 1973: Electromagnetic radiation from severe storms in Oklahoma during April 29–30 1970. *J. Geophys. Res. 78*, 8761–8777.

Turman, B.N. and *Tettelbach, R.J.*, 1980: Synoptic-scale satellite lightning observations in conjunction with tornadoes. *Mon. Weather Rev.108*, 1878–1882.

Wiens, K.C., Rutledge S.A., and *Tessendorf, S.A.*, 2005: The 29 June 2000 supercell observed during the STEPS. Part II: Lightning and charge structure, *J. Atmos. Sci. 62*, 4151–4177.

Williams, E.R., 1985: Large-scale charge separation in thundercloud, *J. Geophys. Res. 90*, 6013–6025.

Williams, E.R., Boldi, B., Matlin, A., Weber, M., Hodanish, S., Sharp, D., Goodman, S., Raghavan, R., and *Buechler, D.*, 1999: The behavior of total lightning activity in severe Florida thunderstorms. *Atmos. Res. 51*, 245–265.

Williams, E.R., Mushtak, V., Rosenfeld, D., Goodman, S., and *Boccippio, D.*, 2005: Thermodynamic conditions favorable to superlative thunderstorm updraft, mixed phase microphysics and lightning flash rate. *Atmos. Res. 76*, 288–306.

IDŐJÁRÁS

Quarterly Journal of the Hungarian Meteorological Service
Vol. 117, No. 3, July – September, 2013, pp. 315–358

Agrometeorological research and its results in Hungary (1870–2010)

Gábor Szász

University of Debrecen, Centre for Agricultural and Applied Economic Sciences, Institute for Land Utilisation, Technology and Regional Development, Agrometeorological Observatory, Böszörményi út 138, H-4032 Debrecen, gszasz@agr.unideb.hu

(Manuscript received in final form June 12, 2012)

Abstract—Agrometeorology is the branch of atmospheric sciences. Lately, modern agrometeorology has been based on exact principles and its findings are of interdisciplinary nature. The focal questions of agrometeorology are determined by the climate of large regions; therefore, its material division is specified by the local nature of the climate system and its methods are systematized by macro- and micrometeorology. Agrometeorology can be regarded as a group of determinant aspects of economic decisions. This publication summarizes the 150 years of development of agrometeorology in Hungary.

Key-words: history of agriculture in Hungary, agrometeorology, climatology, agroclimatology, productivity, weather sensitivity, hazards, water supply of crop canopy, evaporation, production, fertility, actual and potential production

1. Introduction

The ancient cultures had been continuously extending due to the knowledge created by the accumulation of observations. The specialization of this knowledge base created the fundamentals of specialized sciences as a result of the integration of sciences. Of these, the production activity dealing with the issues of human nourishment was developed, as well as the range of consumers which stems from human needs and these two were equally regulated by the climatic endowments of the environment whose risky significance has a global effect even nowadays. Through the centuries, agricultural production and social consumption, as well as the risk range of these two got into an increasingly close connection with each other which resulted in the forceful development of interests of connections towards each other and the deepening of these interests. During the modernization of agriculture, the climatic risk has been continuously

increasing with the development of the consumer society. As a result, an increasingly complex connection has been developed between the agriculture and the climatic environment. The research area of agrometeorology arose from this field, as agrometeorology is meant to explain the causal chain of the biological consequences triggered by the physical effects of the atmosphere with the consideration of the causal order. It follows from this statement that the database of agrometeorology and the nature of its treatment methods is such a partial complex of the meteorological bases that concludes to the physical explanation and consequences of the effects elicited by the atmosphere.

2. Preliminaries of agrometeorological research in Hungary (1850-1950)

Temperate zone modern agriculture roots back into the 13th–16th century in England and the Netherlands. By this time, the history-forming period of great European migrations was over and a seemingly more permanent agriculture unfolded which rooted in the ancient fundamentals and which also provided the basis for modern agriculture that developed in the subsequent centuries. In the centuries after the millennium, there was no agriculture in a sense of that is called agriculture today. The increased population in the mentioned areas demanded an extremely intensive grazing animal husbandry whose environmental conditions were mainly provided by the favorable climatic endowments. This development resulted in severe natural consequences and they are regarded as the first revolution of agriculture in history. As a result of the heavy use, soils gradually lost their fertility. The soil degradation caused by soil use strongly deteriorated the ecological balance (*Overton* and *Campbell,* 1996; *Allen,* 1999; *Campbell,* 2010). The dilemma of losing the ecological balance resulted in an episode of developing agriculture which was regarded as an imperative condition in relation to the elimination of the crisis. Following the abolition of the aggravating circumstances, a more modern agriculture was developed in a few centuries, involving closed-loop animal husbandry, while crop rotations also became widely used and various methods of cultivation were also becoming increasingly widespread. This modernization became a general characteristic of agriculture inside the continent in a few centuries.

By the middle of the second millennium and the subsequent centuries, the production techniques applied for various climatic characteristics penetrated the Carpathian Basin. The production of western European, relatively more water demanding crops increased, the problems of water management regularly causing mediterranean droughts in the summer became more frequent, new plant species and varieties appeared, and these all contributed to the modernization of the Hungarian agriculture.

The region of Central European agriculture was the meeting point of the effects coming from these three directions, and the simultaneous benefits and

complexity could be detected in the history of the past of Hungarian agriculture. *Fig. 1* shows the direction of the peculiarities characterizing the agriculture which evolved as a result of the mentioned climatic effects and the various large territorial differences.

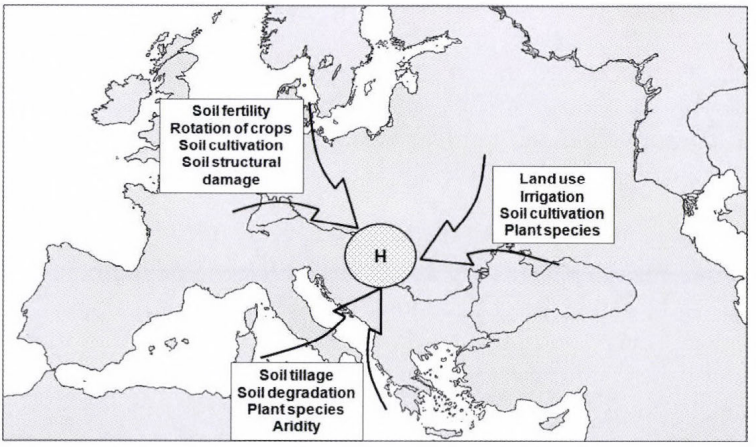

Fig. 1. Development dynamics of modern agriculture in Central Europe (1200-1600)

The conservative layer which is not adjusted to the given climate was struck by the extending cropping area of *newly produced plants* and the lack of *professional knowledge*. Simultaneously with the increasing change and modernization of the production structure, the processing industry was forcibly developed, resulting in what is called technical development.

The growth of agricultural production of this period was characterized by a less powerful prosperity and issues, in which the strong consequences of climatic effects were obvious developed and the dependence on these effects was also necessary. Since agriculture was based solely on natural resources at this time, the various soil characteristics and the consequence of the correlation between climate and soil also had an essential role in addition to climatic factors. The differences in the environment of the areas of the Carpathian Basin which are suitable for agricultural production played a very important role not only in the climate, but also in the soil characteristics. This role provided the basis for getting to know the empirical correlations and phenomena of subsequent agrometeorological knowledge.

There was limited receptiveness concerning development opportunities in the 18th century, mainly due to the social structure. The elements of production modernization were created almost only by the so-called allodial plot system. The smaller feudal farms represented the less favored social class.

In the 19th century, natural sciences developed sharply, resulting in the further intensification of agriculture. As a result of the increasing demand for new

knowledge in the 1800s, agricultural higher education institutions were established which prepared professionals who constituted the intellectual basis of development. These were the institutions (Keszthely 1797, Magyaróvár 1850, Debrecen 1867) where agricultural climatology evolved in Hungary, as "Climatology" was an obligatory subject in the education program. Also, the outstanding teachers of these institutions provided the intellectual basis that was able to accept various forms of modernization. Simultaneously with the scientific basic education, field experiments were launched in a relatively narrow framework. In these trials, the determinant role of climatic effects which regulate yield were of chief importance in addition to cultivation and nutrient management. These issues necessitated the increasing range of research complexity.

The establishment of the National Meteorological and Earth Magnetic Science Institute (1870) was a significant event. Within this institution, an agrometeorological department was also established in addition to the more special data and knowledge collection activities, although it stopped working in the subsequent decades. The station network of the former meteorological institute published climatic data in various forms still used by educated agriculturalists and researchers with significant efficiency. The so-called agricultural experimental stations were also established in this period. In these stations, the climatic information was of significant scientific value.

Mention has to be made of the results of technical development launched in the second half of the 1800s. During the targeted planning processes, this development always considered the climatic parameters that provide information to build various constructions. Last but not least, it has to be noted that agrometeorology is a field of climatology which makes it possible to consider the efficiency of an agricultural technological system. From this viewpoint, Hungarian agrometeorological research left room for development for the succeeding generations.

In the first half of the 1900s, the agricultural use of meteorological information significantly served the research of climatic examination results which cannot be missing from agricultural development. Therefore, the publication of the standard time series of various weather elements was of primary importance. Based on these results, it was possible to launch agroclimatological research subsequently (*Smith*, 1915; *Cserháti*, 1905; *Gyárfás*, 1922; *Kreybig*, 1953; *Boncz*, 1992; *Nyíri*, 1993; *Kemenessy*, 1964; *Birkás*, 2006; *Györffy*, 1990).

The increasing development resulted in a production increase that created the basis of the economic crisis by the first half of the 1800s. As a result, the evaluation and thorough research of climatic effects was done rather slowly. In this period, the main tasks of the National Meteorological Institute were the gradual extension of climatic data collection, the improvement of its system, their collection in a few decades, the publication of the several year averages of the main elements, as well as the performance of technically limited forecasts.

The activity of the institute resulted in the simple information basis on which agrometeorology was built up.

In this period, no specific agrometeorological research was launched, but some researchers were already dealing with climate effect issues that affect agriculture, mainly with the aim to determine the extent of climate damages. The observation series performed between 1901–1930 made it possible to estimate the climate effects based on several decades, but these data were still mainly in connection with climatic extremities, and no more detailed statistical analysis was performed. The basis of examinations was the determination of the climatic differences between low and high yields concerning not more than a few smaller regions. In the subsequent decades of the millennium, there were yield series which provided an opportunity to analyze and explain the fluctuation of yields due to climatic reasons.

The reason for the late launching of agrometeorological research was not the lack of interest, but the simultaneous lack of knowledge about crop production and climate, although this issue arose as a problem independent of historical influences in an agriculturally significant country.

In the first decades of the 1900s, the preparation for war, the difficult economic circumstances caused by the First and Second World Wars, and the subsequent social change did not make it possible to further improve the related research. Despite the fact that the already traditional climatic observations coupled with the poor and significantly mutilated education system became incapable of functioning, tasks driven by new goals and the launching of these tasks became necessary.

3. Expansion of agrometeorological research (1950-2010)

In Hungary, the economic change after the Second World War took nearly ten years. The new fundamentals of the agricultural area and the change of farming methods root back to 1960. Also, this period marks the beginning of the modernization of agriculture. The reorganization of crop production was started, mainly by the replacement of crop species, partially the increasing use of *fertilizers* due to the lack of organic manure and further improvement of soil fertility. Within the *more modern agriculture*, the sensitivity to weather increased in crop production, also resulting in the growing production risk. This large change increased the demand for climatological information. This need was expressed in numerous forms, several different agricultural service research institutes were formed, some of which also performing various meteorological observations, measurements, and research activities that served agriculture directly (see later).

The manifold development elicited the fundamental change of the *agroecological approach* and a change of direction: research built on various natural science bases was becoming wider and the integrated system of

knowledge was also extending. In the initial phase of development, the opportunities of intervention were gradually increasing with the extension of technological elements, but the long-term consequences of the interventions, their mechanisms, and the correlations of these remained unknown for the most part. Practically, the complex representation and mapping of the dynamics which can be observed in the field could not be done. The main question was posed: what could be the most important new method and system which can help in directly exploring the efficiency of interventions? It could be regarded as a historical point when the idea of launching complex *long-term experiments* was conceived.

The examinations covered not only the plant, but also the environmental factors which directly or indirectly affect the vital functions of the plant. These examinations are mainly built on biological, chemical, and physical rules. Only a narrow range of empirical methods can be observed in the basic concept of these examinations. Instead, the system of parameters which can be described in an exact way by explaining the causal conditions became more extended.

The agroecological systems have a specific energy and material flow. The factors governing the whole system are

- created by humans,
- driven by solar energy,
- maintained by the energy and material source and of the environment, as well as its flow,
- regulated by humans.

Therefore, the aim of natural science examinations is not to question the correctness of observations, but to get to know and describe exactly the assumed consequence. The dynamic approach built on the principle of causality lays the main emphasis on the importance of getting to know the processes. While the static approach is condition-focused, the dynamic approach focuses on the process. In addition to climate, soil can also be regarded as an environmental factor, although its characteristics are totally different than those of the atmosphere. Still, its conditions can greatly vary between crop years and the reason of this phenomenon is partly the climate effects, but also the use and effect of technological factors which are adjusted to the climatic conditions, too. Therefore, the effect of climate affects the physical condition of the air space close to the surface, and it has an indirect and altering effect through the soil as well. By doing so, the air, soil, and plants form a specific system in a physical sense, which is basically an ecological system of the nature (*Szász*, 1987; *Petrasovits* and *Balogh*, 1974).

The process-focused analysis of each question of modern crop production can only be performed if their basis is constituted by a scientific information system in which the criteria that meet the hierarchic principles are strictly met. This new approach set an ideal aim to perform the integrity role of cooperating

branches of science; therefore, to be a cooperating research partner of meteorological research (*Monteith*, 1975; *Várallyay*, 2008).

As a matter of course, the development of the approach of agrometeorology cannot neglect climatological and meteorological measurements and the development of a database derived from their data, on which the narrowly interpreted agrometeorology is built. In other words, no agrometeorological examinations can be performed without climatological bases, since these areas of science systematize the effects which act on agriculture over time, and agrometeorology works out the explanation of the responses to these effects. Therefore, this is the reason why the main activity of agrometeorology cannot be observed without knowing the climatic examination of the country which is described by the section about the main characteristics of the climate of Hungary (*Várallyay et al.*, 1980).

4. Climatic description of the flat regions of the Carpathian Basin

The climatological information on which agrometeorological examinations are built could be summarized as follows. It has to be emphasized that these data mainly refer to the relatively flat areas where the widely interpreted crop production has been carried out for centuries.

4.1. Radiation

The measurement of the energy of radiation was started after the 1900s, instruments were used to perform these measurements only on a few stations guided by the National Meteorological and Earth Magnetic Science Institute (OMFI) in the 1930s. Simultaneously with the network measurements, statistical analyses were also performed with the aim to determine the correlation between the measured sunshine duration and the daily duration of relative radiation. The aim was to get to know the average regional distribution of the radiation energy calculated on the basis of the sunshine duration measurements performed at 30-40 stations. In the 1950s, based on the research done by *Dobosi* and *Takács* (1959), the radiation balance could be determined on the basis of calculation. The first measurements aimed at determining the radiation balance were launched by the OMFI and the Agrometeorological Observatory of the former Agricultural Academy of Debrecen, which carried out regular measurements and energy flow examinations.

Radiation measurements were integrated into micrometeorological measurement programs (Berényi-Hesse, Hortobágy, 1962, OMFI-Balaton program 1958-1962, etc.), while some radiation measurements were carried out on demand at various agricultural research institutes (crop production, horticultural, agroecological research programs at Matronvásár MTA, University of Gödöllő, Debrecen, Keszthely, Szarvas, etc.)

The first step towards working out the method of estimating the photosynthetic proportion of radiation in Hungary was made by *Felméry* (1974).

By the millennium, the database of agrometeorological research needs was provided by a network which consisted of around 40 stations. This network helped to establish the research school whose leaders (*Takács,* 1972; *Dobosi,* 1972; *Major,* 1985) laid down the basis of the research and analysis of radiation measurements in Hungary. Furthermore, this network also provided other research locations (universities, research institutes, around 10 stations) with radiation data.

Based on the published measurement results related to the radiation energy supply of the agricultural area and the collected and organized measurements of the components of radiation flow, it can be stated that the energy supply of the Carpathian Basin significantly exceeds that of the agricultural areas at the same latitude.

Radiation is a meteorological element with two components, as the duration of radiation which is generally characterized by sunshine duration and the characteristics of the temporal and spatial features of radiation energy can be used both in theoretical and practical terms.

The temporal and spatial values of *sunshine duration* can be determined on the basis of the following important information:

- astronomic sunshine duration,
- temporal and spatial distribution of the quantity of radiation energy.

The *astronomic sunshine duration* is determined by the position of the Sun and the Earth to each other, and its value is referred to the solid angle of 180° if expressed in hours. The published possible sunshine duration values refer to the latitudinal degree of the country, whose monthly values are summarized in *Table 1*. The extreme values of the yearly solar cycle of the potential sunshine duration refer to the lowest and highest sun height days, expressed in hours/month and hours/day. The monthly and yearly sums (in geographical terms) of the potential sunshine duration slightly differ from each other due to the small range of the related surface. The yearly average sum of the potential sunshine duration is 4450 hours. The daily, monthly, and yearly sums of the actual sunshine duration are determined by geographical and climatological factors, of which the most important are the relief (due to the difference in the reference solid angle) and the clouds (due to climatological reasons). The monthly sums of the potential sunshine duration are shown in *Table 1*, where the actual monthly sunshine duration values are expressed in hours.

Despite the relatively small area of the country, there are average differences in the regional distribution of the sunshine duration mainly due to climatic reasons (clouds, fog). The regional difference of the average yearly sums exceeds 350 hours annually even in flat areas. According to the detailed examinations of *Takács*, the lowest yearly sums develop around the western and

southwestern bordering areas of the Transdanubian region, where the yearly sum does not exceed 1700 hours. The area which is the richest in sunshine is the southern Danube-Tisza mid-region and the southern areas of the Trans-Tisza region, whose regional proportion is shown in *Fig. 2.*

Table 1. Monthly actual, possible and relative sunshine duration in Hungary

Month	Actual	Possible	Relative
	Sunshine duration		
Januar	2.0	8.9	0.22
February	3.0	10.2	0.29
March	4.5	11.8	0.38
April	6.1	13.5	0.45
May	7.8	15.0	0.52
Juny	8.5	15.7	0.54
July	9.2	15.4	0.60
August	8.5	14.2	0.60
September	6.4	12.6	0.51
October	4.3	10.9	0.39
November	2.3	9.3	0.25
December	1.5	8.3	0.18

Based on the research done by *Takács* and *Major*, as well as *Dobosi*, the temporal and spatial distribution of global solar radiation was processed by *Dávid et al.,* (1990), using the data of the period between 1951–1980 (*Distribution of the radiation balance in Hungary based on the data between 1951-1980, 1990.*). This work gives information concerning the monthly energy sums of the global radiation related to 44 polygons of the country, as well as the average values which determine the radiation balance.

4.2. Temperature

Air temperature values determined in accordance with climatological averages provide a wide range of information and they are published to a detailed extent. The agricultural consequences of the variability of temperature are commonly known. Nevertheless, the response reactions of the effect of different variability cannot be neglected either, as the reactive heat demand of the plants are constantly changing. It is one of the tasks of the modernization of agroecological research to analyze the climate sensitivity of various culture plants. While the determination of optimal heat demand was in focus in the past decades, manifold consequences of the effects of tolerance to extremities and heat stress

had to be taken into consideration in the recent decades. The system of related agrometeorological knowledge is still incomplete. The traditional methods of temperature observations and the demand-focused information system of agriculture only partially satisfy this need (*Bacsó*, 1952, 1959).

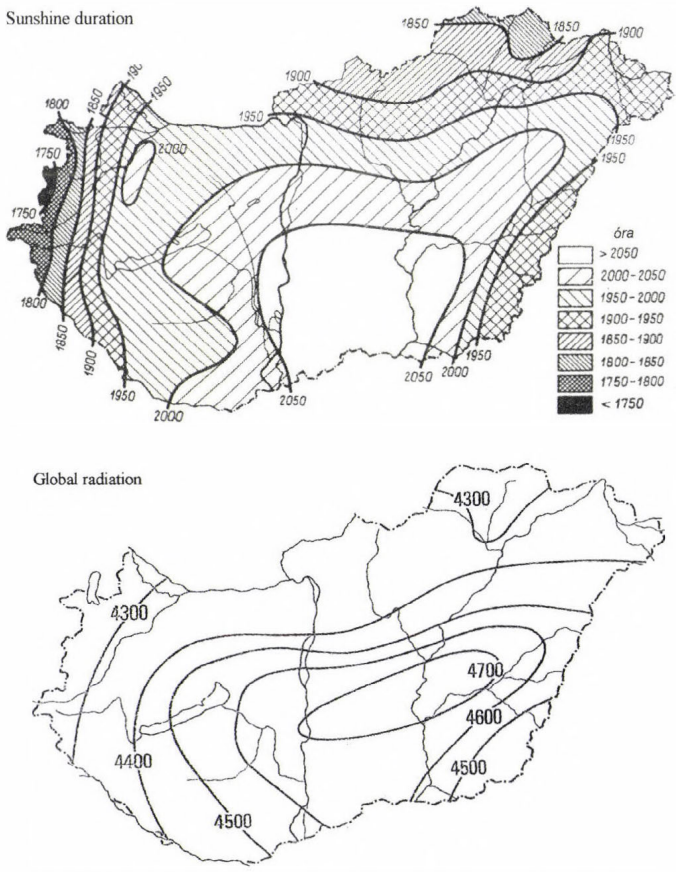

Fig. 2. Annual average of sunshine duration and the sum of global radiation (MJ m^{-2} $year^{-1}$) in Hungary (*Takács*, 1972; *Major*, 1985).

The agroclimatological characterization of temperature could be summarized on the basis of means, standard deviations, and the coefficient of variance. *Table 1* shows monthly mean temperatures of 100 years and the related statistical parameters of the 5 stations. Based on the multiple year mean values of this table, significant difference is shown between the various areas of the country. The yearly mean temperature is between 9–11 °C in Hungary. The yearly fluctuation is characterized by the difference between the mean

temperature in July and January, and the extent of fluctuation continuously decreases from eastern Hungary to the west, whose value is around 20–21 °C. Typically, the interim seasons are long from agricultural aspect and this phenomenon lengthens the vegetation period (*Aujeszky et al.*, 1951).

The 50–50 and 100-year monthly mean values shown in *Table 2* are rather close to each other, but it can only partially be accepted in view of the standard deviation values; therefore, longer periods need to be considered in order to determine the statistical probability of the variability. Nevertheless, these differences are significant from climate statistical aspect, and they do not have any fundamental importance from the viewpoint of agroclimatology. The referred values clearly show the great variability of the winter period. The lowest variability evolves in the second part of summer ($s<1.5$). This statistical parameter is further increasing in the spring and autumn months ($s=1.5–2.5$), which is then finally expressed in the value of coefficient variability (CV) (*Szász,* 1981, 2005).

In field crop production, the cumulated sum of daily mean temperature values is frequently used. This topic cannot be dealt with in detail in this study, since these values represent environmental physical effect and consequence for plants which have different heat demand.

The most perfect and detailed information about the variability of temperature and the probability of its values are provided by the distribution analyses. No such analyzed research results are available from agrometeorological measurements. In order to fill this gap, *Fig. 3* shows the distributions based on daily observations of 100 years in Debrecen, showing the daily mean temperature. The distribution curves of the three summer months make it possible to gain information mainly on the probability of the extremely high or low value ranges which cannot be related to any given day, but they serve the purpose of getting to know the lower and upper limits of the tolerance of plants' needs (*Fig. 4*).

The daily fluctuation of air temperature has a practical significance in agriculture, the extent of its value is shown below:

Season	**Winter**	**Spring**	**Summer**	**Autumn**
Daily average range (°C)	4,2–7,5	7.5–13.0	11.0–14.0	5.0–13.0

The minimum and maximum values of the daily fluctuations can cause irreversible damages to various extents. In the interim seasons, the critical extreme temperature is the minimum value, while it is the maximum value that could cause stress in the summer from the aspect of the heat demand of plants (*Kakas*, 1960).

Table 2. Monthly means, standard deviation, and coefficient variation of temperature (1901–1950, 1951–2000)

Mean temperature (°C)

Station		I.	II.	III.	IV.	V.	VI.	VII.	VIII.	IX.	X.	XI.	XII.	Year
Zalaegerszeg	1901–1950	–1.2	0.7	5.8	10.8	15.8	18.9	20.9	19.9	15.8	10.4	5.0	1.0	10.3
	1951–2000	–1.2	0.7	4.9	9.9	14.6	18.0	19.5	19.1	15.2	9.9	4.6	0.4	9.6
Magyaróvár	1901–1950	–1.4	0.7	5.1	10.2	15.4	18.4	20.3	19.4	15.6	10.1	4.6	0.7	9.9
	1951–2000	–1.2	0.7	5.0	10.3	15.2	18.4	20.1	19.5	15.4	10.1	4.6	0.7	9.9
Túrkeve	1901–1950	–2.3	–0.3	5.3	10.9	16.6	19.7	22.0	21.1	16.7	10.8	4.8	0.3	10.5
	1951–2000	–1.8	0.4	5.3	11.1	16.4	19.9	21.6	21.1	16.7	10.9	4.9	0.5	10.6
Szeged	1901–1950	–1.0	0.8	6.5	11.7	17.2	20.4	22.7	21.7	17.7	12.1	6.1	1.6	11.5
	1951–2000	–1.3	0.8	5.4	11.1	16.2	19.6	21.2	20.8	16.6	11.0	5.2	0.8	10.6
Debrecen	1901–1950	–2.3	–0.5	4.9	10.8	16.4	19.5	21.5	20.5	16.1	10.4	4.7	0.3	10.2
	1951–2000	–2.1	0.0	4.9	10.7	15.9	19.1	20.8	20.2	16.0	10.5	4.7	0.1	10.1

Standard deviation (S)

Station		I.	II.	III.	IV.	V.	VI.	VII.	VIII.	IX.	X.	XI.	XII.
Zalaegerszeg	1901–1950	3.2	3.5	2.4	1.8	1.7	1.4	1.5	1.3	1.4	1.6	2.0	2.3
	1951–2000	2.6	2.7	2.2	1.6	1.6	1.3	1.5	1.6	1.5	1.6	1.9	1.8
Magyaróvár	1901–1950	3.1	3.4	2.2	1.7	1.7	1.5	1.2	1.2	1.5	1.6	1.9	2.3
	1951–2000	2.7	2.6	2.2	1.4	1.6	1.4	1.4	1.5	1.5	1.7	1.8	1.8
Túrkeve	1901–1950	3.5	3.4	2.3	1.9	1.8	1.4	1.3	1.5	1.6	1.8	2.2	2.6
	1951–2000	2.7	3.0	2.4	1.6	1.6	1.4	1.4	1.7	1.7	1.5	2.0	2.3
Szeged	1901–1950	3.5	3.5	2.5	1.9	1.8	1.5	1.5	1.7	1.7	1.7	2.0	2.5
	1951–2000	2.6	3.0	2.2	1.6	1.5	1.3	1.4	1.5	1.6	1.6	2.1	2.3
Debrecen	1901–1950	3.4	3.2	2.3	2.0	1.8	1.5	1.2	1.4	1.6	1.8	2.2	2.5
	1951–2000	2.7	2.9	2.3	1.6	1.6	1.3	1.3	1.5	1.6	1.4	2.0	2.3

Coefficient of variation (CV)

Station		I.	II.	III.	IV.	V.	VI.	VII.	VIII.	IX.	X.	XI.	XII.
Zalaegerszeg	1901–1950	–269.4	540.8	41.0	16.4	10.7	7.3	7.3	6.6	9.2	15.8	40.1	223.5
	1951–2000	–217.9	381.9	44.5	15.7	11.0	7.5	7.5	8.4	10.1	16.4	41.2	415.2
Magyaróvár	1901–1950	–221.3	520.4	43.9	16.6	10.7	8.0	5.8	6.4	9.7	15.5	40.7	343.0
	1951–2000	–221.1	371.8	44.0	13.9	10.8	7.8	7.1	7.5	9.7	16.6	38.8	243.9
Túrkeve	1901–1950	–153.4	–1031.5	43.5	17.4	10.9	7.4	5.9	7.0	9.7	16.8	44.7	877.7
	1951–2000	–146.8	720.4	44.5	14.4	9.8	7.2	6.4	8.2	10.0	13.4	40.8	510.0
Szeged	1901–1950	–336.6	448.1	38.6	16.1	10.5	7.6	6.6	7.8	9.7	14.0	33.5	156.1
	1951–2000	–209.1	391.4	39.9	14.1	9.3	6.7	6.5	7.3	9.6	14.3	40.1	278.0
Deebrecen	1901–1950	–150.3	–660.1	47.5	18.3	10.7	7.6	5.7	6.9	9.8	17.6	47.4	727.9
	1951–2000	–133.5	6405.0	47.4	14.7	10.0	6.8	6.3	7.6	9.9	13.1	42.5	1679.5

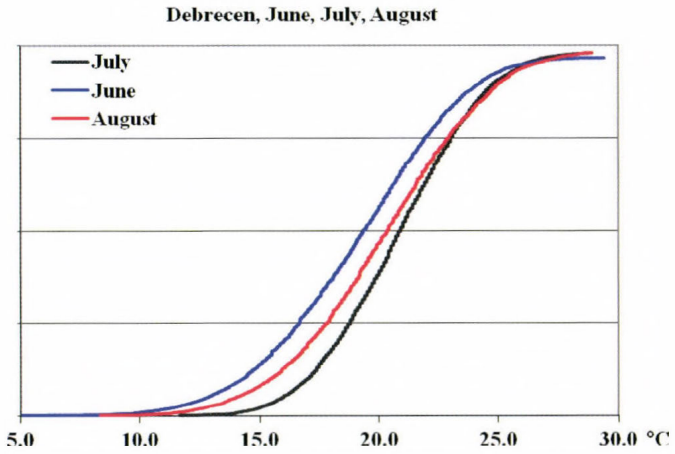

Fig. 3. Probable distribution of the daily average temperatures in summer months (Debrecen, 1901–2000).

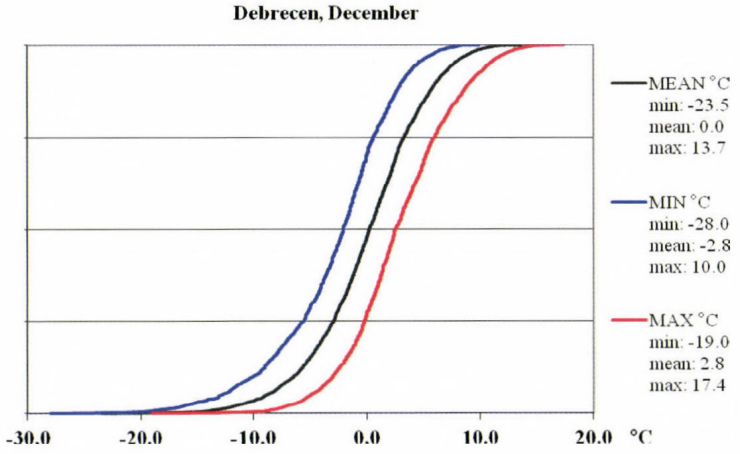

Fig. 4. Frequency distribution of the daily average and extreme temperatures in December with absolute maximun and minimum values (1901–2000).

The spring and partially the autumn temperature damages are mostly caused by radiation frosts which are developed in accordance with local conditions, such as micro relief, heat capacity of soils, etc.

There has been no frost statistical frequency analysis related to a short period of time which is based on several years of observations because of the spatial and temporal heterogeneity of frost sensitivity. *Table 3.* provides

information about the frequency of frost of various strength in the region of Nyíregyháza and Kecskemét broken down to 5-day periods and expressed in a percentage which represents the duration of frost in days (*Szász,* 1988). This table shows the values calculated on the basis of the minimum temperatures measured at 200 cm height, which cannot be regarded as typical values in the lower soil layers.

Table 3. Frequency of five–day minimum temperature (Kecskemét, Nyíregyháza, 1931–1970)

Relativ frequency of different frosts, 1931–1970. Kecskemét											
	III.				IV.						V.
day	**12–16**	**17–21**	**22–26**	**27–31**	**1–5**	**6–10**	**11–15**	**16–20**	**21–25**	**26–30**	**1–5**
Frost days %	49.20	48.20	36.40	25.10	15.90	8.20	10.75	5.75	3.40	1.025	2.05
0 -(–0.9)	17.16	24.50	35.21	32.67	45.15	68.80	66.70	36.40	16.75	50.00	25.00
(–1)-(–1.9)	15.60	19.15	15.50	24.50	35.50	6.20	19.05	45.40	66.60		25.00
(–2)-(–2.9)	16.66	16.00	21.10	12.25	6.45	18.80	4.76	9.10	16.65	50.00	50.00
(–3)-(–3.9)	13.55	8.50	14.10	8.16	12.90	6.30	4.76				
(–4)-(–4.9)	11.45	11.70	5.64	16.30			4.73	9.10			
(–5)-(–5.9)	10.40	9.57	8.45	4.08							
(–6)-(–6.9)	5.21	5.32		2.04							
(–7)-(–7.9)	5.21	2.13									
(8)-(8.9)	3.12										
(–9)-(–9.9)	1.04	2.13									
(–10)-(–10.9)		1.00									

Relativ frequency of different frosts, 1931–1970, Nyíregyháza															
	III.				IV.						V.				
day	**11-15**	**16-20**	**21-25**	**26-31**	**1-5**	**6-10**	**11-15**	**16-20**	**21-25**	**26-30**	**1-5**	**6-10**	**11-15**	**16-20**	**21-25**	**26-31**
Frost days %	62.0	56.5	44.0	32.5	22.5	22.0	12.5	10.0	5.0	4.0	2.0	0.0	0.5	0.5	0.5	
0-(–0.9)	20.2	20.4	26.2	32.3	35.6	47.7	28.0	40.0	50.0	50.0	50.0		100.0		100.0	
(–1)-(–1.9)	22.6	23.0	25.0	30.8	22.2	31.8	40.0	10.0	30.0	25.0	50.0			100.0		
(–2)-(–2.9)	12.9	11.5	23.8	15.4	22.2	9.1	20.0	25.0	0.0							
(–3)-(–3.9)	13.7	11.5	10.2	6.2	15.6	6.8	4.0	15.0	10.0	25.0						
(–4)-(–4.9)	4.8	9.8	8.0	7.8	2.2	2.3		5.0	10.0							
(–5)-(–5.9)	10.5	5.2	6.8			2.3		5.0								
(–6)-(–6.9)	7.3	7.1		1.5			8.0									
(–7)-(–7.9)	4.0	3.5		1.5	2.2											
(–8)-(–8.9)	0.8	6.2		1.5												
(–9)-(–9.9)	0.8	0.9		1.5												
(-10)-(-10.9)	0.8	0.8														
(-11)-(-11.9)	0.8															
(-12)-(-12.9)				1.5												
(-13)-(-13.9)	0.7															

4.3. Precipitation

One of the main elements of agricultural production is precipitation, since the water supply of plants produced in Hungary is provided by natural precipitation with few exceptions. Precipitation is one of the most important aspects which determine yield. It has to be emphasized also because of the fact that the amount of precipitation in Hungary usually does not satisfy the demand posed by plants.

The level of precipitation supply is usually characterized by average sums. Temperate zone areas with continental climate usually have their maximum precipitation in the summer and the minimum precipitation in the winter. In mediterranean areas, this relation of precipitation during the year is the opposite. Since climate borders are rather variable, the different climatic characters are present in a mixed form in the Carpathian Basin (*Berényi*, 1943, 1945). From year to year, precipitation shows a rhapsodic yearly course in comparison with temperature that can be explained by the high variability of this element. Similarly to the description of temperature, the multiple-year mean values of precipitation, as well as its statistical parameters related to the 5 stations are summarized by *Table 4*. One of the most suitable statistical parameter of the variability of precipitation is the coefficient of variation (CV = standard deviation / mean). The coefficients of variation show a specific and strict yearly course in Hungary: the CV values reach their maximum (57–79%) at the beginning of spring – usually in March – and then they decrease until May and June. The minimum values fall around the time of precipitation maximum (44–63%), then they increase again until the end of summer or the first month of autumn to reach a secondary maximum (55–75%); by the winter months, the values will decrease again, but the monthly values will stay between 50 and 70%. CV values calculated for various points of the country are summarized in *Table 4*.

If the distribution of the precipitation sum of the growing season is shown on a similar scale, it can be seen that there is still a difference between the precipitation supply of the eastern and western part of the country. However, the difference between the yearly mean values of the driest and wettest areas is 300 mm per year, and the same difference in the growing season is still 300 mm, but this value refers to a significantly shorter period of time. As a consequence, the difference in the summer precipitation supply has a much stronger effect mainly on crop production, more specifically on the water balance of soils than before and after the vegetation period (*Bacsó,* 1952; *Szepesiné,* 1966).

As a matter of course, the extremes of the yearly precipitation sum take place in the southwestern areas of the Transdanubian region, which can be explained partially by relief-related reasons and partially by the current circulation status. In these areas, the range of fluctuation of the yearly sum significantly exceeds 900 mm, but the minimum amount is below 400 mm. The fluctuation range of the yearly sums of the Great Plain areas, where the usual

amount of precipitation is low, is near 650 mm (*Hajósy*, 1952; *Kéri* and *Kulin,* 1953; *Szász,* 2005; *Goda*, 1966; *Péczely*, 1963, 1968).

Table 4. Sum, standard deviation, and variation coefficient of the monthly precipitation (1901–1950, 1951–2000)

Precipition (mm)													
Station		**I.**	**II.**	**III.**	**IV.**	**V.**	**VI.**	**VII.**	**VIII.**	**IX.**	**X.**	**XI.**	**XII.**	**Year**
Zalaegerszeg	1901–1950	39	38	43	62	74	81	87	81	70	65	59	49	748
	1951–2000	31	31	42	52	72	86	84	74	64	54	63	45	698
Magyaóvár	1901–1950	37	34	38	43	66	58	65	59	52	49	52	49	602
	1951–2000	33	33	36	43	54	66	69	57	45	43	53	44	576
Túrkeve	1901–1950	27	29	33	45	56	68	55	53	44	49	48	38	545
	1951–2000	33	32	30	41	60	71	55	49	41	32	48	46	536
Szeged	1901–1950	32	34	38	49	60	67	50	48	46	51	50	40	565
	1951–2000	28	27	28	40	52	66	53	51	37	31	43	43	497
Debrecen	1901–1950	32	32	34	45	59	69	61	60	46	53	51	41	583
	1951–2000	33	32	29	44	59	77	60	58	38	33	45	45	554

Standard deviation (S)													
Station		**I.**	**II.**	**III.**	**IV.**	**V.**	**VI.**	**VII.**	**VIII.**	**IX.**	**X.**	**XI.**	**XII.**
Zalaegerszeg	1901–1950	23.0	28.6	30.5	33.3	42.6	35.7	53.7	49.3	42.0	42.6	40.9	29.2
	1951–2000	20.2	21.5	22.1	29.8	32.6	45.3	43.5	42.1	34.7	41.9	34.4	26.4
Magyaróvár	1901–1950	19.5	20.3	28.8	25.8	39.1	29.5	37.2	38.3	37.0	34.3	35.0	24.6
	1951–2000	19.9	22.2	19.9	26.0	30.0	36.3	44.4	32.2	29.4	30.2	30.6	22.9
Túrkeve	1901–1950	14.3	20.3	22.8	25.1	33.0	32.8	35.9	34.6	30.7	35.5	28.0	25.6
	1951–2000	20.9	19.7	19.5	20.2	35.8	36.7	33.2	33.2	30.0	29.9	35.2	26.3
Szeged	1901–1950	18.6	26.1	24.4	28.3	34.2	31.6	31.0	28.8	29.1	36.2	30.9	22.9
	1951–2000	17.9	19.7	18.0	18.8	33.4	36.3	32.9	31.4	25.7	27.7	29.7	27.8
Debrecen	1901–1950	19.0	21.6	25.5	27.4	29.8	33.3	38.1	38.5	30.5	33.7	29.8	27.6
	1951–2000	18.4	19.0	18.5	19.4	34.9	40.0	33.5	37.8	28.9	30.0	27.5	22.9

Coefficient of variation (CV)													
Station		**I.**	**II.**	**III.**	**IV.**	**V.**	**VI.**	**VII.**	**VIII.**	**IX.**	**X.**	**XI.**	**XII.**
Zalaegerszeg	1901–1950	59	75	71	54	58	44	62	61	60	65	69	60
	1951–2000	66	70	53	57	45	53	52	57	54	78	55	58
Magyaróvár	1901–1950	53	60	76	60	59	51	57	65	71	70	67	50
	1951–2000	60	68	55	61	56	55	64	56	65	71	58	52
Túrkeve	1901–1950	53	70	69	56	59	48	65	65	70	72	58	67
	1951–2000	64	63	65	49	60	52	61	67	72	94	73	58
Szeged	1901–1950	58	77	64	58	57	47	62	60	63	71	62	47
	1951–2000	64	72	65	47	64	55	63	62	70	90	69	65
Debrecen	1901–1950	59	68	75	61	51	48	62	64	66	64	58	67
	1951–2000	56	60	63	44	59	52	56	66	75	90	61	51

Due to the variable nature of precipitation, exact precipitation maps can only be prepared with lots of imperfections, since the areas bordered by isohyets could also form patches of different variability. Apart from a few exceptions, a precipitation map is drawn on the basis of a *linear scale*, in accordance with the arbitrarily chosen value ranges of the so-called isohyets. Drawing up such a map is a relatively simple task, but the role of isohyets to function as borders is questionable. In reality, the difference in precipitation supply in the mentioned range has more or less similar variability. If high standard deviation is associated with the nearly identical mean values, it is possible to lose the reality of the map, since the difference between the areas limited by the isohyets which have the same values could show different probability. In order to prevent this error, the extent of distinction can be modified in accordance with the principles of statistical probability. If these principles are taken into consideration, a parting line can only be drawn between two stations if not only the mean, but also the standard deviation values of the related precipitation sums differ (*Szász*, 1968). If the standard deviations are considered, the *limit of the probability significance* can be calculated that will not necessarily be different from the averages, but the standard deviations from the mean values. The statistical precipitation map of Hungary shown in *Fig. 5* was prepared by *Szász* (1971). The precipitation sums of the areas delineated by the isohyets significantly differ from each other, while the sums did not significantly differ in the related period within the areas. Therefore, areas with homogeneous precipitation supply can be separated by using this principle. The advantage of this method can be reached by determining the number of precipitation measurement stations. Within the homogeneous fields, nearly exact precipitation sums can be determined at each optional point in the area delineated by the isohyets, even at the point where the standard deviation of the line, which is in accordance with the measurement location, is accepted. In other words, the mean values do not necessary mean identity or difference in themselves, but the standard deviation values of the two locations to be compared need to be considered in order make a decision. The determination of the difference in supply based on the statistical probabilities is necessary mainly in the areas where the mean precipitation and the related standard deviations are close to each other. The editing of homogeneous fields is by all means a complicated task, but the computerized processing removes this difficulty.

Considering the fact that the analysis of the precipitation in the country is rather manifold and numerous bibliographical sources were published in the last 50 years, we do not wish to describe any further matter of detail (*Péczely*, 1963, 1968; *Goda,* 1966; *Bacsó,* 1967; *Schirokné*, 1983).

4.4. Air humidity, evaporation

As a result of the radiation energy, significant amount of water gets into the air from wet surfaces by means of evaporation. Evaporation is a process

which uses heat energy: its approximate value is 2500 kJ g^{-1}. Although the *quantity of water vapor in the air* is negligible in comparison with the mass of the atmosphere, its physical significance is rather great. The commonly known greenhouse gas effect is mostly created by water vapor. The highest possible quantity of water vapor in the air depends on temperature. The saturated vapor pressure (mbar) is the highest vapor pressure which is determined by temperature; the difference between the saturated and the actual vapor pressure is the saturation gap, a value very often used mainly during practical calculations. The ratio of the current and possible vapor pressure at a given temperature is the relative humidity, which serves the quantified expression of saturation. It has to be emphasized that the amount of water vapor present in the air space of the Carpathian Basin varies in a rather wide range (*Száva-Kováts*, 1937), which is mainly caused by the large differences in water vapor content of the air masses arriving from areas which have rather different climate.

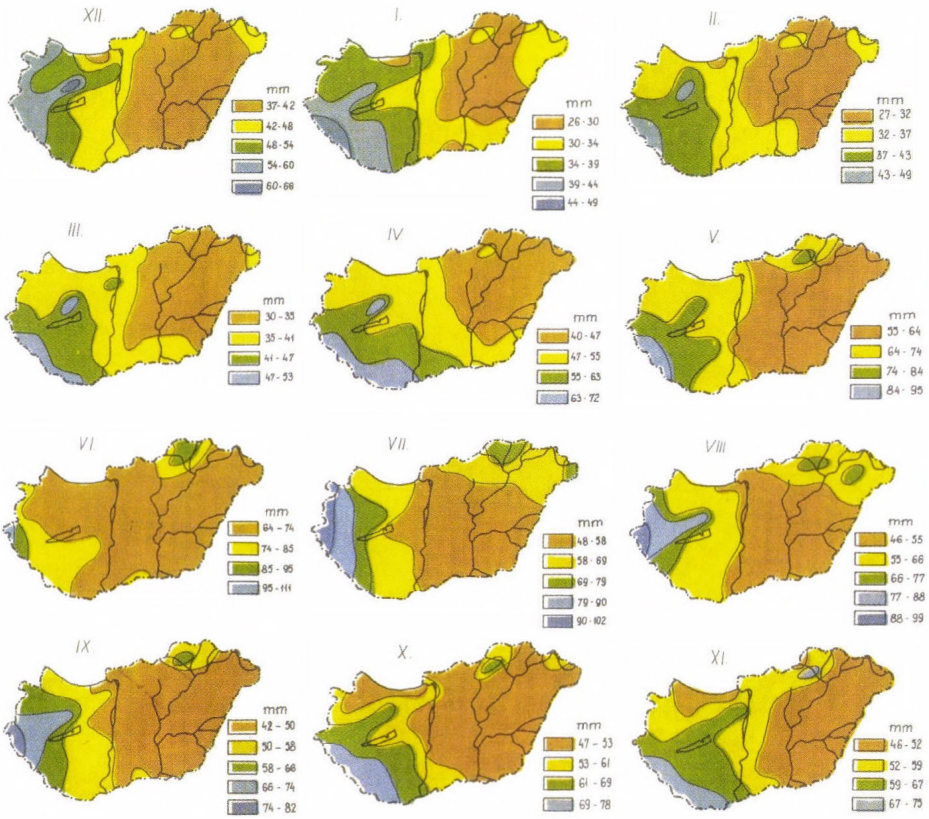

Fig. 5. Significant probable heterogeneity of monthly average precipitations in Hungary (1901–60) (*Szász*, 1971).

Nearly every meteorological element has a role in forming the conditions of *evaporation* to a different extent. The strongest regulatory factor is the incoming energy on the surface that is the absolute value of the radiation balance per unit of time. A high percentage of this energy can be used for evaporation above wet and water surfaces. The saturation deficit or the relative humidity define the intensity of the evaporation process, similarly to the increase of wind speed, which makes the *process of evaporation* more intensive with the increase of turbulence.

Evaporation is the meteorological element which cannot be measured directly; therefore, the mentioned significant factors determine the actual evaporation in a ratio which is in accordance with their importance. The actual evaporation can be estimated with various physical correlations. The amount of water which gets into the air in the form of water vapor in the case of the given physical condition of the atmosphere is called potential evaporation (P_0) (*Thornthwaite*, 1948). As a matter of fact, potential evaporation is a physical constraint, and it expresses the highest evaporation ability if the lack of water hinders evaporation. Measurements show that the evaporation of the open water surface is close to the potential evaporation. Instead of the rather complicated but reliable findings, various empirical formulae are used generally. The high number of these formulae makes it necessary to use them with precaution, because the weights of the various factors are different in areas with different climate. Theoretically, without the certification of the empirical formulae, the mentioned correlations cannot be appropriate and usable (*Fisher* and *Yates*, 1957).

Various formulae become popular in Hungary, of which the research considers the following to be worth mentioning:

Antal's method (1968): $P_0 = 0{,}74 \cdot (E-e)^{0{,}7}(1+\alpha T)^{4{,}8} \quad \left[mm\ day^{-1}\right]$,

Szász' method (1973): $P_0 = \beta\left[0{,}0056(T-21)^2\left(1-RN_a\right)^{2/3} f(v)\right] \quad \left[mm\,day^{-1}\right]$,

Varga-Haszonits' method (1977): $P_0 = \dfrac{1-RN_a}{1+RN_a} \cdot T_k$,

where T_k is the temperature, RN is the relative humidity, v is the wind speed, $(E–e)$ is the saturation deficit.

By using the empirical formulae, it is possible to determine the evaporation ability of the air (P_0), thereby providing the temporal and spatial change of the P_0 values in a wide range. Independently of climatic conditions, the extent of potential evaporation cannot exceed the equivalent of the radiation energy balance (expressed in mm) if rigorous physical criteria are considered. This form of evaporation is usually called balanced evaporation.

In order to determine the evaporation ability of the air, the evaporation-related water loss of different-sized, but standard water-filled tubs is determined.

Based on the water level differences measured in these tubs, the sum of evaporation in a day or in several days can be observed. For agricultural purposes, the evaporation loss of natural water surfaces is usually compared to this value. The examination of evaporation is almost indispensable from the practical aspect during the examination of the climatic characteristics of the country, since this is one of the strongest limiting factors in the development of crop production. In this relation, the climatic analysis of water supply problems have to be performed in order to work out the practical solutions (*Szász*, 1973a,b).

The Hungarian agrometeorological research has reached significant achievements in examining the potential evaporation in the country. Altogether, these results are suitable for the competent authorities to take the steps which are essential to implement developments such as water replenishment, irrigation, and drainage (*Kéri* and *Kulin,* 1953; *Péczely,* 1963; *Pálfai,* 2004).

The regional distribution of potential evaporation in Hungary is between 120–150 mm in the summer months. In the interim seasons, the monthly values range between 60–90 mm, while they are between 10–12 mm in the winter months. In the northern half of the Great Hungarian Plain, the value of P_0 ranges between 660–680 mm, while it reaches 800 mm in the southeastern areas of the Great Plain (*Antal*, 1968; *Szász,* 1973a,b).

The difference between the actual and potential evapotranspiration is the highest in the summer period, its regional distribution is shown in *Fig. 6*. Based on the curves in this figure, the lack of water and the difference between the actual and potential evaporation can be quantified (*Berkes,* 1946; *Antal,* 1966, 1987; *Füri* and *Kozma,* 1972, 1975, 1978; *Posza* and *Stollár*, 1983; *Dunkel et al.,* 1990; *Ács et al.,* 2007).

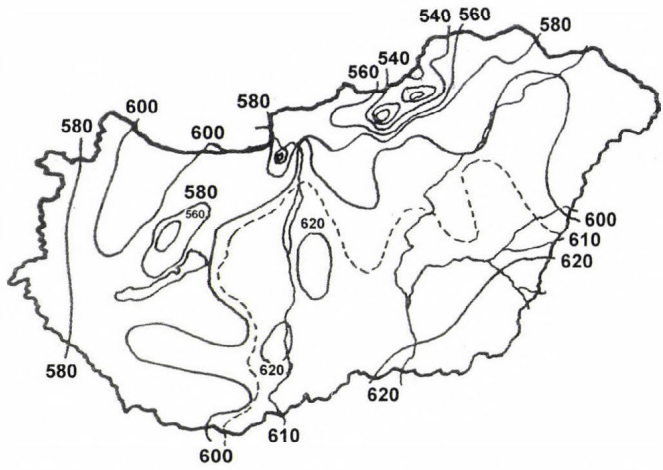

Fig. 6. Areal distribution of potential evapotranspiration in the summer half-year (1901–60).

Due to the high complexity of the problem to be solved, no numerical empirical formulae were prepared to estimate the actual evaporation, and the result of the estimation could contain non-negligible errors. The actual evaporation is significantly modified not only by the amount of available water, but also the speed differences between the water transfer of the soil and plants (*Szász,* 1988; *Ács,* 2004).

4.5. Wind

The interest of modern analyzing agrometeorology in wind speed became extraordinarily wide and deep in the last decades. The motion of air can have different direction and speed. As a matter of fact, wind is only one specific form of this motion system, representing the horizontal component of the motion of the air. The vertical movement is an especially important component of agrometeorology in the existing motion system. Wind speed increases with height, maintaining the process of energy and material transport which is directed towards the heights. The transport processes (sensible and latent heat, CO_2, pollutants, etc.) towards high levels are maintained by the air motion which has a turbulent structure, in which its vertical component plays a very important role.

In Hungary, high energy winds are relatively infrequent, the average wind speed is 2–3 m/s above flat regions. The maximum wind speed can be observed in one of the spring months and the minimum occurs usually in October. The highest wind speed values in the spring could reach 8–10 m/s and the rarely forming tornado-like speed is close to or even exceeds 20 m/s. The change of wind speed is characterized by strengthening during the day and lower values at dawn (1984).

High wind speed results in strong pressure of air. Wind pressure is proportional to the squared wind speed in reference to the surface perpendicular to the motion. These motions can cause significant mechanical damages mainly in forests or in large-leaved herbaceous plants (*Wágner* and *Papp,* 1984; *Papp,* 1974; *Tar,* 1991).

5. Climatic effects in crop production

The physical and dynamic effects on different branches of agriculture can be derived from the database of the climatological information system, and they could be either favorable or unfavorable in a differentiated way. Based on these effects, the responses or reactions whose theoretical and practical significance constitutes the basis of scientific advancement became known, and the system of effects and responses increases the concept range of agrometeorology.

We have a rather wide range of information about climate which provides the increase of knowledge with the accelerating technical development. Also, the increasing amount of information makes it more difficult to interpret

research findings. Considering the fact that the information need is becoming increasingly manifold, a differentiated information system needs to be worked out. Crop production constitutes one component in the science which demands agricultural information. This means that crop production is not satisfied anymore by the traditionally processed climatic data, but it became necessary to get to know the consequences of their effects so that decisions can be made in relation to the introduction of yield-increasing technologies. The research of climate is the concern of meteorologists, but the effect of climate is a social concern. It is necessary to search for the opportunity for sciences dealing with the effect of climate to get to know the complex physical system of processes which is commonly known as agrometeorology.

The summarized findings in this area refer to the crop production-related framework of climate while looking for the opportunity of regional distinguishability in a geographical sense. These research projects could be regarded as agroecological examinations which cover the climatic factor group of the condition system of agriculture, more specifically crop production. This area of research restricts itself to the quantified determination of productivity also in relation to the approach to and the solution of modeling analyses while trying to explore the climatically potential production size in a quantified way for each region of the country based on the climatic *"constraint"* acting on various plants. The model which was worked out on the basis of this concept assumes certain simplified limit conditions, but this fact does not exclude the possibility of development. The most important objective is that the findings should well represent the role of climate in altering productivity; therefore, the climatically potential production expresses the size of climatic value (*Antal*, 1978; *Györffy*, 1976; *Hunkár*, 1990; *Jolánkai*, 1993).

For this reason, the following section provides the partial results which became commonly known as the findings of the main foreign and Hungarian research projects. All these results aimed at the quantified expression of climate as a factor which determines yield. The basis of the characterization of agrometeorology is the collection of climatic elements, which make it possible to describe the effects in an exact way in order to be able to quantify them. The brief overview of the climate of the examined area is done from this aspect.

5.1. Crop development and production

The quantified description of crop development is possible with using various models. Usually, an empirical correlation related to an impact factor in a certain form is used as a basis in an analytical form, which can be theoretically substantiated and it can be easily handled. The change of crop mass, height, its other organs over time describes the rate of development in which mass growth, development phases and the calendar dates of these phases can be determined in an exact way. The related field of science is called phenology, in which not only

crop production but also genetics are significantly interested. Despite the fact that a non-linear process needs to be described, it still has to be expressed in the form of higher level functions in a mathematic form based on the temporal change of usually one climatic element (*Berzsenyi*, 2000). The use of non-recent formulae is significant and the most commonly used ones are worth mentioning here:

$$w/dt = k_1 \cdot m^{c1} - k_2 \cdot m^{c2} \qquad (Bertalanffy,\ 1941),$$

$$w = A\left(1 - b \cdot e^{-kt}\right) \qquad (Mitscherlich,\ 1909),$$

$$w = A\left(\frac{1}{1 + b \cdot e^{-kt}}\right) \qquad (Verhulst,\ 1838),$$

$$w = w_0 \cdot e^{kt} \qquad (Blackman,\ 1919),$$

$$w = w_0\ exp\left(\frac{\mu_0\left(1 - e^{Dt}\right)}{D}\right) \qquad (Gompertz,\ 1825),$$

$$w = w_0\ exp\left(a_1 t - a_2 t^2\right) \qquad (Richards),$$

$$\frac{dw}{dt} = \mu w\left(1 - \frac{w}{B}\right)e^{-Dt} \qquad (Chanter,\ 1976),$$

where w is the growth, k_x is a coefficient, t is the time, D is the coefficient of integration, μ is the coefficient of growth rate.

The number of optional functions is high, but the change of ontogenesis mass over time is different in the case of each species and crop year; therefore, the mentioned correlations and analyses provide a good opportunity to fulfil the target task (*Ábrányi,* 1978; *Berzsenyi*, 2000; *Szász,* 1988; etc.). According to Hungarian observations, growth curves can be effectively used in distinguishing crop year effects. Due to the changing distribution types of the parameters of multivariate functions, the extent of their usability is much lower. The growth curves are mainly realized with the use of continuous climatic elements, considering the fact that these functions describe a certain cumulative curve on various mathematical bases which necessitates the equidistant value series of the independent variable. The temporal distribution of the partial crop mass often becomes necessary to be used, e.g., stem mass, leaf mass, root mass, etc. Processing of the phenological and phenometric values in the mentioned form becomes valuable information, because the character of the curve describes the correlation between both the genetic and climatic effects. This latter question becomes useful information, because the parameters of these functions could be used to express the quantified values of the climatic reactions. For the sake of completeness, it has to be noted that the accumulation of the active temperature values above the basis temperature is a widespread method to classify the

environmental conditions of several plants and also in phenological forecasts in other cases (*Berzsenyi*, 1993).

In the case of any functions which are used to describe growth, it has to be emphasized that the results do not refer to the whole vegetation period, but they mostly express the period between sprouting and flowering; therefore, they can be used for the vegetative development phase. The description of the generative phase is a more complex task, since the inner physiological processes regulate the yield increase and ripening instead of the environmental factors.

5.2. Correlation between weather and yield

This topic looks for an answer to the most important question of meteorology and crop production: in what way and to what extent do different elements regulate yield and yield quality in a separated form or together? This question is rather complex, and although we do not have universal and general equations, it is still worth summing up the currently reliable correlations, which were developed into what they are now.

The simplest correlation is the empirical one which usually verbally refers to the correlation between precipitation, temperature, and yield. Their time-enduring character is questioned and it is only rarely proven. *Bauman* (1949) worked out an empirical correlation used in crop production research by separating the crop years of high and low yields after classifying yields based on their extent. Bauman had the assumption that the best and most unfavorable weather type prevailed in these two categories. This procedure was also used in Hungary by *Berényi* in 1952 (*Berényi* 1945, 1954; *Berényi et al.,* 1959) who also analyzed the significance of the statistical difference of results. Later it was proved that Bauman's method can only be used if the weather effect is parabolic. In these cases, the optimal condition (temperature and precipitation) can be found at the intersection of two lines and its direct statistical surrounding (*Bocz* and *Szász*, 1962).

In the 1900s, correlation and regression analysis became widely used in agricultural research based on the method of *Smith* (1915). This method became common in the first half of the past century in Europe (*Holdefleiss,* 1930; *Smith,* 1915). In parallel with this, the method based on the examination of standard deviation was most commonly used in England (*Fischer* and *Yates,* 1957).

In the Hungarian agrometeorological research, the correlation methods were used in uni- and multivariate forms in order to determine the temperature and precipitation need of the main produced plants as well as their role in regulating yield (*Aujeszky, et.al.,* 1951). With this work, Berényi laid the foundations of one of the most important agrometeorological topic; therefore, several followers used this method within the framework of the yield analysis of plants (*Kerék,* 1934; *Szász,* 1955; *Justyák,* 1989; *Erdős* and *Lambert,* 1987; etc.). The correlation analysis was further developed, and the path analysis became widespread for the

purpose of expressing the modification of the weight of different variables during the plant development process (*Botos* and *Varga-Haszonits,* 1974).

In the last 50 years, standard deviation analysis was used as a multifactor analytical method which can be applied to several purposes as a result of the extraordinary mathematical advancement. Its mathematical-statistical one-sidedness is shown by the fact that it is mainly widespread in the field of technical development. One of its main products is factor analysis which is only used by high-level mathematical analysts, and it is only applied in computerized model-based examinations.

Apart from these, further modern methods became very widely used which can be applied in the form of procedures built into complex systems based on probability-focused principles.

The analytical form of the correlation between weather elements and yield built on physical bases was first used in the 1950s with the following physical concept: the development of the organism of plants happens by taking up organic and inorganic substances from the soil in a chemical way, as well as by absorbing solar energy through plant vital processes and by incorporating this energy in the presence of water. This recognition immediately shows that the atmosphere has an almost exclusive role in this process, since the solar and soil surface sources of energy and water get to plants in the form of precipitation by means of meteorological processes. If the active role of solar energy is clarified, we can conclude that, through CO_2 and water – the constituents of the atmosphere –, plant life is not possible without development, growth, energy, water, and nutrients taken up from the soil. In other words, this means that the maximum mass of plant organism developed through vital processes is clearly determined by energy and water supply; that is the generator of production is energy and the fuels are CO_2 and water. The task of agriculture is to achieve the highest genetically possible vegetable production in a given place using the energy, and material stock provided by nature. The physical condition of nature is constant, while the genetic potential is changing and it can be altered by humans; therefore, only these two climatic factors form the basis upon which the mentioned criterion is expected to be realized in the form of organic matter in the future.

Temporal characterization of growth and development can be done with biophysical and chemical methods by describing photosynthesis in detail. The dry matter to be formed can be estimated on the basis of the rules of gross net assimilation and carbohydrate production. From the agrometeorological aspect, it is a fundamental question how actual and potential photosynthesis is going on and what is the ratio of the dry matter which was formed. The answer for this question is known in agrometeorology, although this ratio also involves the effect of other, non-meteorological roles of the production site, i.e., nutrient supply, soil effect, etc. This explains why the potential production can be estimated in the mentioned form since the 1950s (*de Wit*, 1954). Although the first analyses were done mainly in a global or climatic zone-focused relation

(*Lieth,* 1976), the aim of these examinations was primarily vegetation research. Also, one of the energetic research projects was launched by the author (*Szász*, 1981), who determined the energetically potential production size on the basis of the water analogue of Penman and the PAR values with 0.03 energy efficiency. In the following decades, the further developed form of this work also incorporated the effect of temperature and water supply, and an attempt was made to analyze the typical climatic potential of production sites by considering the proportion of the role of the level of plants' nutrient supply. It has to be noted that *Antal* (1978) and *Varga-Haszonits* (1987b) defined the size of climatic potential, but they used the proportion of the energy balance and water balance to characterize the climatic potential of various regions, that is the size of the dry matter mass which was approximated from the values of energy and water balance that were incorporated in the examination. *Szász* (1981) wished to determine the size of the actual production from the value of climatic potential. The basic correlations of this method could be summarized as follows:

$$EP_0 = \varepsilon(1-a)\,PAR/\eta,$$
$$KP_k = \varepsilon[(1-a)PAR/\eta]\,f(T,W)^{-1},$$
$$KP_{k\cdot N} = \varepsilon[(1-a)PAR/\eta]\,f(T,W)^{-1},$$
$$KP_{k\cdot N}/EP_0,\quad PAR = G/2,$$

where η is the coefficient of conversion (15.7 MJ/kg), KP_{kN} is the plant factor referring to productivity, W is the humidity, G is the global radiation, KP_k is the sensitivity factor referring to temperature and humidity.

Based on these latter, the method was used on the yield series from 23 regions of the county with typically different climatic and soil endowments. As a result of the analyses, the following parameters were arrived at:

energetic potential $\approx$ EP_0 (t/ha),

climatic potential $\approx$ KP_k (t/ha),

genetic potential $\approx$ $KP_{k\cdot N}$ (t/ha),

proportion $\approx$ $KP_{k.N}/KP_0$.

The correlation system shown above constituted the basis of examinations whose database was the 30-year average yields from 23 production regions and the related meteorological database. The author used the method for agricultural purposes by means of estimating the role of genetic potential for various plant species as a parameter of determination. As a matter of fact, the genetic potential, i.e., productivity is a mobilizing factor which could be made usable to

express maximum climate effects. A part of this correlation is shown in *Fig. 7* which demonstrates the energetically and climatically potential average yields, as well as the actual average yield and the level of production which can be achieved from the genetic aspect. These results were used in Hungarian and also in foreign research.

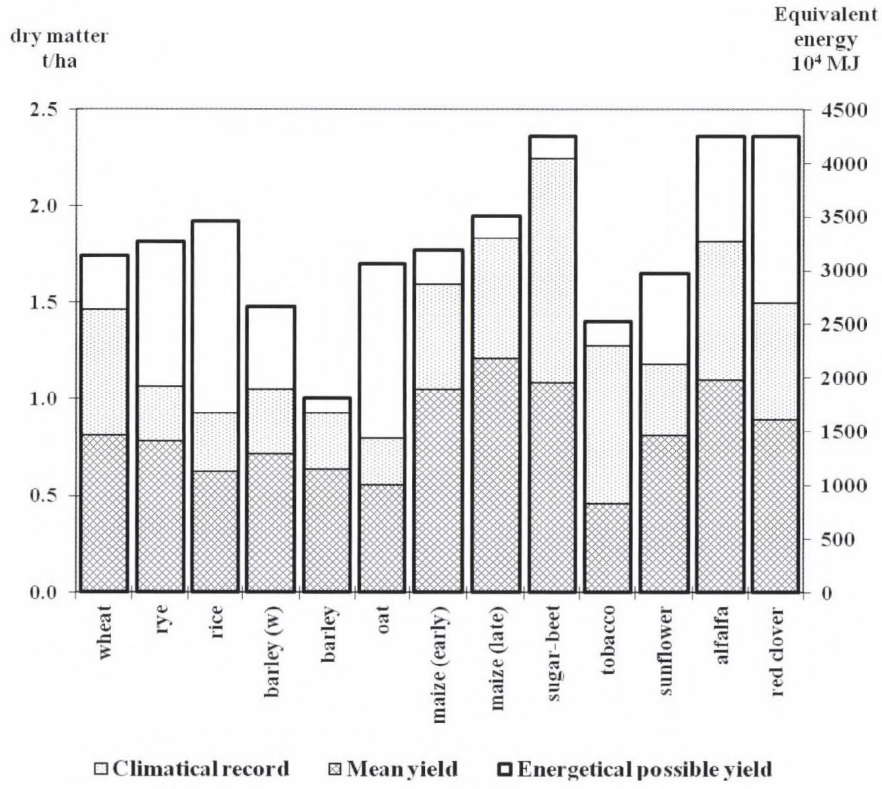

Fig. 7. Climatic records, energetically possible and mean yields of different plants.

It has to be emphasized that significant analyses were performed by the National Meteorological Service in the last 50 years in order to get to know the climate sensitivity of the main produced plants. Of these, the weather dependence findings of wheat (*Varga-Haszonits,* 1974), maize, and potato (*Berényi,* 1943, 1945, 1948*;*, *Szász,* 1961*; Ajtay,* 1979; *Hunkár,* 1990), paprika (*Erdős* and *Lambert*, 1987), barley (*Varga-Haszonits,* 1974), and various vegetable (*Cselőtei*, 1987) and fruit species are worth mentioning. Detailed and programmed examinations were performed in forests (*Justyák,* 1987). It also has to be mentioned that various governing authorities and ministries, such as the

employees of the Agrometeorology and Forecast Department of the National Meteorological Service, cooperated in solving numerous agrometeorological problems by participating in various research programs directed by the government and professional departments.

The agrometeorological research turned into and have been going on in a rather manifold direction for decades, but two factors have especially important role due to the climatic endowments of the country. These are a) the natural water supply of agriculture and irrigation and b) the climatic effects of nutrient management. Details of these two topics still represent a current problem in guiding and developing agriculture on a country level.

5.3. The importance of water supply in crop production

The water cycle has one of the most important roles in the meeting point of the soil-plant-atmosphere system as the activity of all three spheres is peculiar at all times. The water cycle and the broadly meant balance-like record of water in the soil, i.e., *water balance* is an important natural phenomenon whose quantity can be detected by the form of the distinguished processes of the various production sites. The concept of *water cycle* can be approached in any possible ways, as it becomes clear that it refers to a specific motion system that is perpetuated by solar energy, and the transported material is water itself which is the main element of the material flow in plants. The limits of interpreting field crop production can be defined in physical terms; therefore, the limits of the atmospheric part and space of the water balance of various plant communities can be set, where certain physical parameters of the frictional boundary layer of the surface do not significantly change at a given distance from the surface. The lower boundary layer is located in the soil layer where the plant's root mass and the capillary boundary layer below the root mass meet.

The soil of the continent is a vast water reservoir also in global terms. Its upper layer contains all moisture, while its rhythmical change is regulated by the climate. The change is regulated by the simultaneous course of evaporation and precipitation. These two phenomena establish the water need of the plant cover in an optimal or – incidentally – extreme way. One of the main tasks of agrometeorology is to track the temporal change of soil moisture which originates from precipitation and to determine evaporation or evapotranspiration.

Nearly from the beginnings of the agrometeorological research, they tried to get to know the relative value of the available water stock. The numerical value of this stock is the water demand of plants which is the same as the measureable extent of the soil moisture content at all times (accessible soil moisture). The amount of precipitation only refers to the amount of water on the surface, while the water stock that can be stored is 30–40% of precipitation. This is the reason why the total amounts of precipitation and soil moisture are not in balance in the Carpathian Basin, depending on climate. In fact, their

correlation is quite the opposite. Considering the physical characteristics of the most valuable soils from the agricultural aspects, the actual stored water stock and the monthly values of the balance components were the following:

- precipitation,
- stored water stock,
- evaporation.

These few data represent the yearly change of the cycle, the moisture content of the soil, and the values of the balance. As a matter of course, the variability of these values may greatly depend on the physical structure of the soil, the temporal distribution of precipitation, as well as the evaporation ability.

One of the most important ecological parameters of crop production is the water stock which can be taken up by plants, as well as its regional homogeneity. Since the physical heterogeneity of the soil is rather different along the profile, the change of the extent of moisture can hardly be determined from the quantities of the balance components. If the physical reality of the water balance equation is not harmed, it is possible to simplify the correlations of which several forms are known. There are no available long series (in climatic terms) of the soil moisture content, but *Varga-Haszonits* (1987a) estimated county mean values by means of calculation for the whole country. As a matter of course, this method has all those errors which could come from the inaccuracy of the equation used during the calculation. Based on a database which contains more than 30 years of measurement data, these components of the balance provided an opportunity to express the relative values of the water stock of the root zone related to a culture which has an average water need (grass). The relative value of crop water supply (*CWS*) can be estimated by using the following, seemingly simple equation:

$$CWS = \left[\frac{1}{F} \cdot R\left(XII - V\right) \cdot \frac{10 \cdot \sum R\left(VI - VIII\right)}{0.2 \cdot \sum T_d\left(VI - VIII\right)} \right] \cdot \frac{\left(e/E\right)_a}{\left(e/E\right)_m},$$

where (R) in the numerator is the amount of precipitation, the value in the denominator is the potential evapotranspiration, while $(e/E)_a$ represents the actual ratio of vapor pressure and saturation vapor pressure, and $(e/E)_m$ means the average ratio of vapor pressure and saturation vapor pressure for the same period, and T_d is the mean air temperature. The first member of the equation on the right is the value which depends on the physical condition of the soil, and it can be used to express the after-effect of soil moisture before the period of examination. Therefore, the equation expresses a recursive estimation. The value of water supply can be used to characterize the soil endowments, while it can also be interpreted from the climatic aspect; therefore, it can be regarded as a pedoclimatic correlation.

The regional distribution of the water supply (CWS) value – if the summer period is considered to be determinant – is the following: If the CWS value is <20, the region can be considered dry, CWS = 20–40 shows favorable water supply, while CWS > 40 is abundant and overabundant water supply. Due to the simplicity of the map, no extra explanation is needed.

5.4. Correlation between weather and agrotechnical effects

So far, the main characteristics of the range of findings were covered by the correlation between the climate and plants. With the advancement of agriculture, more specifically, modern crop production, the interest in various agrotechnical procedures got into focus. The main reasons for this phenomenon are the increase of soil fertility, the substantial unfolding of genetic potentials, and the protection of the physical condition and the living resources of the soil.

The organic medium of the soil and its health status makes it possible for plant nutrients to form continuously as a result of microbial activity. While the physical structure of the soil is a constant characteristic, the microbial processes in the soil greatly depend on its physical and chemical conditions. Significant research was carried out on the dependence of the nitrogen supply ability of soils on weather (*Szász* and *Lakatos*, 1991; *Nagy,* 2007). The nutrient stock of soil is an important component of the mentioned factor, since the dimension of the conceptual level of soil fertility mainly depends on this aspect. The determination of actual fertility is even more difficult, because the yield of plants cannot be increased without changing the actual fertility. Also, *Kreybig* (1953), *Sipos* (1979), and *Nagy* (1995, 2007) had a similar viewpoint as they emphasized that soil fertility is a dynamic characteristic and it significantly changes even within one crop year. Atmospheric effects play an important role in the change of soil fertility between seasons. The extent of soil fertility can be expressed by the collective of the chemical elements (e.g., mass fraction, etc.) that regulate the nutrient content of plants. In these series of factors, the available nitrogen forms develop in the phases of the C and N cycles. The activity of the microbial system which maintains this process depends on the quantity of bacteria at a given pH value, as well as the temperature and moisture content of the soil. The microbial activity, therefore, the dependence of the nitrate-nitrogen development on temperature is regulated by the Arrhenius equation concerning the value of the daily temperature fluctuation of soil:

$$v_M = K(\Delta T_{min}) exp(-E/RT),$$

where K is the dimensionless adjusting factor of living resources (currently referring to the bacteria sustaining nitrification) and T_{min} is the environmental temperature at which production is zero. This temperature can be considered to be nearly linear in the T_{min}–T_{max} range.

In addition to the theoretical statements, it is also necessary to talk about its significant role in practice. The amount of NO_3-N in 100 g soil (mg) is determined by soil temperature and its water content simultaneously: it is rapidly increasing with temperature in the case of average spring moisture, reaching its maximum at 15–20 mg/100 g in May at the time of the maximum precipitation. By the end of summer and in the early spring, the extent of forming drops back to a low level as a result of dried out soil, and then a secondary maximum develops by the end of autumn after the increase of moisture when the frequency of NO_3 decreases to about half of its highest possible value.

The dependence of the mentioned nitrification process on weather can be increased with favorable cultivation; therefore, it is worth maintaining a proper soil moisture content (water preservation, irrigation) and developing adequate soil moisture by loosening and compacting to be able to regulate the temperature. Most importantly, these tasks call for different cultivation methods on different soils in order to increase or maintain the level of soil fertility.

The natural soil fertility is not enough for the abundant nutrient supply of plants; therefore, its artificial increase became necessary by adding organic and mineral fertilizers into the soil. In relation to this procedure, the previously mentioned rule is applied again, since sustaining of the power of the soil is nothing else than the increase of the intensity of nitrification processes which is the consequence of microbial activity. The regulation of the extent of nitrification is done in an experimental way by artificially applied fertilizers. Usually, the yearly dose of nitrogen replenishment of soils with high fertility amounts to 120–150 kg/ha nitrogen fertilizers that are applied together with potassium and phosphorus (NPK) in order to increase efficiency. The effectiveness of fertilizers can be assured mainly by keeping the moisture content of the soil on the proper level. In other words, this means that the efficiency of fertilization is low in drought, and this effect reaches its maximum with maintaining around 70% of the relative moisture content of soils. Water abundance reduces efficiency in the form of leaching. Since each crop year has different characteristics, the efficiency is always different, too. *Fig. 8* shows the change of yield against different precipitation supplies depending on different NPK fertilizer doses in maize (*Rácz* and *Nagy,* 2011; Nagy, 2007). Providing fertilizer has an extraordinary importance in modern crop production, as if adequate soil moisture and fertilizer quantity is provided, 10–15% or even higher yield surplus can be reached in the case of water-demanding crops, while the lack of precipitation or the overdose of fertilizers could result in yield depression. In addition to the above, it has to be emphasised that the theoretical basis and the practical implementation of yield regulation in the mentioned form of fertilization calls for wide climatological knowledge, since economical yield increase with high efficiency can only be reached this way or by knowing how to conform to the climatic conditions.

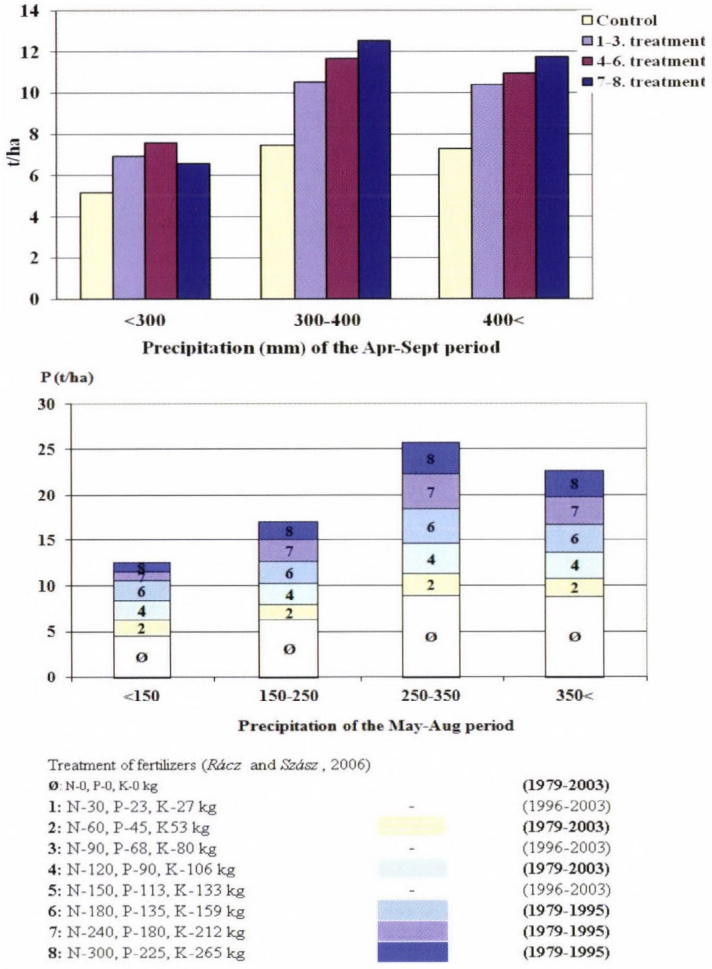

Fig. 8. Effects of mineral-fertility on corn yield by different natural water supply.

Fig. 8 shows the time series of the average yield of maize with different fertilization. On the horizontal axis the amount of precipitation are shown for the given period. Based on these time series, it can be established that the same fertilizer quantity provides significant yield surplus in the case of better precipitation supply. This statement shows that the nutrient effect will only unfold if the increased water demand is satisfied. These data were taken from a long-term field experiment carried out at the Hajdúság loess ridge (*Nagy,* 2007).

The effect of nutrient supply on water need was a generally researched topic. This issue was analyzed within the framework of numerous

agrometeorological experiments (Keszthely, Szarvas, National Meteorological Service). As a general observation, it is known that if the average amount of precipitation is supplemented with around 50 mm irrigation water, the efficiency of fertilization increases significantly (*Antal,* 1968; *Posza* and *Tóth,* 1975; *Antal et al.,* 1977; *Tóth,* 1978; *Dávid,* 1981).

The two mentioned agrotechnical interventions: irrigation + fertilizer effects are the most influential factors concerning the efficiency of crop production; therefore, the research of these factors is among the most important topics even today. One should not neglect the fact that these two agrotechnical effects amount to 30–40% of the prime production costs in crop production. This high amount of costs makes it important to explore the correlations of this topic to an even deeper extent, since they could contribute to the reduction of production risk.

In addition to field experiments, the joint examination of water and nutrient supply is also carried out in so-called evapotranspiration model experiments in a rather manifold way in two locations (Szarvas, Keszthely). The model experiments clearly show that this bifactoral experiment makes it possible to determine the optimal ratio of interaction between water and nutrients which can have a significant role from the aspect of producing crops with average and high water needs. Solving this problem would not only have professional significance, but it could also satisfy an economic requirement.

In addition to the above, it has to be emphasized that these sections summarize only the historical framework of the Hungarian agrometeorological research. There were numerous research results in various topics – mainly in relation to issues close to agriculture – which constitute the problems of various long-term experiments. As a matter of fact, these and similar cooperations should be regarded praiseworthy, due to their successfulness (*Dávid*, 1981, *Berényi*, 1945).

In the agricultural crop production in Hungary, there was a significant change in the modernization of the nutrient management of soils in the 1950s in addition to numerous other processes. In the early fifties, the once traditional organic manure use was switched by the widespread use of mineral fertilizers. The new technology raised new problems, one of which is the determination of the quantity and proportion of mineral fertilizer supply in the case of crops with various nutrient needs. As a matter of fact, Hungarian soils have rather heterogeneous structure and this characteristic is also shown by their nutrient supply. By properly building up the nutrient balance of soils, the specific fertility of soils can be improved which can mainly be expressed in yields. There are numerous well known approaches which say that increasing nutrient supply could moderate yield reduction (*Bocz* and *Szász*, 1962). According to other examinations, the yield fluctuation of different crops is still significant, even though it has changed – some decreased, others increased – for other reasons not mentioned here. From this aspect, the reason of fluctuation is mainly the climatic endowments. In order to clarify this issue, there was a wide survey in

the eighties in Hungary to find an explanation to this phenomenon. Although the ratio of the variability of yield and each weather element did not change substantially, the dependence of plants on weather; therefore, their climate sensitivity still existed as shown by standard deviation analyses. It seems that this question is still not fully answered, as further examinations are necessary to explore the causal correlation between weather variability and the standard deviation of yield. *Table 5* shows the 30-year-long time series of wheat and maize which are the two main crops in Hungary. During the analysis of these series, it was established that the correlations between the two phenomena did not change substantially – r=0.6–0.8 – which shows that there was no significant change in the ratio of standard deviations, only the yield level increased. In other words, the relative yield fluctuation really decreased with the increase of yields, but its absolute value did not increase. Based on this, it can be stated that the average yield of crops moderately increase as a result of yield level increase in the case of the same climatic effect. This issue is one of the fundamental points of the modernization of crop production.

Table 5. Average corn and wheat yield, standard deviation (S) and coefficient of variation (CV)

Soil region	Corn yields (t/ha)			Wheat yields (t/ha)		
	Mean 1961-90	S	CV	Mean 1961-90	S	CV
Szeghalom	3.04	0.79	25.80	2.13	0.78	36.52
Edelény+Encs	3.19	1.25	39.15	2.73	1.01	36.94
Kiskőrös	3.19	1.25	39.31	2.79	0.95	34.20
Fehérgyarmat	3.26	1.03	31.57	2.81	0.94	33.46
Nyírbátor	3.38	1.06	31.29	2.88	1.03	35.76
Gyöngyös	3.64	1.37	37.56	3.10	1.06	34.34
Gödöllő	4.05	1.48	36.64	3.16	1.03	32.63
Pápa	4.08	1.26	30.93	3.16	1.15	36.43
Barcs	4.17	1.23	29.45	3.22	1.06	33.04
Vas	4.19	1.44	34.33	3.29	1.08	32.86
Zalaegerszeg	4.22	1.40	33.04	3.30	1.24	37.69
Siófok	4.28	1.29	30.14	3.47	1.20	34.73
Kunszentmárton+Szentes	4.56	1.58	34.63	3.47	1.27	36.52
Siklós	4.57	1.52	33.30	3.57	1.35	37.94
Csorna	4.60	1.40	30.52	3.58	1.33	37.28
Komárom	4.66	1.66	35.74	3.62	1.32	36.57
Szolnok	4.73	1.70	35.89	3.80	1.26	33.21
Baja	4.86	1.48	30.39	3.83	1.22	31.92
Sárbogárd	5.04	1.69	33.56	3.90	1.22	31.29
Hódmezővásárhely	5.31	1.94	36.57	4.08	1.51	36.88
Szekszárd	5.35	1.78	33.27	4.19	1.63	38.84
Mezőkovácsháza	5.54	1.56	28.14	4.25	1.35	31.75
Hajdúhát	6.49	1.98	30.49	4.62	1.45	31.47

Fig. 9 shows yearly yield of wheat and corn in different growing regions between 1961–90 in Hungary. The increase of nutrient supply results in the increasing water demand of crops. Since the variability of precipitation supply did not decrease, the increased yields could react more powerfully to the extent of water supply. The reaction to water supply is increased by the increased water need, although the amount of precipitation showed a decreasing tendency over the past decade. As a result, drought periods and crop years are becoming more frequent. (*Ruzsányi,* 1974, 1992)

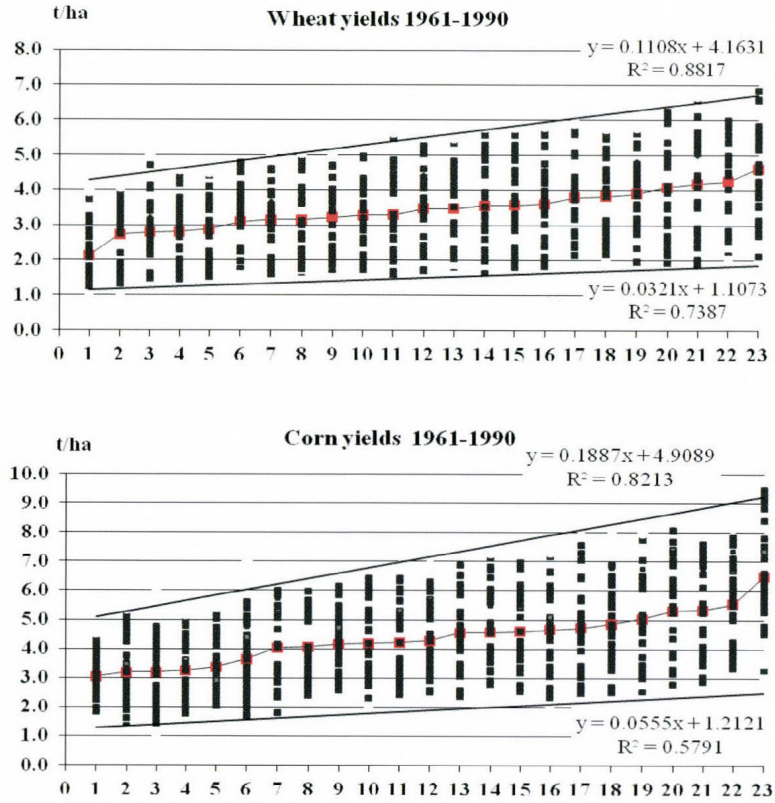

Fig. 9. Yearly yield of wheat and corn indifferent growing region between 1961–90 in Hungary.

Explanation of numbers on horizontal axis is given below in details.

Soil type	Nr.
Low-fertility soils (skeletal soils, bog soils, salt-affected soils)	1, 3-5
Brown forest soils	2, 6-11
Meadow soils, alluvial and sedimentary soils	13, 17, 22
Chernozem soils	15, 18-21, 23

The increase of nutrients and the associated yield increase reach its maximum if the nutrient effect unfolds in the case of favorable water supply. It is an undisputed fact that the extent natural water utilization became more favorable with the increase of yield, while this phenomenon is further intensified by the modest natural water supply level. This latter is favorable until a certain critical value, but the stronger unfolding of water shortage reduces the extent of water utilisation and develops disorders in crop growth, finally resulting in yield decrease.

5.5. Micrometeorology in agrometeorology

Within the framework of complex meteorological research, the physical problems of meteorology are often raised from theoretical and practical aspects in various areas of meteorological practice. As a matter of fact, this phenomenon is ordinary, since it represents two sides of a problem. The predecessor of agrometeorology is the complex and complication of empiricism, physics, micrometeorology, and energetic and aerodynamic processes in the frictional space of the surface. Agrometeorology gets increasingly involved in the interpretation of various parts of agriculture, but its methods are based on physical principles, and it mainly uses the direct physical findings of the surface boundary layer while interpreting biological processes. Today, this phenomenon is clearly shown by the fact that well known international journals feature lots of practically usable findings of agrometeorological research which are based on physical principles among studies that show the aims of nearly sterile meteorological examinations. Despite the fact that agrometeorology and micrometeorology are only narrow branches of science, neither of them can exist without the other concerning the issues they are dealing with; therefore, disciplinarity can be clearly recognized from both sides. In Hungary, agrometeorology originated from empiricism and it also took elements from climatology in order to survey meteorological impacts. From this position, agrometeorology builds a more detailed physical basis while gradually leaving climatology behind in order to provide solution to various problems. Based on this path, it can be established that agrometeorology was not separated from meteorology. On the contrary, it increasingly utilizes the new physical knowledge that formed in the field of micrometeorology. However, agrometeorology attempts to show them "in different clothes" in the area of a more practical science. This process was clearly expressed in the past 50 years in Hungary.

At the beginning, the process described above was shown in the instructions of the former German "Geiger" school, which described the phenomena in the air space close to the surface in a descriptive way under the summarizing name of microclimate and it also attached a speculative explanation to the description of these phenomena, assuming the causal aspect of their background. Microclimatology was widespread mostly in European countries; therefore, there is a large number of related case studies among Hungarian micrometeorological publications, especially from the previous decades.

Agricultural microclimatology observes the yearly and daily cyclic condition changes triggered by plants, the change of temperature and moisture profiles in plant populations and the difference from the profiles above the flat surface and grasslands free from plants. In Hungary, agricultural microclimatology was known as "population climate" both in agriculture and meteorology. At the beginning, the research dealing with this branch of science did not aim at finding the physical explanation for the development of profiles. Instead, the goal was to explore the relationship between the developed profile and some physiological processes of the plant. Therefore, the population climate, or, in other words, vegetable microclimate did not consider the difference between the profiles to be the production of a dynamic process, but mainly of its biological consequence (*Endrődi,* 1967, 1974; *Hunkár,* 1985; *Justyák,* 1989). According to this point of view, the plant population does not intend to explain the quantified evaluation of the physical processes going on in the air space. Instead, the primary subject of interest was the impact of the air condition on plants in high detail. It is not a coincidence that the erroneous nature of this approach did not provide the importance of the new knowledge from the physical aspect from which it could have been the initiator of various biophysical conclusions. It is an undoubted fact that the correlation between the air space of the canopy and the physiological processes of the plant can be considered an especially important knowledge, but the new observations provided usable scientific information mostly in the field of plant biophysics (*Dunkel,* 1984; *Cselőtei,* 1987; *Varga-Haszonits,* 1987b; *Anda* and *Lőke,* 2005).

Canopy climate research was launched in the decades after the turn of the century in Hungary and abroad. In Hungary, *Kálmán Kerpely* performed various population climate-related examinations with the aim to determine the resulting impact between temperature, moisture and evaporation ability in various grown crop populations. The mentioned examinations were carried out in the field experiments established at the Debrecen Agricultural Academy with notable results. The main findings of these examinations referred to the exploration of the joint efficiency of the nutrient and water supply. The work performed in the mentioned field is still significant today.

Later, German researcher *Geiger* organized highly detailed canopy climate research projects in the populations of field crops and forests. The aim of this research was to emphasize the population climate modification role of water supply. *Berényi* extended the population climate research while also considering the microclimate modification impact of the relief in addition to the biological need of plants (*Berényi,* 1954, 1958; *Justyák,* 1960; *Borhidi* and *Dobosi,* 1967; *Szász,* 1973a,b, 1988).

While we acknowledge the agrometeorological significance of population climate research findings, it can be established that the static-focused work needs to be renewed, which was first recognized in foreign research stations. The meteorological use of the physical examination results of the boundary

layer – Prandtl's layer – provided an extensive space for evolving new directions while accepting the findings of the previous population climatological research. The modernization was founded by the general use of energetic measurements, as well as the detailed exploration of the aerodynamic rules of energy and material transfer, further extending the possibilities of complex agro- and biophysical research which justified and explained the previously observed change of conditions with proper physical reality. The simpler energy balances and the implementation of the quantified analysis of turbulent sensible and latent heat transfer provided new bases for a significant part of agrometeorology both in macro- and microclimatic senses. This way, agrometeorology became an interdisciplinary science which made use of atmospheric physical and agricultural knowledge jointly. The theoretical cognition and methodical use of turbulent transport processes made it possible to describe the processes with mathematical correlations based on physical principles – an opportunity that had only been a desire until this point. Furthermore, based on these correlations, a phase of processes can be built up bases on which model-based research findings can be obtained.

Today, modeling can be considered a reachable goal in agrometeorology, despite the fact that gathering and arranging theoretical knowledge still calls for numerous tasks to be done. It is possible to describe the processes which will serve the purpose of the basic model of scientific life by building together separate processes later, based on the results of measurement systems built on digital bases. It has to be emphasized that the most critical point of this problem is the development of the right algorithms that could be regarded as bricks in the building of science (*Ábrányi,* 1978; *Hunkár,* 1984, 1986, 1990; *Szász,* 1987; *Dunkel et al.*, 1987, 1989; *Szabó,* 1988, 1989; *Justyák,* 1989; *Ács,* 2004).

From this viewpoint, the Hungarian agrometeorological research is successful, since numerous research findings were obtained which provided model-based results in order to make progress. The modeling activity that is becoming increasingly accurate is a hopeful tendency that has enormous progress today in international relations. It has to be emphasized that the professional representatives of this tendency do not only increase the values of the agrometeorological research in a narrow sense, but they have high significance in developing practical agriculture both from theoretical and practical points of view. The high level economic utilization of the model system of agricultural activities is recognized in a definite form today, but it can only be hoped to become more extensive if the branches of science associated with agriculture, e.g., agrometeorology will contribute actively to this joint activity. In this field, the Hungarian agrometeorological research calls for further development in order to carry out joint development. The sum and collective of partial potentials represent the level of total active potential concerning all areas. In other words, this means that without the cooperation of

the related branches of knowledge, it could become doubtful to reach the potential borders; therefore, the performance level of the scientific society stays under the potential borders.

In addition to the above, it has to be emphasized that these sections summarize only the historical framework of the Hungarian agrometeorological research. There were numerous research results in various topics – mainly in relation to issues close to agriculture – which constitute the problems of various long-term experiments. As a matter of fact, these and similar cooperations should be regarded praiseworthy, due to their successfulness.

6. Conclusions and results

The Hungarian events and findings of the more than one and half-century-long history of agrometeorology could be summarized as follows:

1. Modernization of agriculture in Hungary was extended in the second half of the 1800s, mostly due to Western European impacts.
2. Around the middle of that century, agricultural higher education institutions were established, providing a professionally educated expert basis for the subsequent periods.
3. In the years between 1850–2000, research institutes were established which helped Hungary becoming increasingly effective in launching international agricultural research.
4. The National Institute of Meteorology and Geomagnetics started to work in 1870 and launched organized and controlled climatological observations at its stations while connected to the international network.
5. At the beginning of the 20th century, the first standard climate elements appeared in the form of 30-year averages (1870–1900).
6. Empirical climate-based agrometeorological research was launched, dealing mostly with the issues of successful prevention of damages caused by weather (e.g., frost, drought, water logging, wind).
7. There was a restructuring in the Hungarian climate network at the time of the World War II.
8. Effect functions, indexes and statistical indexes in accordance with the empirical or physical correlations serving the characterization of the climate and the temporal and spatial change of agrometeorological processes were worked out.
9. By the middle of the 20th century, a national climatic database was established as a result of the joint work of the Hungarian Meteorological Service and the main research institutes. This database made it possible to

establish an agrometeorological information system.

10. The research order of agrometeorological research started to unfold characteristically in the 1960s:
    a. statistical agrometeorology,
    b. agrometeorology built on biophysical bases,
    c. model-based agrometeorology.

    The interpretation range of all specialized branches was continuously becoming increasingly widespread, thereby establishing theoretical bases in a way that they could finally be clustered into a complex research system.
11. For today, the findings of this branch of science which is built on climatic and micrometeorological bases contribute to the development of agriculture in a manifold way. Therefore, the requirements of increasing the natural energies by man also increased.
12. The need for the cooperation between meteorology and agriculture resulted in the further increase and efficiency growth of both fields of science.

References

Ábrányi, A., 1978: Matematikai modell az őszi búza termésének időjárás okozta ingadozásaira. *OMSZ. Hiv. Kiadv. XLVI.* 157–163. (In Hungarian)

Ács, F., 2004: A talaj-növény-légkör rendszer modellezése a meteorológiában. ELTE TTK, Budapest. (In Hungarian)

Ács, F., Breuer, H. and *Szász, G.*, 2007: A tényleges párolgás és a talajvízkészlet becslése egy módosított Thornthwaite-féle modell alapján. *Agrokémia és Talajtan 56*, 217–236. (In Hungarian)

Ajtay, Á., 1979: A burgonya terméshozamának előrejelzése meteorológiai paraméterek segítségével. In (Szerk: *Lőrincz J.*) A burgonya termesztése. Mezőgazdasági Kiadó, Budapest. (In Hungarian)

Allen, R.E., 1999: Tracking the agricultural revolution in England. *Ec. History Rev., LII.*, 209–235.

Anda, A. and *Lőke, Zs.*, 2005: Microclimate simulation in maize with two watering levels. *Időjárás 109*, 21–37.

Antal, E. 1965: Öntözés és meteorológia. *Időjárás 69*, 248–256. (In Hungarian)

Antal, E., 1966: Egyes mezőgazdasági növényállományok potenciális evapotranszspirációja. *Öntözéses Gazd. 4*, 69–86. (In Hungarian)

Antal, E., 1968: Az öntözés előrejelzése meteorológiai adatok alapján. Kandidátusi értekezés, (In Hungarian).

Antal, E., 1978: A növénytermesztés felső határát meghatározó éghajlati potenciál. *OMSZ. Hiv. Kiadv. XLVI*, 164–170. (In Hungarian)

Antal, E., 1987: Agrometeorológiai kutatások az Országos Meteorológiai Szolgálat keretében. *Időjárás 91*, 68–79. (In Hungarian)

Antal, E., Posza, I. and *Tóth, E.*, 1977: Az időjárás és éghajlat hatása a műtrágya érvényesülésére. *Időjárás, 79*, 95–104. (In Hungarian)

Aujeszky, L., Berényi, D., and *Béll B.*, 1951: Mezőgazdasági meteorológia. Akadémiai Kiadó, Budapest. (In Hungarian)

Bacsó, N., 1952: A hőmérséklet szélsőértékei Magyarországon. *OMSZ Hiv.Kiadv. XV*, 8–26. (In Hungarian)

Bacsó, N., 1955: Az egyórás csapadékok gyakorisága és hozama. *Időjárás 59*, 13–28. (In Hungarian)
Bacsó, N., 1959: Magyarország éghajlata. Akadémia Kiadó, Budapest. (In Hungarian)
Bacsó, N., 1967: A mikroklíma fizikai szemlélete. Tudományos értekezés, Gödöllő. (In Hungarian)
Baumann, H., 1949: Wetter und Ernteertrag. Dtsch. Bauernverlag, Berlin.
Berényi, D., 1943: Magyarország Thornthwaite-rendszerű éghajlati térképe és az éghajlati térképek növényföldrajzi vonatkozásai. *Időjárás 47*, 81–90. (In Hungarian)
Berényi, D., 1945: A kukorica termelése és összefüggése az időjárással. Tiszántúli Mezőgazd. Kamara, Debrecen. (In Hungarian)
Berényi D. 1948: A növényklíma fogalmi elhatárolása. *Időjárás 52*, 175–176. (In Hungarian)
Berényi, D., 1954: Az időjárási elemek és a terméseredmények közötti összefüggések kutatásának eredményei. *KLTE Meteorol. Int. Közl. 10*, 193–204. (In Hungarian)
Berényi, D., 1958: Az állományklímát alakító tényezők. *MTA Agr. Tud. Oszt. Közl. XIV*, 155–193. (In Hungarian)
Berényi, D., Nagy, L., and *Szász, G.*, 1959: A talajművelés hatása a talaj hő- és vízgazdálkodására. *KLTE Meteorol. Int. Tud. Közl. 15*, 311–328. (In Hungarian)
Berkes, Z., 1946: A Kárpát-medence vízháztartása. *Időjárás 96*, 5–13. (In Hungarian)
Berzsenyi, Z., 1993: A N-műtrágyázás és az évjárat harása a kukoricahibridek (Zea mays L.) szemtermésére és N-műtrágyareakciója tartamkisérletekben az 1970-1991 években. *Növénytermelés* 49–63. (In Hungarian)
Berzsenyi, Z., 2000: Növekedésanalízis a növénytermesztésben. Veszprémi Egyetem, Georgikon Mezőgazdaség. Tud. Kar, Veszprém. (In Hungarian)
Birkás, M., 2006: Földművelés és földhasználat. Mezőgazdasági Kiadó, Budapest. (In Hungarian)
Bocz, E., 1992: Szántóföldi növénytermesztés. Mezőgazda Kisdó, Budapest. (In Hungarian)
Bocz, E. and *Szász, G.*, 1962: A műtrágya szerepe a kiegyenlítetten nagy termések elérésében. *MTA Agr. Tud. Oszt. Közl. XX.* 109-123. (In Hungarian)
Borhidi, A. and *Dobosi, Z.*, 1967: A felszíni albedó területi eloszlása Magyarországon. *Időjárás 71*, 150–159. (In Hungarian)
Botos, L. and *Varga-Haszonits, Z.*, 1974: Agroklimatológia és növénytermesztés. MÉM, Budapest. (In Hungarian)
Campbell, B.M.C., 2010: Agriculture and national incomes in Europe, c 1300–1850., Univ. Belfast 29.
Cseháti, S., 1905: Általános és különleges növénytermelés. Nirtsmann József Könyvkiadója, Győr. (In Hungarian)
Cselőtei, L., 1987: A meteorológia szerepe a mezőgazdaságban. *Időjárás 91*, 60–67. (In Hungarian)
Dávid, A., 1981: Összefüggés az időjárás, a műtrágyázás és a kukorica fejlődésének jellemzői között. *Időjárás 85*, 103–111. (In Hungarian)
Dávid, A., Takács, O. and *Tiringer, Cs.*, 1990: A sugárzási egyenleg eloszlása Magyarországon az 1951–80-as időszak adatai alapján. *OMSZ Kisebb kiadv. 66.* (In Hungarian)
Dobosi, Z., 1972: A sugárzási egyenleg területi eloszlása Magyarországon. Doktori Értekezés Budapest. (In Hungarian)
Dobosi, Z. and *Takács, L.*, 1959: A globális sugárzás területi eloszlása Magyarországon. *Időjárás 63*, 82–84. (In Hungarian)
Dunkel, Z., 1984: Szántóföldi növények fejlődésének (tömeggyarapodásának) dinamikus (szimulációs) modellezése. *OMSZ Beszámolók, 1981.* 269–284. (In Hungarian)
Dunkel, Z., Hunkár, M., and *Zárbok, Zs.*,1987: A kukorica fejlődésének leírása dinamikus-szimulációs növénynövekedési modell segítségével. *Időjárás 91*, 197–208. (In Hungarian)
Dunkel, Z., Stollár, A., Szabó, T., and *Tiringer, Cs.*, 1990: A területi párolgás meghatározása Magyarországon. *Időjárás 94*, 149–155. (In Hungarian)
Dunkel, Z., Bozó, P., Szabó, T., and *Vadász, V.*, 1989: Application of Thermal Infrared Remote Sensing to the Estimation of regional Evapotranspiration. *Adv. Space Res. 9*, 255–258.
Endrődi, G., 1967: A növényállomány hatása a talaj felmelegedésére. *Időjárás 71*, 39–43. (In Hungarian)
Endrődi, G., 1974: A cukorrépa vízszükségletének és öntözővíz-igényének agrometeorológiai alapjai. *OMSZ Beszámolók 1971.* 186–199. (In Hungarian)
Erdős, L. and *Lambert, K..*,1987: Modellek a fűszerpaprika festéktartalmának és termésátlagának előrejelzésére. *Időjárás 91*, 187–196. (In Hungarian)

Felméry, L., 1974: A fotoszintézisben aktív sugárzás mennyisége a tenyészidőszakban. *Időjárás 78*, 235–239. (In Hungarian)
Fischer, R.A. and *Yates, F.*, 1957: Stastistical tables or biological, agricultural, and medical research. Oliver & Boyd. London.
Füri, J. and *Kozma, F.*, 1972: Az öntözés hatása a szőlőállomány energiafogalmára. *Szőlő- és gyümölcstermesztés 8*, 61–73. (In Hungarian)
Füri, J. and *Kozma, F.*, 1975: A szőlő evapotranspirációja. *Időjárás 79*, 112–120. (In Hungarian)
Füri, J. and *Kozma, F.*, 1978: A szőlő tényleges evapotranspirációja és öntözővíz szükséglete. *OMSZ Beszámolók 1975*. 181–194. (In Hungarian)
Goda, L., 1966: A többnapos nagy csapadékok gyakorisága. *VITUKI Tanulmányok és kutatási eredmények XX*. 1–15. (In Hungarian)
Gyárfás, J., 1922: Sikeres gazdálkodás szárazságban. Magyar Dry Farming. Mezőgazdasági Kiadó, Budapest. (In Hungarian)
Győrffy, B., 1990: Tartamkisérletek Martonvásáron. In (Ed.: *Kovács, I.*)Martonvásár második húsz éve. Martonvásár. 114–118. (In Hungarian)
Győrffy, B., 1976: A kukorica termelésére ható növénytermesztési rényezők értékelése. *Agrártudományi közlemények 35*, 239–266. (In Hungarian)
Hajósy, F., 1952: Magyarország csapadékviszonyai 1901–40. OMSZ, Budapest. (In Hungarian)
Holdefleiss, P., 1930: Agrometeorologie. Verl. P. Parey. Berlin.
Hunkár, M., 1984: A simle calculation of the vertical profile of average PAR flux density within a maize stand. *Időjárás 88*, 139–153.
Hunkár, M., 1985: A fotoszintetikusan aktív sugárzás vertikális profilja kukoricaállományban. *OMSZ Beszámolók 1982*, 125–139. (In Hungarian)
Hunkár M., 1986: A növényfejlődés dinamikus modelljében alkalmazott növekedési függvények. *OMSZ Beszámolók 1983*, 111–120. p. (In Hungarian)
Hunkár, M., 1990: Kukoricaállomány mikroklímájának szimulációja. *Időjárás 94*, 221–229. (In Hungarian)
Jolánkai, M., 1993:A búzatermesztés egyes meghatározó tényezői. Akadémiai doktori értekezés, Martonvásár. (In Hungarian)
Justyák, J., 1960: A művelésmódok hatása a szőlő állományklímájára Tokaj-Hegyalján. Kandidátusi értekezés. (In Hungarian)
Justyák, J., 1987: Energiaháztartás-mérések tölgyerdőben. *Időjárás 91*, 131–146. (In Hungarian)
Justyák, J., 1989: A tokaj-hegyaljai szőlőültetvények mezo- és mikroklimatikus jellemzői. Akadémiai doktori értekezés. (In Hungarian)
Kakas, J. (ed.),1960: Magyarország Éghajlati Atlasza. II. kötet. Országos Meteorológiai Intézet, Akadémiai Kiadó, Budapest. (In Hungarian)
Kemenessy, E., 1964: Talajművelés. Mezőgazdasági kiadó, Budapest. (In Hungarian)
Kerék, J., 1934: Az időjárás befolyása az Alföldön a termés mennyiségére és minőségére. Budapest. (In Hungarian)
Kéri, M. and *Kulin, M.*, 1953: Csapadékösszegek gyakorisága Magyarországon 1901–50. *OMSZ Hiv. Kiadv. XVI*. (In Hungarian)
Kreybig, L., 1953: Az agrotechnika tényezői és irányelvei. Akadémiai Kiadó, Budapest. (In Hungarian)
Lieth, H., 1976: The use of correlation models to predict primary productivity from precipitation or evapotranspiration. In *Lange et al.* Water and Plant Life. Berlin. 392–407.
Major Gy., 1976: A napsütés Magyarországon 1958–1972. *OMSZ Magyarország éghajlata 10*. (In Hungarian)
Major, Gy., 1985: A napenergia-hasznosítás meteorológiai megalapozása Magyarországon. OMSZ, Budapest.
Major, Gy., 2002: Magyarországi éghajlat-energetikai tanulmányok. BKAE, MTA. Budapest. (In Hungarian)
Montheith, J.L., (ed.) 1975: Vegetation and the atmosphere. Academic Press, London, New York, San Francisco.
Nagy, J., 1995: A talajművelés, a műtrágyázás, a növényszám és az öntözés hatásának értékelése a kukorica termésére . *Növénytermelés 44*, 252–260. (In Hungarian)

Nagy, J., 2006: A debreceni kukorica tartamkísérlet kutatási eredményei. Debreceni Egyetem Agrártudományi Centrum. Debrecen. (In Hungarian)
Nagy, J., 2007: Kukoricatermesztés. Akadémiai Kiadó, Budapest. (In Hungarian)
Nyíri, L., 1993: Földműveléstan. Mezőgyzdasági Kiadó, Budapest. (In Hungarian)
Overton, M., and *Campbell B.M.S.*, 1996: Production and productivity in English agriculture, 1086–1871. *Econ. History Rev., Historie et Messure, 1996*, 255–297.
Pálfai I., 2004: Belvizek és aszályok Magyarországon. Hidrológiai Tanulmányok. Közl. Dok. Budapest. (In Hungarian)
Papp, É., 1974: A szélsebesség–óraátlagok gyakorisági eloszlásának sajátosságai. *Időjárás 78,* 342–347. (In Hungarian)
Péczely, Gy., 1963: Csapadékmentes időszakok tartamvalószínűsége Magyarországon. *Időjárás 67*, 33–38. (In Hungarian)
Péczely, Gy., 1968: A szárazsági hajlam évi járása és szingularitásai. *Időjárás 62*, 294–297. (In Hungarian)
Petrasovits, I. and *Balogh, J.*, 1974:Az evapotranspirációs kutatása, magyarországi helyzete és nemzetközi vonatkozásai. MTA Vízgazd. TB – Műsz. TB Kiadv., Budapest. (In Hungarian)
Posza, I. and *Stollár, A.*, 1983: A tényleges párolgás számításához használt növénykonstansok értékei többévi mérés alapján. *Időjárás 87*,170–177. (In Hungarian)
Posza, I. and *Tóth, E.*, 1975: A kukorica vízigényének alakulása az időjárási viszonyok és az NPK szintek függvényében. *OMSZ Beszámolók 1972*, 298–305. (In Hungarian)
Rácz, Cs., and *Nagy, J.*, 2011: A víz- és tápanyagellátottság illetve -hasznosulás megítélésének kérdései kukorica terméseredmények vonatkozásában. *Növénytermelés 60*, 94–117. (In Hungarian)
Ruzsányi, L., 1974: A műtrágyázás hatása egyes szántóföldi növényállományok vízfogyasztására és vízhasznosítására. *Növénytermelés 23*, 249–258. (In Hungarian)
Ruzsányi, L., 1992: Főbb növénytermesztési tényezők és a vízellátás kölcsönhatásai, Akadémiai doktori értekezés tézisei, Debrecen. (In Hungarian)
Schirokné, Kriszton I., 1983: A nagycsapadékok gyakorisági analízise és valószínű legnagyobb csapadékbecslése. *Vízügyi Közlemények LXV*. 167–187. (In Hungarian)
Sipos, S., 1979: Talajművelési kísérletek eredményei réti talajon. In *Bajai, J.* (szek.) Kukoricatermesztési kísérletek 1968–1974. Akadémia Kiadó, Budapest, 213–221. (In Hungarian)
Smith, J.W., 1915: Agricultural meteorology. *Proc. Ohio Acad. Sci. 6*, 239–264.
Szabó, T., 1988: A felszínhőmérséklet, mint agrometeorológiai információhordozó. Kandidátusi értekezés. (In Hungarian)
Szabó, T., 1989: Inverz módszer az aktív felszín hőmérsékletén alapuló energiaháztartási egyenlet megoldására. *Időjárás 93*, 115–120. (In Hungarian)
Szász, G., 1955: A rozs termesztésének összefüggése az időjárással és az éghajlattal. MTA Értekezés. Debrecen. (In Hungarian)
Szász, G., 1961: A rizs termesztésének időjárási feltételei a fő termőtájakon. *Növénytermelés 35*, (In Hungarian)
Szász, G., 1968: A csapadékösszegek szórásának vizsgálata Magyarországon (1901–50). *DATE, Tud. Közl.*, 185–210. (In Hungarian)
Szász, G., 1971: Untersuchungen der räumbichen Homogenität von Niederschlagssummen. *Acta Georg. Debrecina XV-XVI,* 225–237.
Szász, G., 1973a: A potenciális párolgás meghatározásának új módszere. *Hidrológiai Közlöny*, 435–442. (In Hungarian)
Szász, G., 1973b: A termesztett növények vízigényének és az öntözés gyakoriságának meteorológiai vizsgálata. *Növénytermelés 22*, 241–258. (In Hungarian)
Szász, G., 1981: Az időjárási folyamatok és a termelés közötti kapcsolat modellezésének alapjai. *Időjárás 85*, 334–345. (In Hungarian)
Szász, G., 1987: A mezőgazdasági célú távérzékelés jelentősége az agrometeorológiában. *Időjárás 91*, 88–103. (In Hungarian)
Szász, G., 1988: Agrometeorológia – általános és speciális. Mezőgazd. Kiadó, Bp. (In Hungarian)

Szász, G., 2005: Termésingadozás és éghajlati változékonyság a Kárpát-medencében. *„Agro-21" Füzetek 40*, 33–69. (In Hungarian)
Szász, G. and *Lakatos, L.*, 1991: A légköri hatások szerepe a talajok N-szolgáltató képességének alakulásában. *Időjárás 95*. 289–300. (In Hungarian)
Száva-Kováts, J., 1937: A légnedvesség évi ingadozása Európában. *Időjárás 68*, 2–16. (In Hungarian)
Szepesiné Lőrincz, A., 1966: A Kárpát-medence hidroklímájának jellemzői. *OMSZ Hiv. Kiadv. XXIX.*, 86–114. (In Hungarian)
Takács, O., 1972: A teljes besugárzás függőleges felületeken. *OMSZ Beszámolók 1969*, 231–238. (In Hungarian)
Tar, K., 1991: Magyarország szélklímájának komplex statisztikai elemzése. *OMSZ Kisebb kiadv. 67.* (In Hungarian)
Thornthwaite, C.W., 1948: An approach toward a rational classification of climate. *Geogr. Rev. 38*, 55–94.
Tóth, E., 1978: A kukorica evapotranspirációja, terméshozama és vízhasznosítása különböző tápanyag és vízellátás mellett. *OMSZ Beszámolók 1975*, 241–255. (In Hungarian)
Wágner, R. and *Papp, É.*, 1984: A szél néhány statisztikai jellemzője. *OMSZ. Hiv. Kiadv. LVII.* 108–117. (In Hungarian)
Várallyay, G., 2008: Extreme soil moisture regime as limiting factor of plants' water uptake. *Cereal Res. Commun. 36 Suppl.*, 3–6.
Várallyay, G.,Szűcs, L., Rajkai, K., Zilahy, P., and *Murányi, A.*, 1980: Magyarországi talajok vízgazdálkodási tulajdonságainak kategóriarendszere és 1:100000 méretarányú térképe. *Agrokémia és Talajtan 29*, 77–112. (In Hungarian)
Varga-Haszonits, Z., 1974: A meteorológiai elemek hatása az őszi árpa fejlődésére. *OMSZ Beszámolók 1971*, 72–77. (In Hungarian)
Varga-Haszonits, Z., 1987a: Agrometeorológiai információk és hasznosításuk. Mezőgazd. Kiadó. Budapest. (In Hungarian)
Varga-Haszonits, Z., 1987b: Az időjárás-növény modellek elvi-módszertani kérdései. *Időjárás 91*, 176–186. (In Hungarian)
Wit, C.T. de, 1954: Photosynthesis of leaf canopies. Centre f. *Agricult. Publ. Doc. Wageningen*, 1–57.

INSTRUCTIONS TO AUTHORS OF *IDŐJÁRÁS*

The purpose of the journal is to publish papers in any field of meteorology and atmosphere related scientific areas. These may be

- research papers on new results of scientific investigations,
- critical review articles summarizing the current state of art of a certain topic,
- short contributions dealing with a particular question.

Some issues contain "News" and "Book review", therefore, such contributions are also welcome. The papers must be in American English and should be checked by a native speaker if necessary.

Authors are requested to send their manuscripts to

Editor-in Chief of IDŐJÁRÁS
P.O. Box 38, H-1525 Budapest, Hungary
E-mail: journal.idojaras@met.hu

including all illustrations. MS Word format is preferred in electronic submission. Papers will then be reviewed normally by two independent referees, who remain unidentified for the author(s). The Editor-in-Chief will inform the author(s) whether or not the paper is acceptable for publication, and what modifications, if any, are necessary.

Please, follow the order given below when typing manuscripts.

Title page: should consist of the title, the name(s) of the author(s), their affiliation(s) including full postal and e-mail address(es). In case of more than one author, the corresponding author must be identified.

Abstract: should contain the purpose, the applied data and methods as well as the basic conclusion(s) of the paper.

Key-words: must be included (from 5 to 10) to help to classify the topic.

Text: has to be typed in single spacing on an A4 size paper using 14 pt Times New Roman font if possible. Use of S.I. units are expected, and the use of negative exponent is preferred to fractional sign. Mathematical formulae are expected to be as simple as possible and numbered in parentheses at the right margin.

All publications cited in the text should be presented in the *list of references*, arranged in alphabetical order. For an article: name(s) of author(s) in Italics, year, title of article, name of journal, volume, number (the latter two in Italics) and pages. E.g., *Nathan, K.K.*, 1986: A note on the relationship between photo-synthetically active radiation and cloud amount. *Időjárás 90,* 10-13. For a book: name(s) of author(s), year, title of the book (all in Italics except the year), publisher and place of publication. E.g., *Junge, C.E.*, 1963: *Air Chemistry and Radioactivity*. Academic Press, New York and London. Reference in the text should contain the name(s) of the author(s) in Italics and year of publication. E.g., in the case of one author: *Miller* (1989); in the case of two authors: *Gamov* and *Cleveland* (1973); and if there are more than two authors: *Smith et al.* (1990). If the name of the author cannot be fitted into the text: *(Miller,* 1989); etc. When referring papers published in the same year by the same author, letters a, b, c, etc. should follow the year of publication.

Tables should be marked by Arabic numbers and printed in separate sheets with their numbers and legends given below them. Avoid too lengthy or complicated tables, or tables duplicating results given in other form in the manuscript (e.g., graphs).

Figures should also be marked with Arabic numbers and printed in black and white or color (under special arrangement) in separate sheets with their numbers and captions given below them. JPG, TIF, GIF, BMP or PNG formats should be used for electronic artwork submission.

Reprints: authors receive 30 reprints free of charge. Additional reprints may be ordered at the authors' expense when sending back the proofs to the Editorial Office.

More information for authors is available: journal.idojaras@met.hu

Published by the Hungarian Meteorological Service

Budapest, Hungary

INDEX 26 361

HU ISSN 0324-6329